DESIGN AND DEVELOPMENT OF GRID-INTERACTIVE ELECTRIC VEHICLE CHARGER

A Thesis Submitted
In Partial Fulfillment of the Requirements
for the Degree of

DOCTOR OF PHILOSOPHY

by

GAURAV YADAV

(Roll No. 2K21/PHDEE/17)

Under the Supervision of

Prof. Mukhtiar Singh

Department of Electrical Engineering

Delhi Technological University, Delhi - 110042

Department of Electrical Engineering

DELHI TECHNOLOGICAL UNIVERSITY

(Formerly Delhi College of Engineering)

Shahbad Daulatpur, Main Bawana Road, Delhi - 110042. INDIA

June, 2025

DELHI TECHNOLOGICAL UNIVERSITY

(Formerly Delhi College of Engineering)
Shahbad Daulatpur, Main Bawana Road, Delhi-42

CANDIDATE'S DECLARATION

I hereby certify that the work which is being presented in the thesis entitled **DESIGN AND DEVELOPMENT OF GRID-INTERACTIVE ELECTRIC VEHICLE CHARGER** in partial fulfillment of the requirements for the award of the degree of Doctor of Philosophy and submitted in the Department of Electrical Engineering of the Delhi Technological University is an authentic record of my own work carried out during the period from July, 2021 to June, 2025 under the supervision of Dr. Mukhtiar Singh, Professor, Department of Electrical Engineering.

The matter presented in this thesis has not been submitted by me for the award of any other degree of this or any other Institute.

(Gaurav Yadav)

This is to certify that the student has incorporated at the corrections suggested by the examiners in the thesis and the statement made by the candidate is correct to the best of our knowledge.

Signature of Supervisor

Signature of External Examiner

DELHI TECHNOLOGICAL UNIVERSITY

(Formerly Delhi College of Engineering)
Shahbad Daulatpur, Main Bawana Road, Delhi-42

CERTIFICATE BY THE SUPERVISORS

Certify that **Gaurav Yadav** (2K21/PHDEE/17) has carried out their work presented in this thesis entitled "**DESIGN AND DEVELOPMENT OF GRID-INTERACTIVE ELECTRIC VEHICLE CHARGER**" for the award of **Doctor of Philosophy** from Department of Electrical Engineering, Delhi Technological University, Delhi, under our supervision. The thesis embodies results of original work, and studies are carried out by the student himself and the content of the thesis do not form the basis for the award of any other degree to the candidate or to anybody else from this or any other University/Institute.

(Mukhtiar Singh)
Supervisor

Date:

Abstract

Electric vehicles (EVs), with their increasing penetration into the power grid, present a significant opportunity to support grid reliability by functioning as distributed energy resources rather than passive loads. On average, an EV remains plugged in and available for energy interaction for approximately 22 hours per day, providing a unique chance to utilize its battery for valley filling, load shifting, and grid de-stressing. Smart chargers can dynamically synchronize with the grid, discharging power during peak demand periods and recharging during low-demand or surplus-generation periods. By aggregating multiple EVs across the network, this approach reduces strain on conventional generation units and transmission infrastructure while promoting a more balanced and flexible grid operation. The intelligent orchestration of these charging events contributes to frequency stability, defers network upgrades, and improves the overall operational economy of the power system. This work develops an advanced control strategy for bidirectional EV chargers, enabling them to support both grid-to-vehicle (G2V) and vehicle-to-grid (V2G) operations while enhancing grid stability, power quality, and distributed flexibility. The control framework leverages the Cascaded Non-Identical Second-Order Generalized Integrator (CNISOGI) a high-selectivity fourth-order quadrature signal generator to extract highly accurate unit vector templates and fundamental components of grid and load currents under conditions of unbalance, harmonics, and dynamic voltage events such as sags and swells. These extracted signals serve as reference inputs to a synchronous reference frame-based current controller, which governs the charging converter. The controller is further augmented to provide dynamic reactive power compensation at the Point of Common Coupling (PCC), reducing the burden on the utility by handling the var requirements of nonlinear residential and emergency loads. This results in unity power factor operation at the interface, minimizing transmission losses and supporting grid voltage profiles.

Beyond conventional power exchange, the proposed smart charger exhibits adaptive behavior through its grid-synchronized logic, which prioritizes energy dispatch based on real-time grid conditions and demand-response signals. During periods of low grid load or high renewable penetration, the charger transitions into G2V mode, while in peak periods, it seamlessly shifts to V2G mode thus contributing to peak shaving, frequency regulation, and voltage support. A flexible state machine and decision-making algorithm manage this energy flow based on priority flags such as grid demand, vehicle state-of-charge, and local load requirements. The integration of such smart decision capabilities not only supports decentralized energy management but also forms the backbone for future vehicle-centric virtual power plants (VPPs).

To evaluate performance, the proposed strategy is rigorously tested using real-time Hardware-in-the-Loop (HIL) simulations on the OPAL-RT OP5600 platform, simulating various grid conditions including load switching, harmonic distortion, voltage sag/swell, and PCC disturbances. These simulations confirm fast dynamic response, high selectivity in frequency extraction, and effective real-time control action. In parallel, a laboratory-scale hardware prototype was developed using a bidirectional DC-AC converter, TI F28379D DSP controller, and programmable AC/DC sources to replicate grid conditions. Experimental validation shows that the system significantly reduces Total Harmonic Distortion (THD) below IEEE-519 standards, achieves voltage regulation within ±5% during transients, and dynamically maintains power factor above 0.98 across a range of load scenarios.

The holistic design presented in this work positions EV chargers not just as energy sinks or sources, but as multi-functional grid-interactive assets capable of contributing to power quality enhancement, grid support services, and real-time energy balancing. As the number of EVs on the grid continues to grow, the proposed smart charging control framework offers a scalable and modular solution to manage bidirectional energy flow, improve power factor, support reactive demand, and reduce the stress on centralized grid infrastructure. The results advocate for the large-scale deployment of such intelligent chargers within smart cities, microgrids, and future decentralized power systems, marking a critical step toward the realization of a resilient, low-carbon, and digitally managed electric grid.

Acknowledgements

First and foremost, my gratitude and appreciation must go to my advisors Professor Mukhtiar Singh, Department of Electrical Engineering, Delhi Technological University, Delhi, for their invaluable support and guidance during the course of my PhD studies. I consider this as the highest degree of privilege to have completed my studies under their supervision.

I owe my deepest gratitude to my PhD research committee for their valuable comments and input: Professor S.K Valluru, Professor, Department of Electrical Engineering, Delhi Technological University; Professor Kapil Sharma from the Department of Information Technology, Delhi Technological University; and Professor D. R. Bhaskar from Department of Electrical Engineering, Delhi Technological University.

I would like to express my deepest gratitude towards my father, Mr. Virendra Singh Yadav; my mother, Mrs. Shushma Yadav; my uncle, Late Vijay Singh Yadav, Mr. Ram Vilas Yadav; my aunt, Mrs. Rajeshwari Yadav, Mrs. Pushpanjali Yadav; my sisters, Mrs. Neha Yadav, Mrs. Swati Yadav, Mrs. Jyoti Yadav, and Miss Vaishali Yadav; my brothers, Mr. Saurabh Yadav, Mr. Maneesh Yadav, Mr. Shubham Yadav, and Mr. Himanshu Yadav; my brothers-in-law, Mr. Arvind Yadav, Mr. Pankaj Yadav, and Mr. Dev Yadav; and my nephew and niece, Ayansh Yadav and Ayanshi Yadav, for their love and patience, which kept me going on this journey. Their faith and unconditional love towards me are the reason for whatever I have achieved in my life. Without my friends Dr. Brijendra Sangar, Dr. Shudhanshu Mittal, Dr. Atul Avasthi, Dr. Dipak Prasad, Dr. Philemon Yegon, Mrs. Poonam Dhaka, Mr. Divyansh Shailly, and Mr. Mohd. Farman, because of their constant support, research work would not have been so easy. I am indebted to all of them for their support, valuable input, and constant encouragement.

Date: Gaurav Yadav

Contents

List of Figures

List of Tables

Chapter 1

Introduction

1.1 Introduction and Motivation

Global initiatives to decarbonize the transportation industry and lessen reliance on fossil fuels are led by electric vehicles, or EVs. The broad use of EVs is now a realistic possibility because to developments in battery technology, the incorporation of renewable energy sources, and advantageous governmental regulations. Additionally, the electric car is a singular technical marvel that has influenced human civilization and fueled societal advancement for decades [1]. The importance of cars on a worldwide scale must also be recognized [2].

Therefore, the worldwide trend is towards the augmentation of charging infrastructure. Here, the chargers could be divided into various categories depending on their size and configuration. Normally, utility-scale charging stations are used for multiple vehicles charging at a commercial level while onboard chargers (OBC)/wall-mounted chargers are used for individual vehicle charging. EV chargers comprise power electronic converters performing the task of AC/DC as well as DC/DC conversion and are further categorized as single-stage or two-stage chargers [3]. Further, the grid-interactive bidirectional chargers are preferable as they have several in-built active functions to support power utility operations especially, in the context of the vehicle-to-grid (V2G) concept [4] - [5]. In the V2G mode of operation, the energy stored in an EV battery may be utilized in regulating the voltage, frequency as well and load harmonics by actively controlling its output active and reactive (PQ) power at the point of common coupling (PCC) [6], [7].

Further, the key to efficient bidirectional power transfer lies in the stability of

the DC-link voltage, which serves as the interface between the AC grid and the DC battery [8]. Maintaining a stable DC-link is crucial for ensuring smooth energy exchange, yet it is particularly challenging due to grid disturbances such as voltage sag, swell, and fluctuations in load. Voltage sag can cause a drop in the DC-link voltage, reducing the performance of the charging system, while voltage swell may overcharge the DC-link, risking damage to the converter [9]. Sudden load fluctuations, whether increases or decreases, can destabilize the DC-link voltage, degrading power conversion efficiency and impairing energy transfer during charging and discharging cycles [10], [11]. Traditional controllers, like Proportional-Integral (PI) controllers, have been widely used to regulate DC-link voltage but exhibit several limitations. PI controllers are known for their relatively slow dynamic response to transient events like voltage sag and swell, and they often struggle to maintain stability under non-linear conditions such as fluctuating grid loads or changes in battery State of Charge (SoC) [12], [13]. Additionally, tuning PI controllers is a complex task, and improper tuning can lead to overshooting, undershooting, and even system instability. These drawbacks make PI controllers less suitable for modern, dynamic V2G systems.

In grid interactive EV chargers, the front-end converter (FEC) plays a pivotal role in absorbing the grid side fluctuations while charging the battery and may provide ancillary services such as reactive power support and load harmonic compensation at PCC if required. Under normal grid conditions, there is no issue in FEC control. However, a problem arises under non-ideal voltage conditions due to the presence of negative sequence and DC-offset components. To get rid of the negative sequence components in grid voltages, a Quadrature Signal Generator (QSG)-based two-channel method works well. Although QSG exhibits satisfactory performance in rejecting the negative sequence component as well as total harmonic distortion (THD), it has limitations in dealing with the DC-offset component [14]. To achieve DC-offset rejection & improved harmonic attenuation, fourth-order QSGs (FO-QSGs) have been proposed in [15]. Conventionally, the FO-QSGs utilize either SOSOGI [16] or CSOGI filters [17], while approximating the fourth-order system to a lower-order system for parameter selection. In the case of CSOGI, the filter is constructed by successively arranging two SOGIs with similar properties. However, in case the damping factor for a single SOGI-QSG is improperly configured, cascaded

SOGIs may become excessively damped & respond more slowly than a single SOGI. The parallel connection of two SOGIs results in SOSOGI, where settling time is taken into consideration while determining its parameters. However, as stated in [15], the approximation to a reduced-order system may occasionally result in a substantial discrepancy between the predicted & current settling timeframes in terms of harmonic attenuations only while ignoring the amplitude variations. Here, it is worthwhile to mention that ignoring the amplitude variations may have a significant impact on the overall control performance of FEC under non-ideal voltage conditions [18].

A central component enabling EV adoption is the Electric Vehicle Charger (EVC), which serves as the energy interface between the grid and the EV battery. These chargers are categorized into two main types:

Unidirectional Chargers: Allow energy flow only from the grid to the vehicle (G2V).

Bidirectional Chargers: Enable two-way energy transfer, both G2V and Vehicle-to-Grid (V2G), turning EVs into mobile energy storage systems.

Among these, single-phase bidirectional chargers are commonly used in residential and light commercial applications. These systems are typically built around a power electronics interface comprising:

- A grid-side AC/DC converter that ensures power factor correction and synchronizes with the utility grid.
- A DC-Link stage with energy storage capacitors to buffer power between stages.
- A battery-side DC/DC converter for controlling the charging and discharging process.
- A control unit responsible for monitoring power flow, managing transitions between G2V and V2G modes, and ensuring grid compliance.

Grid synchronization is a critical requirement in such systems. While conventional Phase-Locked Loops (PLLs) are widely used, they often suffer from performance degradation under distorted or unbalanced grid conditions. To address this, Quadrature Signal Generators (QSGs) are used in this research.

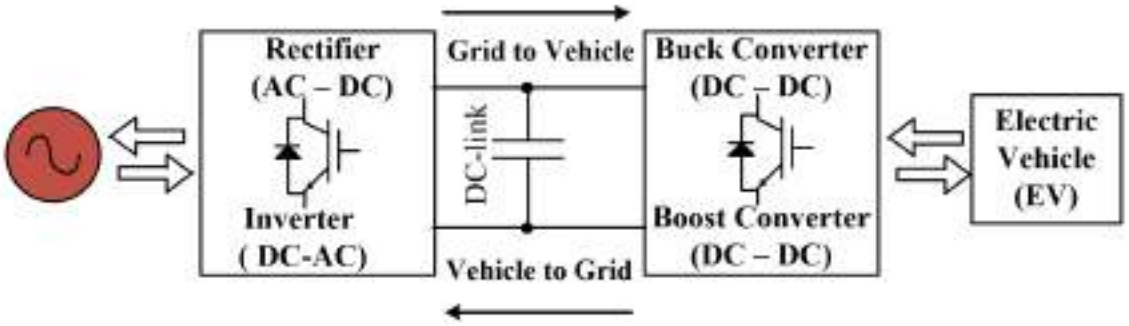

FIGURE 1.1: Block Diagram of a Grid-Interactive Bidirectional EV Charger

QSGs extract orthogonal components of the grid voltage without relying on PLLs, offering faster response, better noise immunity, and lower computational burden features, especially beneficial for embedded control implementations in bidirectional chargers.

Fig. 1.1 illustrates the key components of a grid-interactive EV charger, showing bidirectional power flow between the grid and the EV battery, coordinated by a control unit that utilizes QSG-based synchronization.

1.2 Problem Statement

- Lack of research on the use of chargers that can act smartly in managing the active as well as reactive power support to the grid as and when required. It may also be very helpful in meeting the local load demands in the absence of a grid.
- Insufficient research on the impact of grid-interactive EV systems on grid reliability.
- Most system parameters are acquired in some works of literature under the premise of linear and traditional control techniques. However, because an EV charger is a nonlinear load, system parameters must be intelligently tuned in practice.

- Limited implementation of advanced control filters such as CNISOGI for accurate signal decomposition in distorted and dynamically changing grid environments.
- Inadequate consideration of voltage events such as sags, swells, and harmonics in EV charger control design, which significantly affects performance in real-world distribution systems.
- Scarcity of laboratory-based hardware validation and real-time Hardware-in-the-Loop (HIL) testing of smart bidirectional EV chargers under realistic grid operating conditions.
- Lack of algorithms for adaptive energy dispatch in EVs that account for grid demand fluctuations, user energy preferences, and real-time priority-based decision-making.
- Insufficient attention to the potential of EV fleets to contribute toward ancillary services such as frequency regulation, peak shaving, and voltage support through coordinated V2G strategies.
- Existing systems often ignore reactive power management at the point of common coupling (PCC), which is essential for maintaining unity power factor and minimizing grid-side losses.
- Inadequate integration of predictive control or artificial intelligence (AI)-based tuning mechanisms that adaptively optimize EV charger performance across diverse load and grid profiles.

1.3 Research Objectives

- **Study and analysis of different charging control strategies of EVs:**
  This objective focuses on reviewing and comparing existing EV charging control methodologies, including unidirectional, bidirectional, centralized, and decentralized schemes. The goal is to identify limitations in conventional approaches and explore advanced techniques that allow dynamic interaction between the grid and EV. Emphasis is placed on power quality, efficiency, and grid support capabilities.

- **Design and Development of a Bidirectional EV Charger:**
  This involves the conceptualization and implementation of a power electronic interface that allows seamless operation in both Grid-to-Vehicle (G2V) and Vehicle-to-Grid (V2G) modes. The charger must be capable of handling energy flow in both directions while supporting real-time voltage and current regulation. It should also offer modularity and compatibility with smart grid infrastructure.

- **Design of a simple and robust control technique for improving system response:**
  The objective here is to develop a control strategy based on advanced filtering methods such as CNISOGI, enabling accurate signal decomposition and robust current control. The control algorithm must ensure fast dynamic response, stability under distorted grid conditions, and support reactive power compensation. Simplicity in implementation and computational efficiency are also key considerations.

- **Development of a hardware prototype of V2G/G2V to validate the control approach:**
  To verify the effectiveness of the proposed system, a laboratory-scale hardware prototype will be built using a bidirectional converter and a real-time DSP controller. This prototype will test the control algorithm's response to dynamic grid events, voltage disturbances, and nonlinear loads. The experimental validation will confirm real-world feasibility and performance.

1.4 Structure of the Thesis

The remainder of the thesis is organized as follows:

- Chapter 1 gives the introduction to the grid-interactive charger system. Also, it gives the motivation behind this research, and I am able to find the research objective based on that.

- Chapter 2 provides a comprehensive overview of electric vehicle (EV) charging systems. It starts with the fundamentals of EV charging

infrastructure, categorization of chargers, and the working principles of grid-connected EV chargers. The chapter also explores existing control schemes used in grid-interactive charging systems.

- Chapter 3 focuses on the modelling and development of a hardware prototype for a grid-interactive bidirectional EV charger capable of both G2V and V2G operation. The prototype is built to validate the proposed control scheme under real-time conditions. This includes the selection and integration of power electronic components, sensors, DSP-based control platforms, and safety mechanisms.

- Chapter 4 presents the study and analysis of different charging control strategies for EVs. It includes a review of classical methods such as PI control and PWM-based regulation and a comparative evaluation of various filtering techniques, including CNISOGI (cascaded non-identical second-order generalized integrator), SO-SOGI (second-order-second-order generalized integrator), CSOGI (cascaded second-order generalized integrator), LLMF (leaky least mean fourth), LMS (least mean squares), and LMF (least mean fourth) for grid synchronization and current control.

- Chapter 5 details the real-time implementation of the proposed control strategy. Further, to test the efficacy of the charger system, it is tested for different grid voltage scenarios like sag, swell, and harmonic-injected conditions and dynamic conditions at the point of common coupling (PCC). Also, it includes the mathematical modelling of the filter technique.

- Chapter 6 deals with the design and implementation of the proposed control strategy. A QSG-based robust and efficient control approach is developed for both G2V and V2G modes. The real-time performance of the control logic is demonstrated using the developed hardware prototype. The robustness of the controller is tested under the increment/decrement of the emergency loads connected at the point of common coupling (PCC). Also, analysis under wide voltage range scenarios (e.g. 10% sag, swell and harmonics)

- Chapter 7 concludes the thesis with a summary of contributions and key outcomes. It discusses the limitations of the present work and suggests future research directions in the field of grid-supportive EV charging.

1.5 Conclusions

The rapid adoption of Electric Vehicles (EVs) necessitates the development of intelligent charging systems that not only meet user demands but also support the power grid in real-time. This research addresses critical gaps such as limited reactive power support, inadequate control under nonlinear and distorted grid conditions, and the lack of experimental validation. By studying various control strategies, designing a bidirectional charger, and implementing a robust CNISOGI-based control algorithm, the work aims to enable smart energy exchange between the EV and grid. The development and testing of a hardware prototype further ensures practical viability. Overall, the proposed system contributes toward making EVs active participants in grid stabilization, power quality improvement, and flexible energy management within future smart grid environments.

Chapter 2

Literature Review

2.1 Overview of EV Charging Technologies

Electric vehicle (EV) charging technologies are rapidly evolving to meet the increasing demand for sustainable transportation solutions. These technologies encompass a variety of approaches, each addressing different aspects of the charging process, from infrastructure to energy management. One significant advancement in EV charging is the integration of artificial intelligence (AI) to optimize charging infrastructure. AI frameworks are being developed to enhance charge-demand profiling, data augmentation, demand forecasting, and charge optimization, which are crucial for managing distributed energy resources effectively in the context of EV adoption [19]. This approach helps in addressing the challenges posed by the increasing number of EVs on the grid. Renewable energy sources, particularly solar power, are increasingly being integrated into EV charging stations. For instance, a PV-assisted grid-connected multi-output charger has been developed, which utilizes a modified Z-source inverter to manage power from both solar panels and the grid, ensuring efficient energy conversion and distribution [20]. Similarly, hybrid charging stations that combine solar power with battery energy storage systems are being designed to provide uninterrupted power supply and reduce grid dependency [21]. Load forecasting is another critical area in EV charging technology. Advanced deep learning models, such as those using Long Short-Term Memory (LSTM) networks, are employed to predict charging station loads by incorporating multi-feature data, including weather conditions, which significantly influence EV charging patterns [22]. This predictive capability is essential for optimizing

energy distribution and meeting the dynamic demands of EV charging stations. The coordination of multiple power exchange modes is also being explored to enhance the efficiency and cost-effectiveness of EV charging. This includes strategies like battery swapping, building-to-vehicle (B2V), and grid-to-vehicle (G2V) charging, which leverage distributed renewable energy sources and optimize power exchange to reduce costs and battery degradation [23]. Moreover, intelligent energy management algorithms are being developed to optimize EV charging schedules. These algorithms, such as the intelligent scatter search (ISS) and actor-critic learning-based smart charging algorithms, aim to minimize charging costs and smooth the daily load profile by employing advanced optimization techniques [24], [25]. These methods are crucial for managing the uncertainties in EV charging behaviors and ensuring efficient energy use. Finally, the integration of IT infrastructure for managing energy usage through a token-based system is proposed to handle the dynamic nature of EV charging, especially for plug-in hybrid electric vehicles (PHEVs). This system aims to balance energy production and consumption, ensuring grid stability despite the unpredictable nature of renewable energy sources like wind power [26]. In summary, EV charging technologies are advancing through the integration of AI, renewable energy, predictive modeling, and intelligent energy management systems. These innovations are crucial for addressing the challenges of grid stability, energy efficiency, and cost-effectiveness in the face of growing EV adoption. Each approach contributes uniquely to the development of a robust and sustainable EV charging infrastructure, highlighting the multifaceted nature of this rapidly evolving field.

2.1.1 Overview of EV charging types (Level 1, Level 2, DC Fast Charging)

Electric vehicle (EV) charging infrastructure is a critical component in the transition to sustainable transportation. The charging process is categorized into three main types: Level 1, Level 2, and DC Fast Charging, each with distinct characteristics and applications. This overview will explore these charging types, their technical specifications, and their roles in the EV ecosystem.

Level 1 Charging

Definition and Characteristics: Level 1 charging uses a standard 120-volt AC outlet, typically found in residential settings. It is the most basic form of EV charging and requires no additional installation beyond a standard electrical outlet. Charging Speed: This method provides a slow charging rate, typically adding about 2 to 5 miles of range per hour of charging. It is suitable for overnight charging or for users with low daily mileage requirements [27], [28]. Use Cases: Level 1 charging is ideal for home use, where vehicles can be charged over extended periods, such as overnight. It is also a cost-effective solution for users who do not require rapid charging capabilities [29].

Level 2 Charging

Definition and Characteristics: Level 2 charging operates at 240 volts and requires a dedicated charging station. It is commonly found in residential, commercial, and public charging environments. Charging Speed: This method significantly reduces charging time compared to Level 1, providing 10 to 60 miles of range per hour, depending on the vehicle and charger specifications [30], [28]. Use Cases: Level 2 chargers are suitable for both home and public charging stations, offering a balance between cost and charging speed. They are often used in workplaces and shopping centers, where vehicles are parked for several hours[27], [31].

DC Fast Charging

Definition and Characteristics: DC Fast Charging (DCFC) uses direct current to charge EVs at a much higher power level, typically ranging from 50 kW to 350 kW. This requires specialized equipment and is usually found in commercial and public charging stations [31], [32]. Charging Speed: DCFC can add 60 to 80 miles of range in just 20 minutes, making it ideal for long-distance travel and quick top-ups[33]. Use Cases: These chargers are strategically placed along highways and in urban areas to facilitate long-distance travel and reduce range anxiety. They are essential for fleet operations and in areas with high EV adoption rates [34], [35].

Technical Considerations and Future Trends

Power Electronics and Converter Technologies: The efficiency and performance of EV chargers are heavily influenced by power electronic converters. Innovations in converter topologies, such as buck-boost converters and multi-level inverters, are enhancing the efficiency and reducing the size of charging systems [36], [32]. Integration with Renewable Energy: There is a growing trend towards integrating renewable energy sources with EV charging infrastructure to enhance sustainability and reduce grid dependency. This includes the use of solar panels and energy storage systems in charging stations [28], [35]. Grid Impact and Stability: The widespread adoption of EVs poses challenges to grid stability, particularly with high-power DC fast chargers. Advanced control strategies and grid-supportive technologies are being developed to mitigate these impacts [27], [33]. While the development of EV charging infrastructure is progressing rapidly, challenges remain, particularly in terms of grid integration and the high costs associated with fast-charging stations. Continued research and innovation in power electronics and renewable integration are essential to address these issues and support the growing demand for EVs.

2.1.2 Discussion of existing charging systems and their limitations

Electric vehicle (EV) charging systems are evolving rapidly to meet the increasing demand for sustainable and efficient energy solutions. However, existing systems face several limitations that need to be addressed to optimize their functionality and security. One significant limitation of traditional EV charging systems is their vulnerability to cyber-attacks, such as distributed denial of service (DDoS) and insider attacks. These systems often rely on a central server, which, if compromised, can lead to significant disruptions. To address these security concerns, blockchain-based charging systems have been proposed. These systems enhance security by ensuring key protection, secure mutual authentication, anonymity, and perfect forward secrecy, while also preventing replay and man-in-the-middle attacks. Despite these advancements,

the challenge remains to efficiently integrate these systems into practical applications without incurring high computational and communication costs [37]. Another limitation is the mismatch between electricity generation and consumption times in photovoltaic (PV) charging systems. PV systems generate electricity during the day, while EV owners typically require charging at night. This discrepancy necessitates the use of batteries, which can lead to either oversizing or undersizing of the PV system, depending on the time period for which full coverage is claimed. This can result in financial losses due to unused generated electricity or insufficient energy supply during peak demand times. Optimizing the design of PV systems to align with real consumption patterns and weather conditions is crucial to overcoming these limitations [38]. Furthermore, the integration of renewable energy sources, such as solar power, into EV charging stations presents additional challenges. Hybrid charging stations that combine solar power with battery storage and grid electricity can reduce reliance on fossil fuels and minimize grid overload. However, the complexity of managing these systems, including the use of maximum power point tracking (MPPT) techniques and charge controller algorithms, requires sophisticated design and simulation to ensure continuous power supply and efficient operation [39]. The emergence of charger sharing markets offers a potential solution to expand existing charging networks without significant infrastructure investments. These markets operate on a sharing economy model, where charger owners rent out their under-utilized chargers to EV drivers. The success of such markets depends on innovative designs that incorporate game theory, mechanism design, and large-scale optimization to maximize social welfare and ensure market growth. However, achieving high efficiency and budget balance in these markets remains a challenge [40]. In summary, while advancements in EV charging systems, such as blockchain security measures and hybrid solar power integration, address some existing limitations, challenges remain in optimizing system design, ensuring security, and aligning energy generation with consumption patterns. The development of innovative solutions, such as charger sharing markets, presents promising opportunities to enhance the efficiency and sustainability of EV charging infrastructure. However, these solutions require careful consideration of economic, technical, and security aspects to be effectively implemented in real-world scenarios.

2.2 Grid-Interactive Charging Systems

2.2.1 Basic Concepts of Grid-Interactive Charging

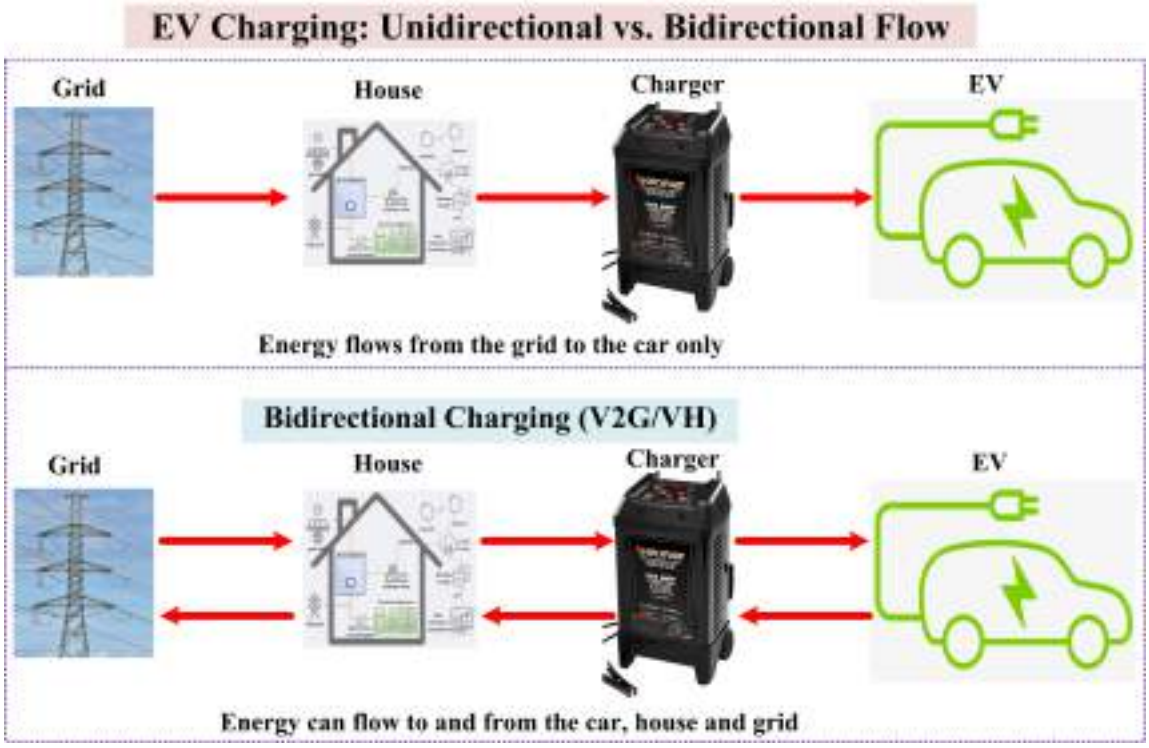

FIGURE 2.1: Unidirectional and Bi-directional power flow

The technical requirements for bidirectional power flow in electric vehicle (EV) chargers are crucial for enabling efficient grid-to-vehicle (G2V) and vehicle-to-grid (V2G) operations as shown in Fig. 2.1. These requirements include advanced power electronics, control strategies, and system architectures that ensure seamless integration with the power grid while maintaining grid stability. The impact on grid stability is significant, as bidirectional chargers can both support and challenge grid operations depending on their implementation and control.

Technical Requirements for Bidirectional Power Flow

Advanced Power Electronics: Bidirectional chargers require sophisticated power electronic systems capable of handling both AC-DC and DC-AC conversions.

These systems must operate efficiently across a wide range of voltages and power levels. For instance, modular multilevel converters (MMCs) and dual active bridges (DABs) are used to link AC distribution voltages to DC grids, facilitating bidirectional power flow and enhancing system stability [41], [42].

- Control Strategies: Effective control strategies are essential for managing bidirectional power flow. Techniques such as phase-shift control, adaptive virtual synchronous generator (VSG) control, and gain adaptive sliding mode control (ASMC) are employed to ensure precise power transmission and minimize power mismatches [43], [44]. These strategies help maintain power quality and grid stability by dynamically adjusting to grid conditions and EV charging requirements.

- System Architecture: The architecture of bidirectional chargers often includes features like energy storage integration and modular design to enhance flexibility and efficiency. For example, replacing capacitors with energy storage batteries in the DC bus allows for smoother scheduling of EV and grid instructions, reducing interference and improving response times [43]. Additionally, multi-phase operation and universal charging blocks are designed to handle full power ranges without additional components, ensuring cost-effectiveness and high power density [45].

Impact on Grid Stability

- Frequency and Voltage Stability: Bidirectional EV chargers can significantly impact grid frequency and voltage stability. By participating in frequency support strategies, EVs in V2G mode can help stabilize grid frequency during fluctuations, improving overall grid reliability [46], [47]. Moreover, optimal planning and control of EVs can enhance the voltage profile of the grid, maintaining power quality within acceptable standards [46].

- Power Quality: The integration of bidirectional chargers can introduce challenges such as total harmonic distortion (THD) in grid currents. However, with proper design and control, these effects can be minimized, ensuring that power quality remains within the limits set by standards like IEEE 519-2014 [46], [47].

- Grid Support and Renewable Integration: Bidirectional chargers can support grid operations by providing ancillary services such as peak shaving and valley filling. They also facilitate the integration of renewable energy sources by stabilizing intermittent power supply through dynamic interaction with the grid [41], [42].

While bidirectional EV chargers offer numerous benefits for grid stability, they also present challenges that need to be addressed through advanced technology and strategic planning. The development of high-efficiency, compact, and cost-effective solutions is crucial for maximizing the potential of bidirectional power flow in EV chargers. As the technology evolves, the focus will likely shift towards integrating wide-bandgap semiconductors and other innovations to further enhance performance and grid compatibility [48].

2.2.2 Key Features

The integration of Vehicle-to-Grid (V2G), Vehicle-to-Home (V2H), and Vehicle-to-Building (V2B) technologies significantly impacts energy efficiency by enhancing the utilization of renewable energy sources, optimizing energy storage, and reducing energy costs. These technologies leverage the energy storage capabilities of electric vehicles (EVs) to provide a flexible and efficient energy management solution, which is crucial for addressing the intermittency of renewable energy sources and improving grid stability. The following sections detail the key features and impacts of these technologies on energy efficiency.

Vehicle-to-Grid (V2G) Technology

- Renewable Energy Utilization: V2G technology allows EVs to feed electricity back into the grid, which helps in balancing the supply and demand of renewable energy. This reduces wastage and enhances the efficiency of renewable energy utilization [49].

- Grid Stability and Load Management: By enabling bidirectional energy flow, V2G can stabilize power grids through load balancing during peak hours, thus reducing the pressure on the grid and improving overall energy efficiency [50].

- Economic Benefits: V2G systems can increase corporate profits and green energy utilization by optimizing the pricing strategies for EVs and offsetting battery costs, which encourages higher adoption rates of V2G-enabled vehicles [49]. Vehicle-to-Home (V2H) Technology
- Energy Cost Reduction: V2H technology allows homeowners to use stored energy from EVs during peak electricity pricing periods, thereby reducing electricity costs and increasing energy self-sufficiency [51].
- Integration with Renewable Energy: V2H systems can be integrated with residential photovoltaic systems to optimize energy consumption and reduce reliance on the grid, enhancing the overall energy efficiency of homes [52].
- Demand Response: V2H can work in conjunction with demand response strategies to further optimize energy usage and reduce the need for additional energy storage capacity [52].

Vehicle-to-Building (V2B) Technology

- Energy Management in Prosumers: V2B technology is particularly effective in prosumer buildings, where it reduces the amount of electricity purchased from the grid and enhances the building's energy efficiency by utilizing EVs as a flexible energy storage solution [53].
- Cost Efficiency and Flexibility: By coordinating battery storage with V2B systems, buildings can achieve cost-efficient operations and increased flexibility, which is crucial for managing the variability of renewable energy sources [54].
- Impact on Building Microgrids: V2B systems contribute to the efficient operation of building microgrids by providing additional energy storage capacity and reducing the mismatch between energy generation and demand [54].

Broader Implications and Challenges

While V2G, V2H, and V2B technologies offer significant benefits for energy efficiency, their implementation faces challenges such as the need for infrastructure development, regulatory support, and market mechanisms to ensure financial feasibility [55]. Additionally, the effectiveness of these technologies is influenced by factors such as EV adoption rates, battery costs, and user acceptance, which require careful consideration and strategic planning [56], [49]. Despite these challenges, the potential of these technologies to transform energy management and support the transition to a sustainable energy future is substantial.

2.2.3 Comparison with Traditional Charging

Grid-interactive electric vehicle (EV) chargers offer significant advantages over traditional charging methods by optimizing energy storage and reducing peak demand. These chargers leverage advanced technologies and strategies to manage the charging and discharging of EVs in a way that benefits both the grid and the vehicle owners. The following sections explore how these systems achieve these optimizations.

Multi-Agent and Distributed Control

Grid-interactive EV chargers utilize multi-agent and distributed control frameworks to optimize charging schedules. This approach allows each charging spot to make independent decisions based on local conditions, such as electricity prices and renewable energy availability, without sharing private information. This method significantly improves scalability and efficiency, reducing energy costs by up to 25% and enhancing user satisfaction by 20% compared to traditional rule-based controllers [57].

Time and Energy-Based Prioritization

Effective management of EV charging demand is crucial for grid stability. A time and energy-based approach prioritizes EVs with shorter deadlines and lower energy demands, maximizing the number of EVs that can be charged without

overloading the grid. This method can fulfill the energy needs of up to 33% more EVs compared to traditional methods, ensuring sustainable energy management and supporting the widespread adoption of EVs [58].

Charge-Discharge Optimization

Charge-discharge optimization strategies consider both grid-side and user-side demands, using dynamic spatiotemporal distribution models and sub-districted dynamic electricity pricing. These strategies significantly reduce peak-to-valley load disparities and active power losses, achieving reductions of more than 15% and 10%, respectively. This approach also reduces the total economic cost for EV owners by up to 97.7% [59].

Bidirectional Charging and Vehicle-to-Grid (V2G) Integration

Bidirectional chargers enable EVs to not only draw power from the grid but also supply power back to it, providing grid support functions such as voltage control and harmonic distortion reduction. This integration allows for more flexible and efficient energy management, reducing grid voltage total harmonic distortion by 24.77% and offering rapid dynamic response and robust steady-state performance [60].

Smart Charging with Renewable Integration

Smart charging strategies, when combined with renewable energy sources like solar photovoltaic (PV) and battery energy storage systems (BESS), enhance energy and economic performance. These systems can reduce network losses by 35.5% and electricity costs by 4.3%, demonstrating the effectiveness of integrating smart charging with renewable energy sources for peak shaving and improved grid stability [61].

Emission Reduction and Peak Demand Shaving

Coordinated charging strategies can reduce CO2 emissions by 18% annually while also decreasing peak power demand by 33%. However, further emission reductions may lead to increased peak power demand, highlighting the need for

a balanced approach to achieve both emission reduction and grid stabilization goals [62].

Advanced Charger Design

Innovative charger designs, such as those using energy storage batteries instead of capacitors, allow for flexible scheduling of EV and grid instructions. These designs ensure that grid and EV requirements do not interfere with each other, enabling efficient peak shaving and valley filling without compromising EV charging needs [63].

While grid-interactive EV chargers offer numerous benefits, challenges remain in balancing the trade-offs between emission reduction and peak demand management. The integration of renewable energy sources and advanced control strategies can help mitigate these challenges, but careful planning and coordination are essential to maximize the benefits of these technologies. As the adoption of EVs continues to grow, ongoing research and development will be crucial in refining these systems to ensure sustainable and efficient energy management.

2.3 Technological Components

2.3.1 Power Electronics

The role of power converters, specifically AC/DC and DC/DC converters, in grid-interactive chargers is pivotal for the efficient integration of electric vehicles (EVs) into the power grid. These converters not only facilitate the charging of EVs but also enable bidirectional power flow, allowing vehicles to act as mobile energy storage units in vehicle-to-grid (V2G) systems. This capability is crucial for enhancing grid stability and accommodating renewable energy sources. The following sections delve into the specific roles and advancements of these converters in grid-interactive charging systems.

AC/DC Converters in Grid-Interactive Chargers

- Bidirectional Operation: AC/DC converters are essential for enabling bidirectional power flow in grid-interactive chargers. This functionality allows EVs to return stored energy to the grid, supporting grid stability and renewable energy integration. For instance, a bidirectional AC-DC converter system using modular multilevel converters (MMCs) and dual active bridges (DABs) has been proposed to link AC distribution voltages to DC grids, facilitating large-scale EV charging infrastructure and stabilizing renewable energy sources [64], [65].
- High Efficiency and Wide Voltage Range: Advanced AC/DC converters, such as the single-stage four-phase interleaved totem-pole converter, offer high efficiency and can operate over a wide voltage range, making them suitable for fast charging applications. These converters reduce total harmonic distortion (THD) and improve power quality, which is critical for maintaining grid stability [66].

DC/DC Converters in Grid-Interactive Chargers

- Efficiency and Control: DC/DC converters play a crucial role in optimizing power exchange between EVs and the grid. The use of model predictive control (MPC) in synchronous boost converters has been shown to enhance efficiency by minimizing switching losses and improving control precision. This is particularly beneficial in V2G systems, where efficient power management is essential [67].
- Advanced Topologies: To address the limitations of traditional DC/DC converters, such as switching losses and electromagnetic interference, new topologies like resonant and multiport converters are being explored. These innovations are crucial for high-voltage EV applications, ensuring reliable and efficient power conversion [68].

Integration with Renewable Energy and Grid Stability

- Grid Interaction and Stability: Power converters are integral to the interaction between EVs and the grid, especially in systems with high

renewable energy penetration. They help manage power quality issues, such as harmonics and transients, which can arise from the increased use of power electronics in the grid [69].

- Renewable Energy Integration: Power electronics converters are vital for integrating large-scale renewable energy sources into the grid. They provide the necessary control and flexibility to manage the variable nature of renewable energy, ensuring efficient and reliable power conversion [70].

Future Trends and Challenges

While power converters are essential for the current and future landscape of grid-interactive chargers, they also present challenges. The increasing penetration of power electronics in the grid can lead to issues such as reduced system inertia and power quality degradation. Addressing these challenges requires ongoing research and development in converter technologies and grid management strategies [67], [71].

In conclusion, AC/DC and DC/DC converters are fundamental to the operation and advancement of grid-interactive chargers. They enable efficient energy transfer, support grid stability, and facilitate the integration of renewable energy sources. However, as the reliance on power electronics grows, addressing the associated challenges will be crucial for the sustainable development of power systems.

Grid-interactive systems are pivotal in modernizing power grids, integrating renewable energy sources, and enhancing grid stability and efficiency. These systems employ a variety of control mechanisms and algorithms to manage energy flow, maintain power quality, and ensure reliable operation under varying conditions. This overview explores the diverse control strategies used in grid-interactive systems, highlighting model-based, learning-based, and hybrid approaches, as well as specific algorithms tailored for different grid applications.

2.3.2 Control Systems

Voltage and Current Control Strategies:-

In grid-interactive EV chargers, voltage and current control strategies typically use a cascaded control structure composed of an outer voltage loop and an inner current loop. The outer loop is responsible for maintaining the DC-link voltage at a desired reference, ensuring power balance between the battery side and the grid side. A Proportional-Integral (PI) controller is commonly used in this loop to regulate voltage fluctuations that result from varying grid or battery power conditions. The inner current control loop regulates the injected or absorbed grid current, enabling control over active and reactive power exchange. This loop ensures that the current drawn by the charger is sinusoidal and synchronized with the grid voltage, which is crucial for grid compliance and power quality. The use of this dual-loop control architecture provides fast dynamic response, decoupled power control, and adaptability to bidirectional power flow, making it ideal for both G2V and V2G operations [72].

Reference Frame-Based Control:-

Reference frame-based control techniques are central to the dynamic regulation of grid-interactive EV chargers. The most widely used method is synchronous rotating reference frame (d-q) control, which transforms three-phase AC signals into DC quantities, thereby simplifying control with PI regulators. This method allows direct control of active and reactive power via the d- and q-axis current components, respectively. However, its performance can degrade under grid disturbances or unbalanced conditions. To address this, control in the stationary - reference frame is often used, particularly when paired with Proportional-Resonant (PR) controllers or Second-Order Generalized Integrators (SOGI). These techniques eliminate the need for a PLL and enable accurate control in the presence of voltage asymmetries, harmonic distortions, or unbalanced loads. The choice between d-q and - control frames depends on grid conditions and computational requirements, with the latter offering superior harmonic rejection and dynamic performance in challenging environments [73], [74].

Grid Synchronization Techniques:-

Grid synchronization is an essential function in grid-interactive EV chargers, enabling phase-coherent current injection and stable operation during both charging (G2V) and discharging (V2G) modes. Under ideal grid conditions, synchronization can be effectively achieved using conventional methods.

However, in the presence of voltage distortions, DC offsets, and negative sequence components common in weak or unbalanced grids synchronization becomes significantly more complex and error-prone.

To address these challenges, advanced Quadrature Signal Generation (QSG) techniques are employed as a foundation for synchronization. These techniques enable the extraction of clean in-phase and quadrature signals required for reference frame transformation and control coordination. Among them, two-channel QSGs have proven effective in rejecting negative sequence components, thereby maintaining synchronization stability even under unbalanced conditions.

However, while basic QSGs are effective at reducing total harmonic distortion (THD) and filtering negative sequences, they exhibit limited performance in rejecting DC offset components. To overcome this limitation, higher-order QSGs, particularly Fourth-Order Quadrature Signal Generators (FO-QSGs), are utilized. Compared to second-order [75], third-order [76], and hybrid QSG structures [77], FO-QSGs offer complete DC offset rejection and superior harmonic attenuation [78], which are critical for stable and accurate synchronization in distorted environments.

Two notable implementations of FO-QSGs are the Second-Order Generalized Integrator (SO-SOGI) [79] and the Cascaded Second-Order Generalized Integrator (CSOGI) [80]. The SO-SOGI relies on system-specific parameters like settling time and damping factor, but its synchronization accuracy can degrade if not properly tuned. On the other hand, the CSOGI structure cascades two identical SOGI units to achieve fourth-order filtering. In this configuration, the first SOGI effectively eliminates DC offsets, while the second enhances harmonic filtering. Nevertheless, improper damping factor selection in the first SOGI can lead to an over-damped overall system and slow synchronization response.

These advanced QSG structures, especially CSOGI and CNISOGI, significantly improve the accuracy and stability of grid synchronization under non-ideal conditions. Their ability to isolate the fundamental voltage component even in the presence of harmonics and transients makes them highly suitable for modern EV charging systems operating in complex grid environments.

Power Quality-Oriented Control:-

Beyond energy transfer, grid-interactive EV chargers can enhance grid

stability through power quality-oriented control strategies. These chargers can be programmed to act as Active Power Filters (APFs), injecting compensating currents to mitigate harmonics introduced by nonlinear loads. This is often achieved using resonant controllers or harmonic observers that allow the charger to detect and suppress specific harmonic orders. In addition, EV chargers can provide reactive power support by modulating the q-axis current component, which helps regulate grid voltage and improve power factor. Another key function is unbalanced load compensation, especially in three-phase four-wire systems. This involves detecting and counteracting phase imbalances and neutral currents using sequence extraction methods such as the Cascaded Non-Identical Second-Order Generalized Integrator (CNISOGI) filters. By integrating these power quality functions, EV chargers serve not only as energy devices but also as distributed assets for grid support, contributing to the overall robustness and reliability of the power system [77], [78].

2.4 Types of Grid-Interactive Charging Technologies

2.4.1 Smart Charging

Smart charging, particularly through demand response (DR) and controlled charging, plays a crucial role in optimizing grid load by balancing energy supply and demand, reducing peak loads, and integrating renewable energy sources. This approach involves various strategies and technologies to manage the charging of electric vehicles (EVs) and other flexible loads, ensuring efficient grid operation and minimizing costs. The following sections explore key aspects of smart charging, drawing insights from recent research.

Real-Time Pricing and Demand Response

Real-time pricing is a pivotal strategy in demand response programs, allowing consumers to adjust their energy usage based on dynamic price signals. This method enhances grid stability by incentivizing users to shift their consumption to off-peak times. A study utilizing the Geometric Mean Optimizer (GMO) algorithm demonstrated that integrating real-time pricing with controlled charging of Plug-In Electric Vehicles (PHEVs) can improve voltage profiles and reduce reactive power consumption during peak hours by 4.5% and

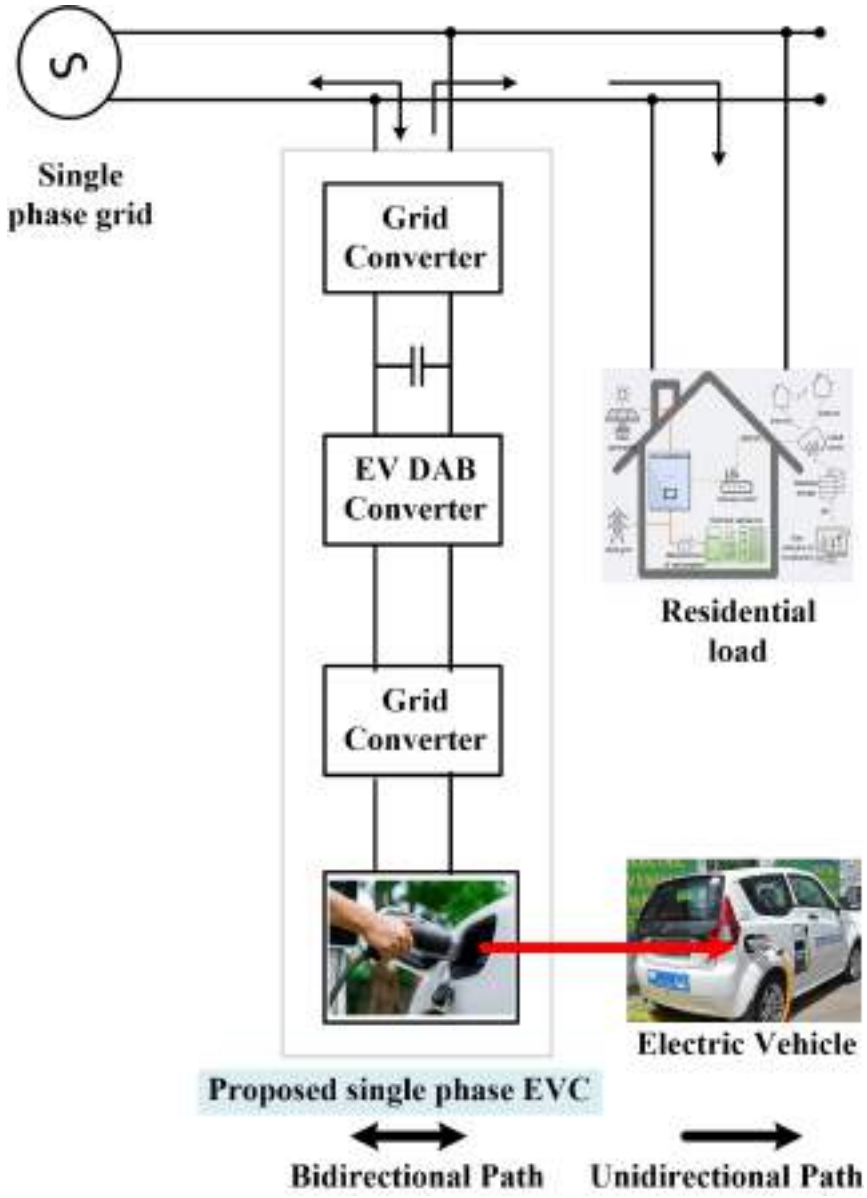

FIGURE 2.2: Schematic of the charger intracting with the grid and the residential loads

23%, respectively. Additionally, the load factor increased by 18%, and transformer capacity was optimized to handle 60% more EVs without overloading [81].

Distributed Demand Response Control

Distributed demand response control involves managing the charging of multiple EV clusters to provide frequency regulation services. By modeling EV

clusters as transport-based load aggregates, a dynamic real-time distributed control algorithm can coordinate charging rates to follow a reference power trajectory. This approach ensures that the aggregate charging power aligns with grid requirements, enhancing the grid's ability to manage load fluctuations effectively [82].

Scheduling and Flexibility

Demand response also extends to scheduling home appliances based on their time and power flexibility. By classifying appliances into time-flexible and power-flexible categories, an energy consumption scheduler can optimize power usage, reducing utility bills and peak-to-average demand ratio (PADR) by 28% and 21%, respectively, without compromising user comfort [83].

Smart Charge Controllers

Advanced smart charge controllers, such as those using neuro-fuzzy particle swarm optimization (PSO), offer enhanced flexibility and control over EV charging. These controllers consider multiple factors, including user requirements, energy tariffs, and grid conditions, to optimize charging operations. The integration of PSO with neural networks provides a global optimum solution, balancing technical constraints and user needs while minimizing processing time [84], [85]. Integration with Renewable Energy and Load Frequency Control Integrating demand response with renewable energy sources and load frequency control (LFC) systems can further optimize grid performance. For instance, a centralized control strategy using a modified crow search algorithm (mCSA) significantly reduced frequency deviations in micro-grids by 27.22%. This approach, combined with energy storage devices, enhances the robustness and reliability of micro-grid systems, accommodating variable renewable inputs and load demands [86]. While smart charging and demand response offer significant benefits, challenges remain in terms of implementation complexity, user acceptance, and the need for advanced infrastructure. Moreover, the integration of renewable energy sources introduces variability that requires sophisticated control strategies to maintain grid stability. As research progresses, these challenges are being addressed through innovative algorithms and technologies, paving the way for more efficient and sustainable energy systems.

2.4.2 Bidirectional Charging (V2G, V2H, V2B):

Bidirectional charging technologies, such as Vehicle-to-Grid (V2G), Vehicle-to-Home (V2H), and Vehicle-to-Building (V2B), enable electric vehicles (EVs) to not only draw power from the grid but also return energy back to it or to buildings as depicted in Fig.2.2. These technologies leverage the storage capacity of EV batteries to provide grid support, enhance energy efficiency, and offer economic benefits. The implementation of these systems involves sophisticated power electronics and control strategies to manage the bidirectional flow of energy effectively. Below, we explore the key aspects of these technologies, their applications, and the challenges they face.

Bidirectional Charging Technologies

Vehicle-to-Grid (V2G): V2G technology allows EVs to discharge stored energy back to the grid, providing ancillary services such as frequency regulation and peak shaving. This is facilitated by bidirectional power converters that enable energy flow in both directions, enhancing grid stability and efficiency [87], [88]. The use of advanced power electronics, such as wide-bandgap semiconductors, improves the efficiency and power density of these systems [89].

Vehicle-to-Home (V2H) and Vehicle-to-Building (V2B): V2H and V2B applications enable EVs to supply power to homes or buildings, reducing reliance on the grid and optimizing energy use. These systems can significantly increase renewable energy consumption and improve energy management within buildings, as demonstrated by higher auto-consumption ratios in V2B setups [90]. The integration of Building Integrated Photovoltaics (BIPV) with V2H systems further enhances energy efficiency and sustainability [91].

Technological Components and Control Strategies

Onboard Chargers (OBCs): Bidirectional onboard chargers are crucial for enabling V2G and V2X (Vehicle-to-Everything) applications. These chargers incorporate advanced converter topologies, such as interleaved bridgeless totem-pole PFC and CLLC resonant converters, to achieve high efficiency and dynamic performance under varying load conditions [92], [89]. The use of asymmetric full-bridge converters with power decoupling capabilities further optimizes energy flow and reduces common-mode currents [93].

Control Strategies: Effective control strategies are essential for managing the

bidirectional flow of energy. Techniques such as phase-shift control, adaptive virtual synchronous generator (VSG) control, and pulse frequency modulation are employed to ensure stable and efficient operation [94]. These strategies help in maintaining power quality and grid stability, even under variable current and pulse heating conditions [95].

Challenges and Considerations

Battery Degradation: Frequent charging and discharging cycles can accelerate battery degradation. Therefore, optimizing charging and discharging controls to minimize battery life impact is crucial. Advanced aging-aware optimization algorithms are being developed to address this issue [96].

Grid Integration and Power Quality: The integration of bidirectional EVs into the grid poses challenges related to power quality, voltage profile, and frequency stability. Strategies to mitigate these impacts include optimal frequency support and power flow analysis to maintain grid standards [95].

Economic and Environmental Benefits: Bidirectional charging technologies offer economic incentives by reducing energy costs and providing grid services. They also contribute to environmental sustainability by enhancing the use of renewable energy sources and reducing greenhouse gas emissions [87], [91].

While bidirectional charging technologies present significant opportunities for energy management and grid support, they also face challenges related to battery degradation, power quality, and economic feasibility. Continued research and development in power electronics, control strategies, and integration with renewable energy systems are essential to fully realize the potential of these technologies.

2.4.3 Dynamic Wireless Charging

Dynamic wireless charging (DWC) is an innovative technology that enables electric vehicles (EVs) to charge while in motion, addressing key challenges such as range anxiety and battery size limitations. This technology is gaining traction due to its potential to enhance the efficiency and convenience of EV charging. Emerging grid-interactive charging technologies are being developed to optimize power transfer, improve interoperability, and integrate with existing

grid systems. Below, we explore the key aspects of these technologies based on recent research.

Interoperability and Power Stability

A significant challenge in DWC systems is maintaining stable power output and ensuring interoperability between different charging systems. A novel approach involves a self-adaptive two-pole receiver that can adjust its polarity based on mutual inductance variations, ensuring smooth power output and compatibility with various transmitter coil configurations [97]. Another approach to achieving stable power output involves a segmented dynamic wireless power transfer system. This system uses a T- series/series topology to minimize cross-coupling effects and improve efficiency during transitions between charging segments [98]. Charging Efficiency and Cost Optimization In wireless rechargeable sensor networks, optimizing the charging sequence can significantly reduce costs and improve efficiency. An improved deep Q-network approach has been proposed to schedule mobile chargers effectively, balancing charging demand with energy consumption [99]. Cost-effective solutions for DWC systems are also being explored, such as using simplified coil structures and control strategies to reduce the number of transmitter segments and associated costs [98]. Grid Integration and Impact High-power DWC systems pose challenges for grid integration due to their unique load profiles and power pulsations. A direct power control strategy has been developed to manage these challenges, ensuring stable operation and minimizing grid impact [100]. The integration of energy storage systems, such as supercapacitors, with DWC systems can help manage energy pulses and reduce strain on the grid. This approach allows for controlled energy storage and release, enhancing the overall efficiency of the charging process [**?**]. Magnetic Coupler Design The design of magnetic couplers is crucial for efficient DWC. A narrow-rail three-phase magnetic coupler has been developed to provide uniform output power while maintaining a compact design. This coupler integrates the benefits of narrow rails and uniform power distribution, reducing output voltage fluctuations during charging [101]. Systematic Design and Implementation A systematic approach to designing DWC systems involves considering various parameters such as charging couplers, compensation networks, and power inverter topologies. This comprehensive design process ensures that the systems are

efficient and capable of integrating with renewable energy sources [102]. Wireless charging systems for EVs are categorized into stationary and dynamic types, with dynamic systems requiring specific control functions to enhance power transfer efficiency and communication between system components [103]. While dynamic wireless charging offers numerous benefits, it also presents challenges such as the need for extensive infrastructure development and potential electromagnetic interference. Additionally, the integration of these systems with existing grid infrastructure requires careful planning and control strategies to ensure stability and efficiency. As research progresses, these challenges are being addressed, paving the way for more widespread adoption of dynamic wireless charging technologies.

2.5 Grid Interface and Synchronization Logic

Grid-interactive charging, particularly through bidirectional electric vehicles (EVs), plays a significant role in enhancing grid stability and reliability. This involves the use of EVs in both grid-to-vehicle (G2V) and vehicle-to-grid (V2G) modes, which can provide frequency regulation and voltage support. However, the integration of such systems also presents challenges that need to be addressed to maintain power quality and system stability.

2.5.1 Frequency Regulation

Bidirectional EVs can significantly contribute to frequency stability by acting as flexible resources that absorb or inject power as needed. This capability is particularly useful during frequency fluctuations, where EVs in V2G mode can provide immediate support to stabilize the grid frequency. An optimal frequency support strategy can leverage these capabilities to improve grid stability during such events [104], [105]. In hybrid AC/DC microgrids, bidirectional virtual inertia support can be introduced to slow down changes in AC frequency and DC voltage, thus enhancing system stability. This approach allows for significant reductions in frequency fluctuations, improving the rate-of-change-of-frequency and frequency nadir, which are critical for maintaining grid stability [106].

2.5.2 Voltage Support

The integration of bidirectional EVs also impacts the voltage profile of the grid. By implementing power flow analysis, it is possible to optimize the use of EVs to improve the voltage profile, ensuring that it remains within acceptable limits. This is crucial for maintaining the overall power quality and reliability of the grid [107], [108].

Fast-charging stations (FCSs) for EVs can cause voltage deviations at the point of common coupling (PCC) due to high current injections. To mitigate these effects, advanced converter control techniques, such as single-stage converter (SSC) control, can be employed to provide inertia and damping support, thus enhancing voltage stability [109].

2.5.3 Power Quality and Stability Challenges

The increasing penetration of power electronics converters, including those used in EV charging, can degrade power quality by introducing harmonics and resonances into the grid. This can lead to waveform distortion and transients, posing risks to grid stability and connected equipment. Effective grid impedance modeling and estimation are necessary to address these challenges and ensure the stability of distribution networks with high numbers of grid-connected inverters [108]. The synchronization stability of grid-following converters (GFL) is also affected by grid voltage and frequency variations. These variations can impact the transient responses and stability boundaries of GFLs, highlighting the need for comprehensive studies to understand and mitigate these effects [110]. While grid-interactive charging offers significant benefits for grid stability and reliability, it also introduces complexities that must be managed. The integration of bidirectional EVs and advanced converter technologies can enhance frequency regulation and voltage support, but they require careful planning and optimization to avoid adverse impacts on power quality and system stability. Addressing these challenges involves developing robust control strategies and improving grid infrastructure to accommodate the dynamic nature of modern power systems.

2.6 Standards and Protocols

2.6.1 Communication Protocols

Interoperability in communication protocols is crucial for the seamless integration and operation of electric vehicle (EV) charging systems and other interconnected technologies. Key standards such as ISO 15118 and the Open Charge Point Protocol (OCPP) play significant roles in ensuring this interoperability. These standards facilitate communication between various entities, ensuring secure, efficient, and reliable operations. This answer explores the importance of these protocols, their security challenges, and the broader context of interoperability standards.

Importance of Communication Protocols

ISO 15118: This standard is pivotal for the communication between EVs and charging stations, enabling features like Plug & Charge, which allows for automatic vehicle identification and billing without user intervention. It enhances user convenience and supports the integration of EVs into smart grids by enabling bidirectional energy flow, which is essential for grid stability and energy management [111].

OCPP (Open Charge Point Protocol): OCPP is widely adopted for managing communication between charging stations and central systems. It supports various functionalities, including remote monitoring, diagnostics, and firmware updates, which are crucial for maintaining the operational efficiency of charging networks. The protocol's latest version, OCPP 2.0, includes enhanced security features to address vulnerabilities such as man-in-the-middle attacks and energy theft [112].

Security Challenges and Solutions

Security Threats in OCPP: Despite its widespread use, OCPP faces several security challenges. Potential threats include unauthorized access, data manipulation, and fraud, which can destabilize power networks. Addressing these threats requires robust security measures, such as encryption and authentication protocols, to protect data integrity and confidentiality [113], [114].

Proposed Security Enhancements: Scholars have proposed various solutions to enhance the security of OCPP, including the implementation of secure

communication channels and the use of digital certificates for authentication. These measures aim to mitigate risks and ensure the reliable operation of EV charging networks [114].

Broader Context of Interoperability Standards

Interoperability Programs: The Open Geospatial Consortium (OGC) Interoperability Program exemplifies how collaborative engineering and open standards development can drive innovation and interoperability across industries. Such programs engage diverse stakeholders to identify interoperability needs and develop solutions that benefit society [115].

Standardization Efforts: Various standardization bodies, such as IEEE and ETSI, are actively working on developing and refining communication standards to ensure interoperability across different technologies and industries. These efforts are crucial for enabling seamless integration and fostering innovation in emerging use cases [116].

Evaluation Frameworks: Systematic evaluation frameworks are essential for assessing the effectiveness and applicability of interoperability standards. These frameworks help organizations select appropriate standards that meet their specific needs and ensure successful integration and operation of their systems [117].

Regulatory and Market Challenges

While technical standards like ISO 15118 and OCPP are critical for interoperability, non-technical barriers such as regulatory policies and market dynamics can impede their adoption. For instance, in the personal health device industry, regulatory barriers have hindered the implementation of interoperability standards, highlighting the need for updated policies that align with industry demands [118]. Addressing these challenges requires collaboration among policymakers, industry stakeholders, and standardization bodies to create a conducive environment for the adoption of interoperability standards.

In conclusion, communication protocols like ISO 15118 and OCPP are vital for ensuring interoperability in EV charging systems and beyond. While these standards offer significant benefits, addressing security challenges and overcoming regulatory barriers are essential for their successful implementation and widespread adoption.

2.6.2 Power and Safety Standards

The integration of electric vehicles (EVs) into the power grid has necessitated the development and adherence to power and safety standards to ensure both efficient operation and safety. Standards such as IEEE 1547 play a crucial role in defining the requirements for grid-interactive charging systems, which include power quality and safety considerations. This overview explores the key aspects of these standards, focusing on power quality issues, safety measures, and the technological advancements in EV charging infrastructure.

Power Quality Standards

IEEE 1547 and Power Quality: IEEE 1547 is a critical standard that addresses the interconnection of distributed energy resources, including EVs, with the grid. It sets requirements for power quality, including voltage regulation, frequency response, and harmonic distortion, which are essential for maintaining grid stability and performance [119], [120].

Challenges in Power Quality: The integration of EVs poses challenges such as voltage sags, harmonic distortions, and grid instability. These issues arise from the nonlinear nature of EV chargers and the bidirectional power flow in vehicle-to-grid (V2G) operations [121], [122]. Standards aim to mitigate these issues by specifying acceptable levels of distortion and providing guidelines for grid support functionalities [123].

Proposed Metrics for DC Grids: New metrics for power quality in DC grids, which are increasingly relevant due to the rise of EVs, are being developed. These metrics address phenomena such as ripple, high-frequency noise, and common-mode disturbances, which are not fully covered by existing AC grid standards [124].

Safety Standards

Battery Safety Standards: Safety standards for EV batteries are crucial due to the potential risks associated with battery failures. In China, national standards have been developed to address these risks, focusing on battery materials, management systems, and vehicle integration. These standards provide a framework for international safety guidelines [123].

Isolation and Protection: Safety in EV charging infrastructure is enhanced through the use of isolation techniques, such as those implemented in dual active

bridge (DAB) converters. These techniques protect EV batteries from disturbances on both the AC and DC sides of the charger, ensuring safe operation [119].

Technological Advancements in EV Charging

Multifunctional Charging Infrastructure: Modern EV chargers are designed to operate in multiple modes, including grid-to-vehicle (G2V), V2G, and active-filtering-mode (AFM). These multifunctional chargers improve power quality by compensating for grid current harmonic distortions and providing voltage sag compensation [119], [122].

Bidirectional Chargers: The development of bidirectional chargers supports both G2V and V2G operations, allowing EVs to act as distributed energy resources. This capability is crucial for grid support, as it enables active and reactive power compensation, enhancing grid stability [121].

While the current standards provide a robust framework for ensuring power quality and safety in grid-interactive charging, there are ongoing challenges and opportunities for improvement. The rapid evolution of EV technology and the increasing complexity of power grids necessitate continuous updates to these standards. Future developments may include more comprehensive metrics for DC grids and enhanced safety protocols for emerging battery technologies. As the energy transition progresses, the role of power quality and safety standards will become even more critical in facilitating the integration of EVs into the grid.

2.6.3 Grid integration of renewable energy sources

The integration of renewable energy sources (RESs) such as solar and wind power is crucial for transitioning to a sustainable energy future. This integration not only addresses environmental concerns but also supports economic growth and technological innovation. The role of renewable energy integration is multifaceted, involving technological, economic, and policy dimensions. Below, we explore these aspects in detail.

Technological Integration and Energy Systems

Energy Storage and Management: The integration of RESs is often challenged by their intermittent nature. Energy storage systems, such as batteries and hydrogen storage, are essential for balancing supply and demand. For instance, a

study on a university campus in Romania demonstrated the use of photovoltaic panels, wind systems, and hydrogen storage to ensure a stable power supply, highlighting the importance of energy storage in renewable integration [125]. Smart Water Systems: Renewable energy can be integrated into water systems to create smart, sustainable, and low-cost solutions. This involves using renewable resources for water pumping and distribution, supported by energy management and intelligent technologies to enhance system efficiency [126]. Microgrids and AI: In remote areas, microgrids powered by hybrid RESs can provide reliable electricity. Artificial intelligence (AI) plays a significant role in optimizing these systems, improving operational accuracy, and managing the integration challenges of RESs [127].

Economic and Policy Implications

Economic Growth and Job Creation: The integration of renewable energy is linked to sustainable economic growth. It fosters job creation, enhances energy security, and stimulates technological innovation. A bibliometric analysis revealed a positive correlation between renewable energy adoption and economic indicators like GDP growth and industrial productivity [128].

Market Integration and Innovation: In China, market integration has been shown to significantly boost renewable energy technology innovation (RETI). This is achieved by optimizing the energy structure and enhancing technological innovation, which are crucial for achieving carbon neutrality goals [129].

Policy Support and Financial Incentives: Policies and financial incentives are vital for promoting renewable energy integration. For example, in the construction sector, subsidies and policy support have been effective in increasing the adoption of renewable technologies, such as solar and wind energy, in building practices [**?**].

Environmental and Social Benefits

Decarbonization and Energy Autonomy: Increasing the share of renewables in power systems is essential for decarbonization. A study on the island of Procida demonstrated that high renewable integration could significantly reduce greenhouse gas emissions and decrease dependency on energy imports [130]. Community Development: Renewable energy projects can drive local community development by providing clean energy and creating local jobs. This is particularly beneficial in regions with abundant renewable resources, where

such projects can lead to equitable development and improved living standards [131]. While the integration of renewable energy sources offers numerous benefits, it also presents challenges such as grid stability and the need for technological advancements. Addressing these challenges requires coordinated efforts in policy-making, technological innovation, and market strategies. The role of renewable energy integration is not only about replacing fossil fuels but also about transforming energy systems to be more resilient, sustainable, and inclusive.

2.7 Conclusion

The literature reveals that effective grid synchronization is fundamental for stable and efficient operation of grid-interactive EV chargers. While traditional PLL-based methods are widely used, their limitations under distorted grid conditions have led to the adoption of advanced quadrature signal generation techniques such as SO-SOGI, CSOGI, and CNISOGI. Among these, CNISOGI offers superior performance in filtering harmonics and rejecting DC offset, making it highly suitable for modern synchronization needs. Furthermore, the review underscores the importance of standardized communication protocols like ISO 15118 and OCPP, while also identifying challenges related to cybersecurity, economic viability, and regulatory compliance. Overall, the integration of bidirectional EV chargers poses both opportunities and challenges for grid reliability, emphasizing the need for advanced control strategies and continued research in power electronics and grid-interface technologies.

Chapter 3

Design and development of the hardware

3.1 System description

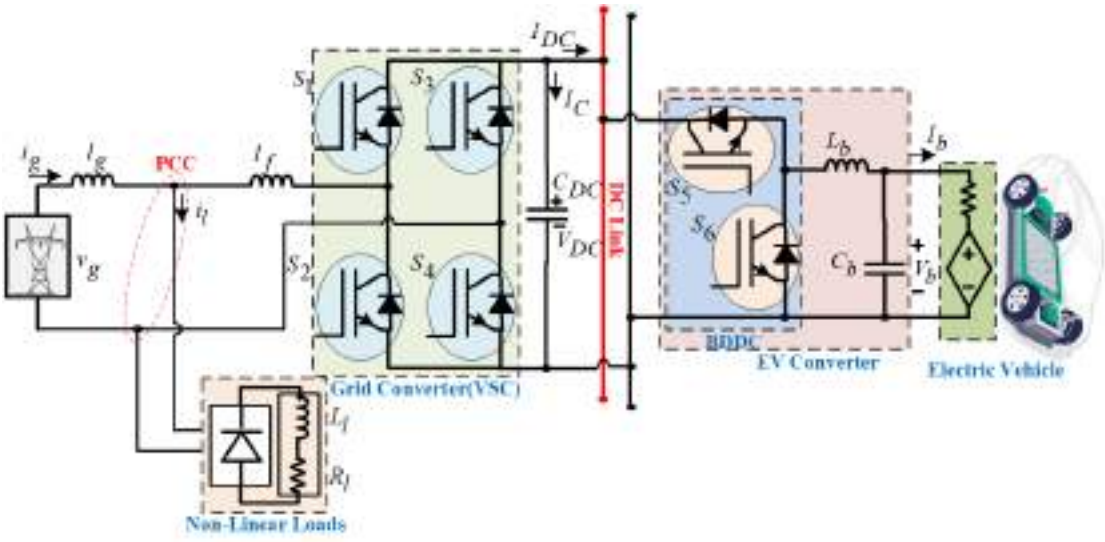

FIGURE 3.1: System description of single phase GIEVC

The configuration of on-board battery charger (OBBC) under consideration comprises two conversion stages as shown in Figure 3.1. The first stage is dedicated to AC-DC conversion, while the second level handles DC-DC conversion. Furthermore, a non-linear load is connected at the PCC. In the suggested control configuration, the first AC-DC converter serves as a controlled rectifier, & its succeeding step employs a bipolar dual-directional DC (BDDC)

converter with two IGBT switches. Following this arrangement, the lithium-ion battery undergoes charging utilizing a combination of constant current (CC) and constant voltage (CV) techniques. The various parameters and components of a complete OBBC system are depicted as the source voltage (v_g), L_s the source inductance, the shunt R_l & L_l act as the load, and L_f the coupling inductance. The AC/DC inverter in which switches (S_1, S_2, S_3, S_4) consequently operate is the Bi-Directional & especially for the rigidity of the DC link voltage (V_{DC}). DC/DC converter that functions as a buck-boost converter that implements buck mode (S_5) for charging and boost mode (S_6) for discharging the battery.

3.2 Modelling of single phase OBBC EV charger

Single phase OBBC EV chargers comprises of two stage AC/DC and DC/DC. In this section modelling of firstly AC/DC converter and secondly DC/DC converter is discussed.

3.2.1 AC/DC Converter

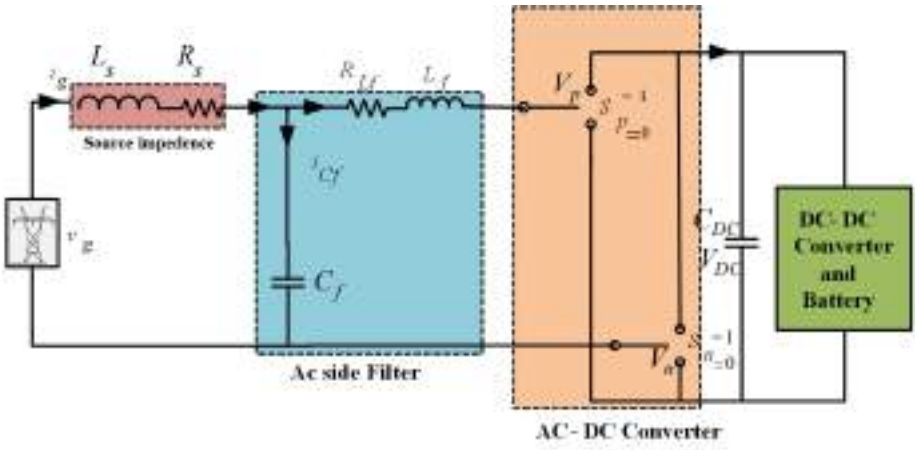

FIGURE 3.2: Switching model of AC/DC converter

The switching architecture for a single-phase AC-DC converter is shown in Fig. 3.2. For each leg, a single pole double throw switch is used. The grid voltage is represented by v_g, the grid side inductor by L_s, the AC side filter inductance and capacitance by L_f and C_f, respectively, and the equivalent series resistance

(ESR) of the filter inductance and capacitance by R_{Lf} and R_{Cf}. For switches S_1 and S_3, the on state is represented by $S_p = 1$ and $S_p = 0$, accordingly. The on states of switches S_2 and S_4 are represented by the values $S_n = 1$ and $S_n = 0$, respectively. As a result, the grid current i_g becomes the DC side current I_{DC} and the variable V_{pn} equals V_{DC} when switches S_1 and S_4 are on and S_3 and S_2 are off.

$$v_{pn} = v_p - v_n \tag{3.1}$$

$$S_p \times V_{DC} - S_n \times V_{DC} = (S_p - S_n)V_{DC} \tag{3.2}$$

$$= S_{pn} \times V_{DC} \tag{3.3}$$

where, $S_{pn} = S_p - S_n$, v_{pn} = Pole Voltage. V_{DC}=Average DC link voltage.

And

$$I_{DC} = (S_p - S_n) \times i_{Lf} = S_{pn} \times i_{Lf} \tag{3.4}$$

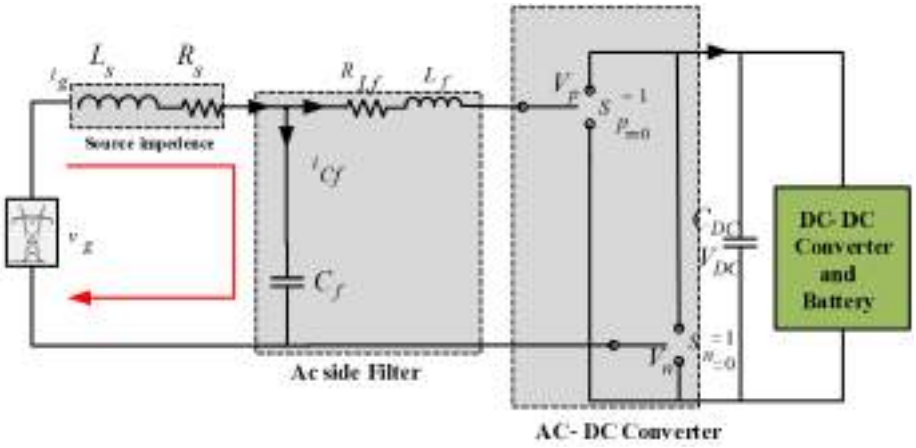

FIGURE 3.3: Outer loop configuration for switching model

Now applying KVL in outer loop and neglecting capacitor ESR as shown in Fig. 3.3,

$$v_g = v_{Ls} + v_{Cf} \tag{3.5}$$

$$v_g = L_s \frac{di_g}{dt} + v_{Cf} \tag{3.6}$$

$$\frac{di_g}{dt} = \frac{v_g}{L_s} - \frac{v_{Cf}}{L_s} \tag{3.7}$$

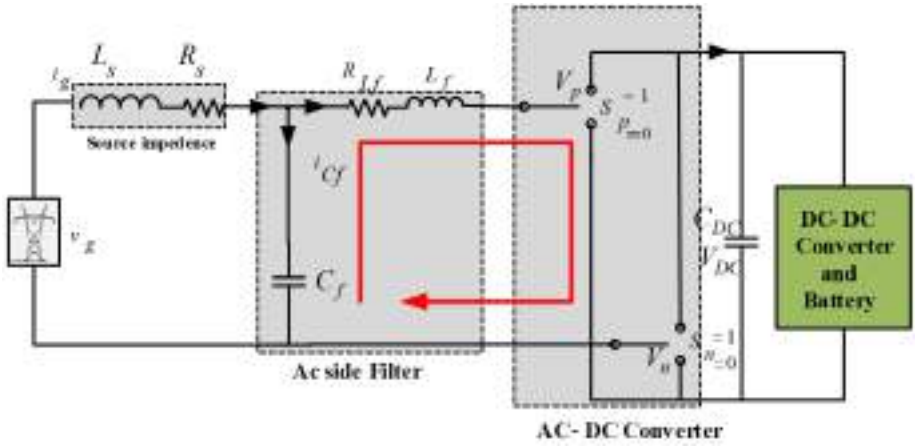

FIGURE 3.4: Inner loop configuration for switching model

Now applying KVL in the inner loop as given in Fig. 3.4,

$$v_{Cf} = v_{Lf} + i_{Lf} \times R_{Lf} + v_{pn} = L_f \frac{di_{Lf}}{dt} + i_{Lf} \times R_{Lf} + v_{pn} \tag{3.8}$$

$$\frac{di_{Lf}}{dt} = \frac{v_{Cf}}{L_f} - \frac{i_{Lf} \times R_{Lf}}{L_f} - \frac{v_{pn}}{L_f} \tag{3.9}$$

Where,

v_{Lf} = AC side inductor filter voltage.

i_{Lf} = AC side inductor filter current.

R_{Lf} = Equivalent Series Resistance of the filter inductor.

L_f = AC side filter inductance.

Now applying Kirchhoff's Current Law (KCL) at the junction as shown in Fig. 3.5,

$$i_g = i_{Lf} + i_{Cf} i_g = i_{Lf} + C_f \frac{dv_{Cf}}{dt} \tag{3.10}$$

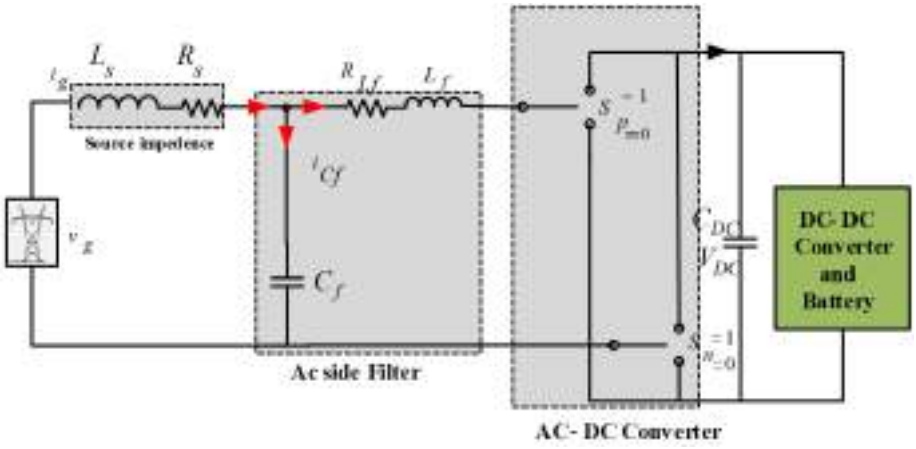

FIGURE 3.5: Junction configuration for Switching model

$$\frac{dv_{Cf}}{dt} = \frac{i_g}{C_f} - \frac{i_{Lf}}{C_f} \tag{3.11}$$

Where, i_g = Grid current.

i_{Lf} = AC side inductor filter current.

i_{Cf} = AC side capacitor filter current.

C_f = AC side filter capacitance.

Average Model

Using one switching period as the switching model, the averaging operator is used, the system average model is acquired. For a time-varying variable y, the averaging operator is illustrated as 3.12.

$$\tilde{y} = \frac{1}{T}\int_0^T y(\tau)\, d\tau \tag{3.12}$$

Where,

$\tilde{y}$ = Average value.

$y(\tau)$ = Time-varying variable.

T = Switching period.

Applying the averaging operator to the above derived state-space equations:

$$\frac{d\tilde{i}_g}{dt} = \frac{\tilde{v}_g}{L_s} - \frac{\tilde{v}_{Cf}}{L_s} \tag{3.13}$$

$$\frac{d\tilde{i}_{Lf}}{dt} = \frac{\tilde{v}_{Cf}}{L_f} - \frac{\tilde{i}_{Lf} \times R_{Lf}}{L_f} - \frac{d_{pn} \times V_{DC}}{L_f} \tag{3.14}$$

$$\frac{d\tilde{v}_{Cf}}{dt} = \frac{\tilde{i}_g}{C_f} - \frac{\tilde{i}_{Lf}}{C_f} \tag{3.15}$$

Where,
d_{pn} = The average value of S_{pn}.

Small Signal Model

The steady state values of the average model are combined with small AC changes that are overlaid to create the small signal model. The resulting Eqns 3.11, 3.12, and 3.14 for small signals are

$$\frac{d\tilde{\tilde{i}}_g}{dt} = \frac{\tilde{\tilde{v}}_g}{L_s} - \frac{\tilde{\tilde{V}}_{Cf}}{L_s} \tag{3.16}$$

$$\frac{d\tilde{\tilde{I}}_{Lf}}{dt} = \frac{\tilde{\tilde{V}}_{Cf}}{L_f} - \frac{\tilde{\tilde{I}}_{Lf} \times R_{Lf}}{L_{Lf}} - \frac{\tilde{\tilde{d}}_{pn} \times V_{DC}}{L_f} \tag{3.17}$$

$$\frac{d\tilde{\tilde{V}}_{Cf}}{dt} = \frac{\tilde{\tilde{i}}_g}{C_f} - \frac{\tilde{\tilde{i}}_{Lf}}{C_f} \tag{3.18}$$

Taking Laplace transform of Eqns 3.16-3.18,

$$\tilde{\tilde{I}}_g = \frac{\tilde{\tilde{V}}_g}{sL_s} - \frac{\tilde{\tilde{V}}_{Cf}}{sL_s} \tag{3.19}$$

$$s\tilde{\tilde{I}}_{Lf} = \frac{\tilde{\tilde{V}}_{Cf}}{L_f} - \frac{\tilde{\tilde{I}}_{Lf} \times R_{Lf}}{L_f} - \frac{\tilde{\tilde{d}}_{pn} \times V_{DC}}{L_f} \tag{3.20}$$

$$s\tilde{\tilde{V}}_{Cf} = \frac{\tilde{\tilde{I}}_g}{C_f} - \frac{\tilde{\tilde{I}}_{Lf}}{C_f} \tag{3.21}$$

Putting Eqn 3.19 in Eqn 3.21

$$s\tilde{\tilde{V}}_{Cf} = \frac{1}{C_f}\left(\frac{\tilde{\tilde{V}}_g}{sL_s} - \frac{\tilde{\tilde{V}}_{Cf}}{sL_s}\right) - \frac{\tilde{\tilde{I}}_{Lf}}{C_f} \tag{3.22}$$

$$\tilde{\tilde{V}}_{Cf} = \frac{\tilde{\tilde{V}}_g}{s^2L_sC_f+1} - \frac{\tilde{\tilde{I}}_{Lf}\times sL_s}{s^2L_sC_f+1} \tag{3.23}$$

Putting Eqn 3.23 in Eqn 3.20

$$\tilde{\tilde{I}}_{Lf} = \frac{\tilde{\tilde{V}}_g}{s^3L_fL_sC_f + s^2L_sC_fR_{Lf} + s(L_f+L_s) + R_{Lf}} - \tilde{d}_{pn}\times V_{DC}\left(\frac{s^2L_sC_f+1}{s^3L_fL_sC_f + s^2L_sC_fR_{Lf} + s(L_f+L_s) + R_{Lf}}\right) \tag{3.24}$$

Let us assume the ideal grid, then the final relation is as follows:

$$\tilde{\tilde{I}}_{Lf} = -\tilde{d}_{pn}\times V_{DC}\left(\frac{s^2L_sC_f+1}{s^3L_fL_sC_f + s^2L_sC_fR_{Lf} + s(L_f+L_s) + R_{Lf}}\right) \tag{3.25}$$

As known that at higher frequencies, the above Eqn results to 3.26.

$$\tilde{\tilde{I}}_{Lf} = \frac{-\tilde{d}_{pn}\times V_{DC}}{sL_f + R_{Lf}} \tag{3.26}$$

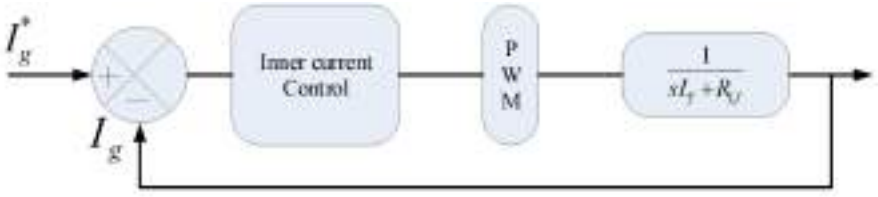

FIGURE 3.6: Inner current control loop

From Eqn. (26), it shows that $\tilde{d}_{pn}$ increases with the decrement in $\tilde{I}_{Lf}$ because of the negative sign. Therefore, the plant function is as follows in Fig. 3.6.

$$G_{P_{ac}} = V_{DC}\times\left(\frac{1}{sL_f+R_{Lf}}\right) \tag{3.27}$$

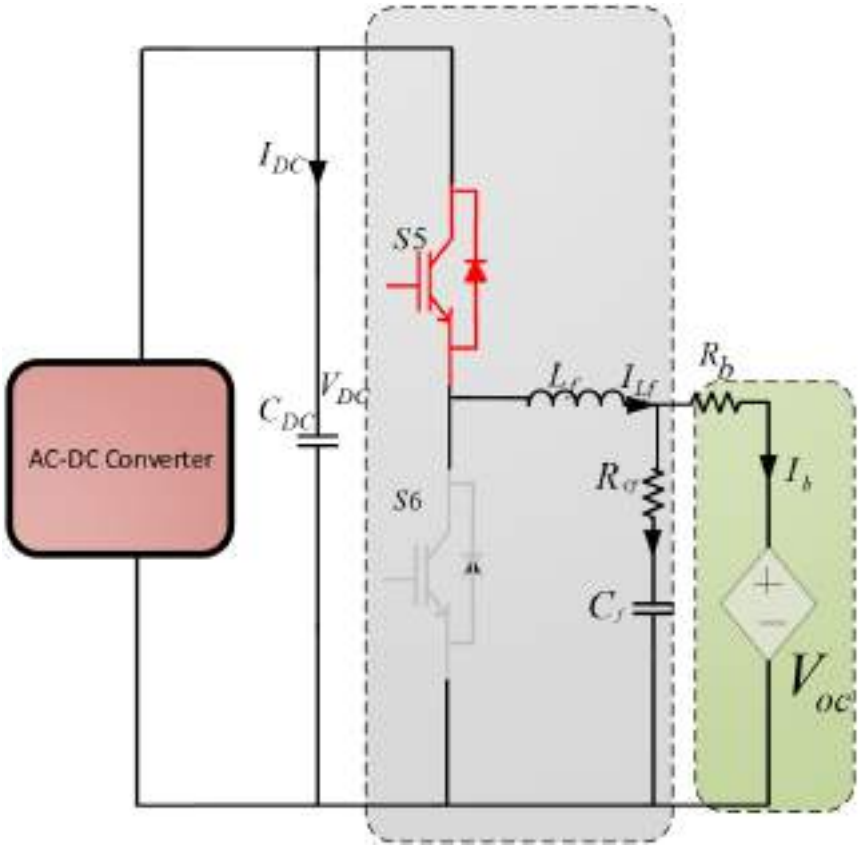

FIGURE 3.7: Switching model of DC/DC converter with S_5 ON

3.2.2 DC/DC Converter

A pair of logical modes for the bidirectional buck-boost converter may be identified assuming complimentary switch control signals for S_5 and S_6 Topological mode 1: In this case, S_5 is ON and S_6 is OFF, yielding:

$$\frac{dI_{L_f}}{dt} = \frac{1}{L_f}V_{DC} - \frac{1}{L_f}V_b \tag{3.28}$$

$$\frac{dV_{DC}}{dt} = \frac{1}{C_{DC}}I_{DC} - \frac{1}{C_{DC}}I_{Lf} \tag{3.29}$$

$$\frac{dV_b}{dt} = \frac{1}{C_f}I_{Lf} - \frac{1}{C_f}I_b \tag{3.30}$$

Topological mode 2: In this case, S_5 is OFF and S_6 is ON, which leads to:

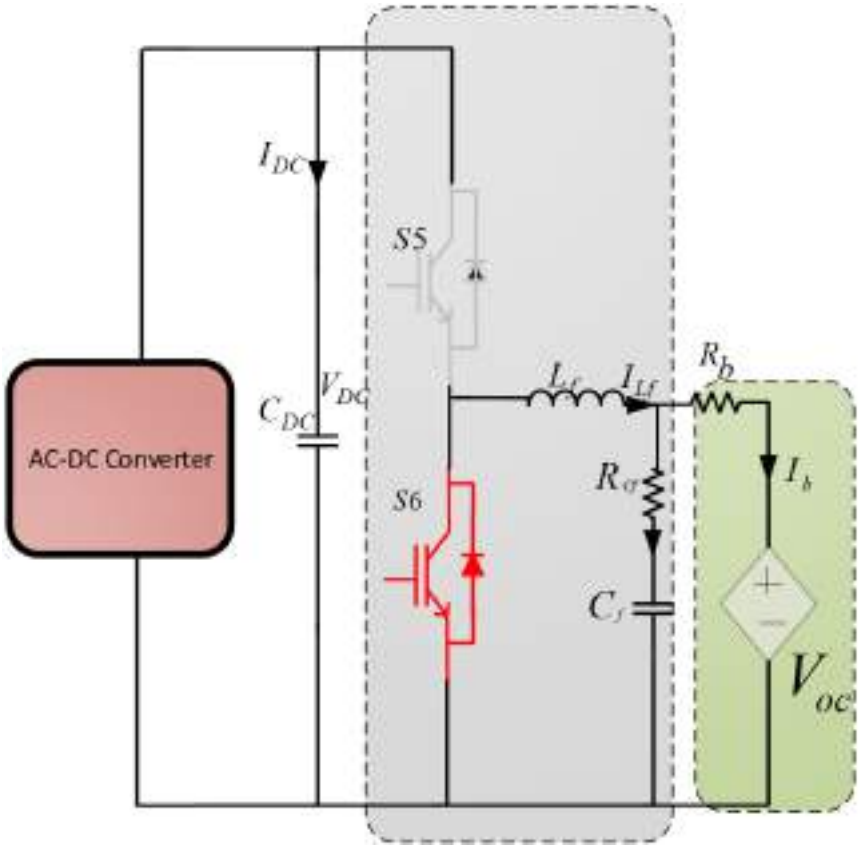

FIGURE 3.8: Switching model of DC/DC converter with S_6 ON

$$\frac{dI_{L_f}}{dt} = -\frac{1}{L_f}V_b \tag{3.31}$$

$$\frac{dV_{DC}}{dt} = \frac{1}{C_{DC}}I_{DC} \tag{3.32}$$

$$\frac{dV_b}{dt} = \frac{1}{C_f}I_{Lf} - \frac{1}{C_f}I_b \tag{3.33}$$

The following formulas may be obtained by averaging the first-order differential Eqns 3.28 - 3.33 over a switching period; where, D_{S_5} is the duty cycle for S_5 :

$$\left(\frac{dI_{L_f}}{dt}\bigg|_{\text{av}} = D_{S_5}\left(\frac{1}{L_f}V_{DC} - \frac{1}{L_f}V_b\right) + (1 - D_{S_5})\left(-\frac{1}{L_f}V_b\right)\right. \tag{3.34}$$

$$= D_{S_5}\frac{V_{DC}}{L_f} - \frac{V_b}{L_f} \tag{3.35}$$

$$\left(\frac{dV_{DC}}{dt}\right|_{\text{av}} = D_{S_5}\left(\frac{1}{C_{DC}}I_{DC} - \frac{1}{C_{DC}}I_{L_f}\right) + (1 - D_{S_5})\left(\frac{1}{C_{DC}}I_{DC}\right) \tag{3.36}$$

$$= \frac{1}{C_{DC}}I_{DC} - D_{S_5}\left(\frac{-I_{L_f}}{C_{DC}}\right) \tag{3.37}$$

$$\left(\frac{dV_b}{dt}\right|_{\text{av}} = \left(\frac{1}{C_f}I_{L_f} - \frac{1}{C_f}I_b\right) \tag{3.38}$$

3.3 Development of the Hardware for GIEVC

For the development of the hardware, several equipment are used as follows:

- Voltage sensor:-

  Voltage sensor is used to sense the voltage, whether it is an AC, DC, pulsed, etc. Fig. 3.9 depicts the circuit as well as the actual hardware of the voltage sensor. LEM LV 25-P is a voltage transducer module for electronic voltage measurements with galvanic isolation between the primary and secondary circuits. This voltage transducer is based on the Hall effect and may be mounted on a PCB. Between primary and secondary circuits, the device offers galvanic isolation. To measure a voltage, a current proportional to the measured voltage must be collected through an external resistor chosen by the user. Hence it is suitable for voltages related to DC, AC, and impulse circuits, which may be measured electronically with this device.

- Current Sensor:-

  Fig. 3.10 shows the current sensor with its circuitry. LEM make LA 25-P is capable of measuring a 25A AC/DC signal. As a similar structure to a voltage transducer, this current sensor is also based on the Hall effect. Also, it offers isolation between primary and secondary circuits. With the

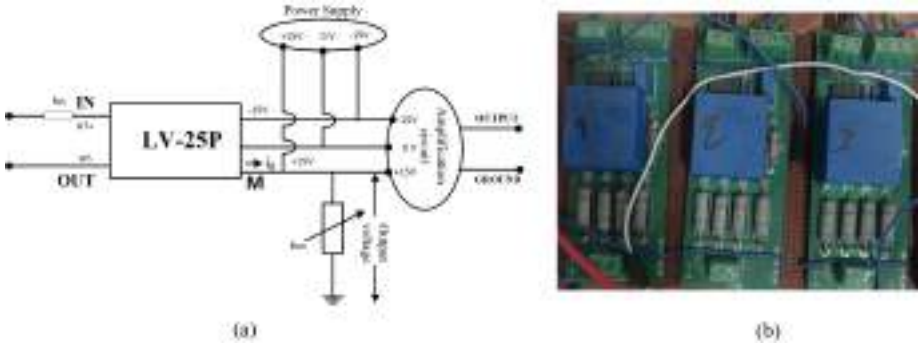

FIGURE 3.9: Circuit diagram and the hardware of Voltage sensor

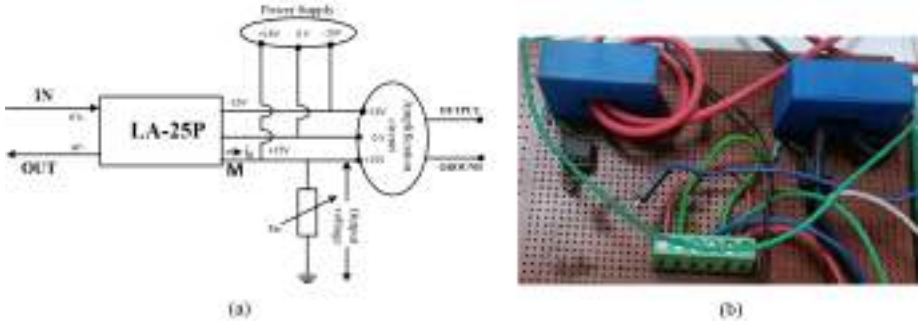

FIGURE 3.10: Circuit diagram and the hardware of Current sensor

accuracy of 1.25%, it is capable of -25 to 85 degrees Celsius temperature and has the closed-loop Hall effect technology.

Henceforth, single-board mounting of three voltage and two current transducers is depicted in Fig. 3.11. Such that grid voltage, DC-link voltage, and battery voltage are measured through voltage transducers. And grid current and load current are measured through the current transducers.

- Gate Driver Circuit:-

  Gate drivers are specialized circuits that amplify and provide the necessary voltage and current to the gate of high-power transistors like MOSFETs and IGBTs as shown in Fig. 3.12. They act as a bridge between a low-power control signal (e.g., from a microcontroller) and the high-power switch. This amplification is crucial for effectively turning the power transistor on and off, especially in applications requiring high switching speeds and efficiency.

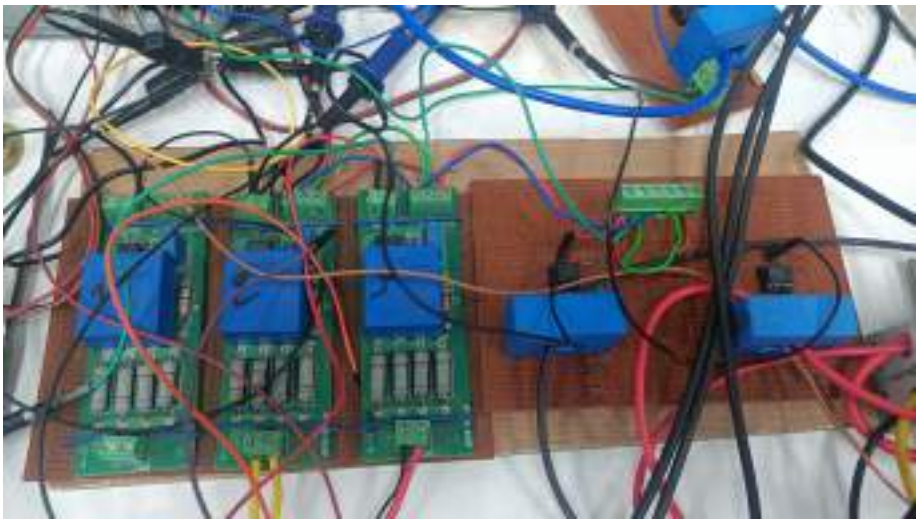

FIGURE 3.11: Voltage and Current sensor

- IGBT module:

  Semikron make an IGBT leg module consisting of two IGBT switches with a power diode as the body diode as shown in Fig. 3.13. Further, the SKM100GB12T4 series is a fast-generation trench, soft-switching-enabled IGBT having an isolated copper baseplate using DBC technology (Direct Bonded Copper). It can go for higher switching frequencies up to 20 kHz.

- Bi-Directional DC power supply:

  Chroma 62000D Series programmable bidirectional DC power supplies shown in Fig. 3.14 have both power source and load characteristics. Capable of feeding power from the device under test (DUT) back to the utility grid, these two-quadrant power supplies are ideal for testing energy storage systems in renewable energy applications such as solar PV/storage hybrid inverters, battery power conditioning systems (PCS), and simulating charging and discharging of energy storage batteries. 62000D also has applications in testing power components in electric vehicles (EVs) as well as bidirectional on-board chargers (BOBC), DC-DC converters, and DC-AC motor drivers, enabling bi-directional power conversion simulation tests without the need for actual batteries.

- Regenerative Grid simulator:

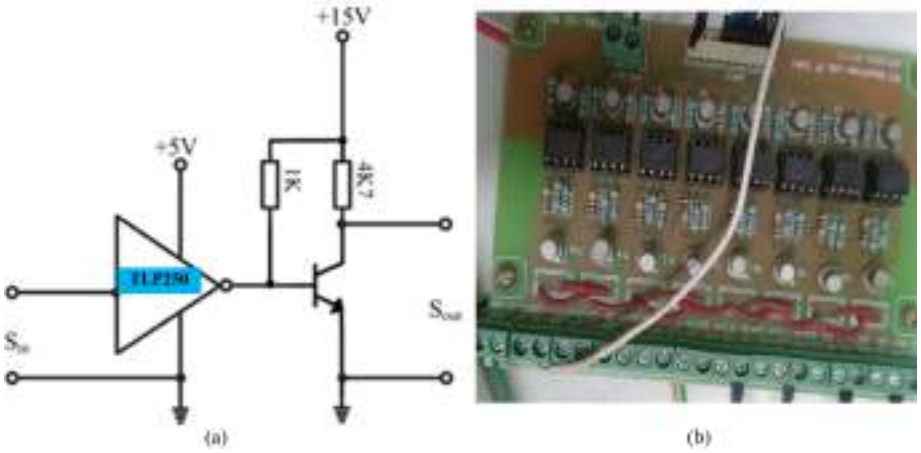

FIGURE 3.12: Gate driver circuit

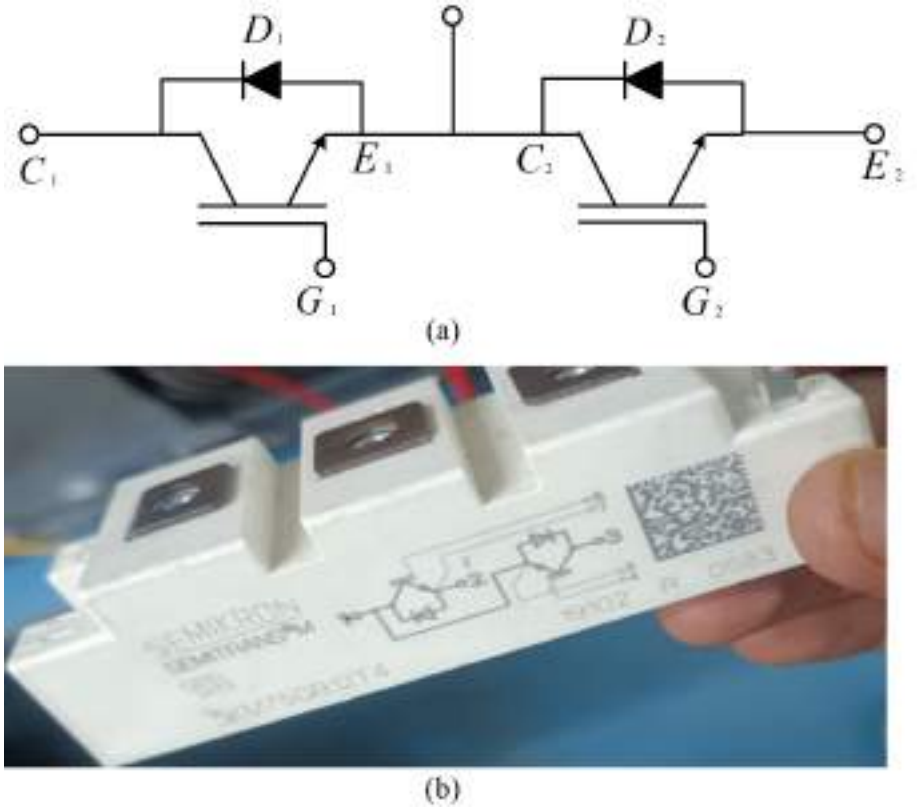

FIGURE 3.13: IGBT module

FIGURE 3.14: Bi-Directional DC power supply

The regenerative grid simulator is used for the AC/DC supply as shown in Fig. 3.15. The simulator is 18 kW, and the output AC voltage ranges from 175 to 350V_{rms} (L-N). In addition, output DC voltage ranges from 200 to 400V_{DC}. It has programmable 1, 2, or 3-phase modes and is capable of sinking power, which is returned back to facility mains.

FIGURE 3.15: Regenerative Grid Simulator

- AC/DC converter:

  The AC/DC converter is mounted on the zero PCB as depicted in Fig. 3.16. Where IRF840 mosfets are used as the switch with the heat sink. Also,

FIGURE 3.16: Hardware setup for AC/DC converter

FIGURE 3.17: DC-Link capacitor

switches are the discrete and through holes capable of 8A, 500V with very low $R_{DS(on)} = 0.85\Omega$.

- DC-Link Voltage:

  For the DC-Bus or the DC-Link voltage a filter capacitor or DC-Link capacitor is used to smoothen the output voltage of the AC/DC rectifier. This capacitor is an aluminum electrolytic capacitor, 1000uF, 315V case size 35X45 mm, high-temperature electrolytic capacitor. To have the capacitance of 2000F a parallel connection of 10001000F has been used as shown in Fig. 3.17.

- DC/DC converter:

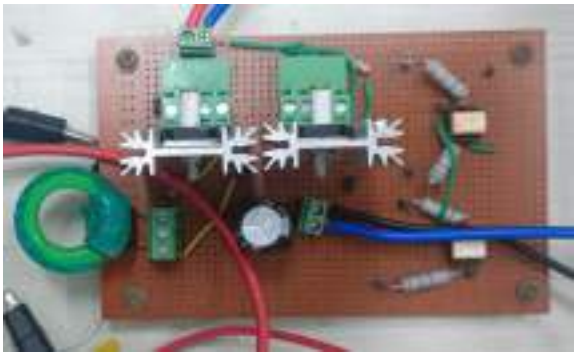

FIGURE 3.18: DC/DC non-isolated converter

For the charging and discharging of the battery, a DC/DC converter is used to integrate with DC Bus. The DC/DC converter is a non-isolated buck-boost converter as depicted in Fig. 3.18. In addition, FGA25N120ANTD IGBT switches have been used for the DC/DC converter, which is capable of 1200V, 50A. Further, a coaxial wound ferrite core inductor of 4mH and 100F 56V has been used as a filter.

- Complete experimental setup:

Fig. 3.19 shows the hardware implementation of the grid-interactive EV charger. To test the efficacy of the charger, there is a need for a distorted grid supply, which is supplied from a regenerative grid simulator. The control scheme is developed on the CP1104 series dSPACE control box. Chroma make 62060D-600 series bidirectional DC power supply, which is used as the battery simulator. A three-leg converter comprising IGBT switches is capable of bidirectional flow of power. Therefore, two legs are used for the AC/DC converter, and the third one is used for the DC/DC converter. Many measuring instruments have been used, such as a current probe, multimeter, differential probe, and DC programmable supply, which is used to give supply of +15 0 -15 to the sensors.

Fig. 3.20 depicts another experimental setup for the GIEVC system. In this setup, the converters used, AC/DC and DC/DC converters, are made on the zero PCB with IRF840 MOSFETs with the heat sink. These MOSFET switches need a gate pulse (amplitude = 15V) at the gate terminal. Henceforth, gate

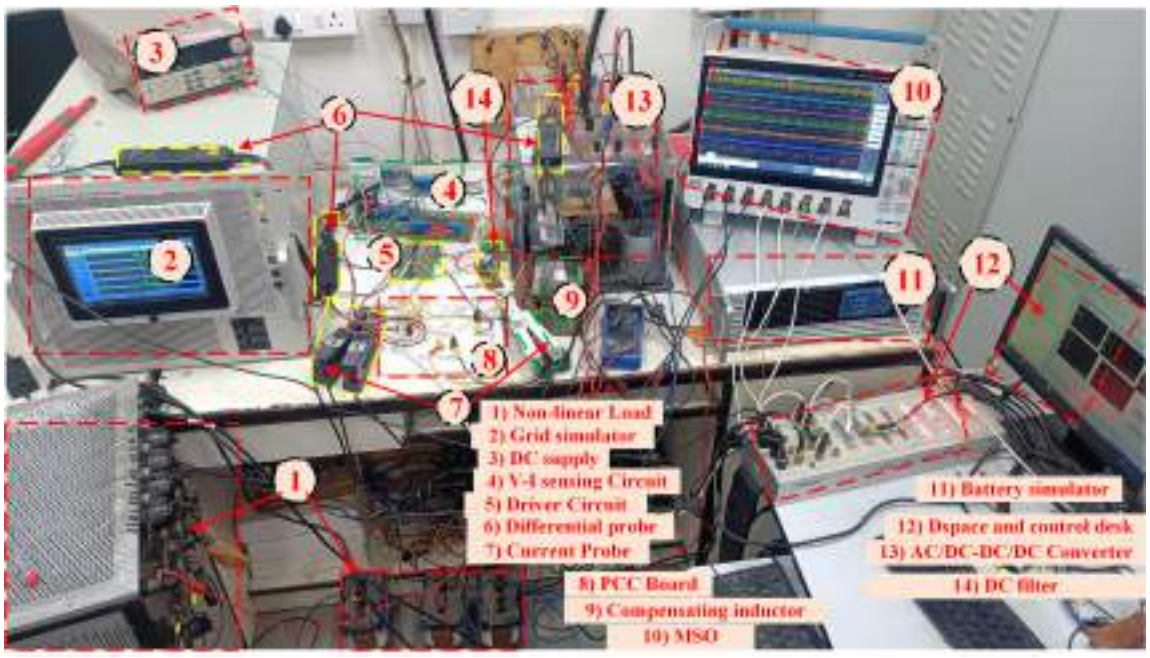

FIGURE 3.19: Complete experimental setup

driver circuits are used for two purposes: firstly, to provide the isolation and secondly, to amplify the pulse from 3.3V/5V to 15V. TI make C2000 series F28379d model is used for the generation of pulses and is used to develop the control schemes.

Lastly, a real-time simulation setup is shown in Fig. 3.21. OPAL-rt technologies make OP-4510 series the real-time simulator with rt-lab enabled. This RT-Lab can be accessed by the desktop. Further, to analyze the output waveform 8 channel Tektronix make 5 series mixed signal oscilloscope is used.

3.4 Conclusions

This chapter presents a comprehensive modeling framework for a two-stage bidirectional grid-connected EV charger consisting of a front-end AC/DC converter and a back-end isolated DC/DC converter, designed to operate seamlessly in both G2V and V2G modes. The system was modeled to ensure efficient energy flow control, voltage regulation, and grid

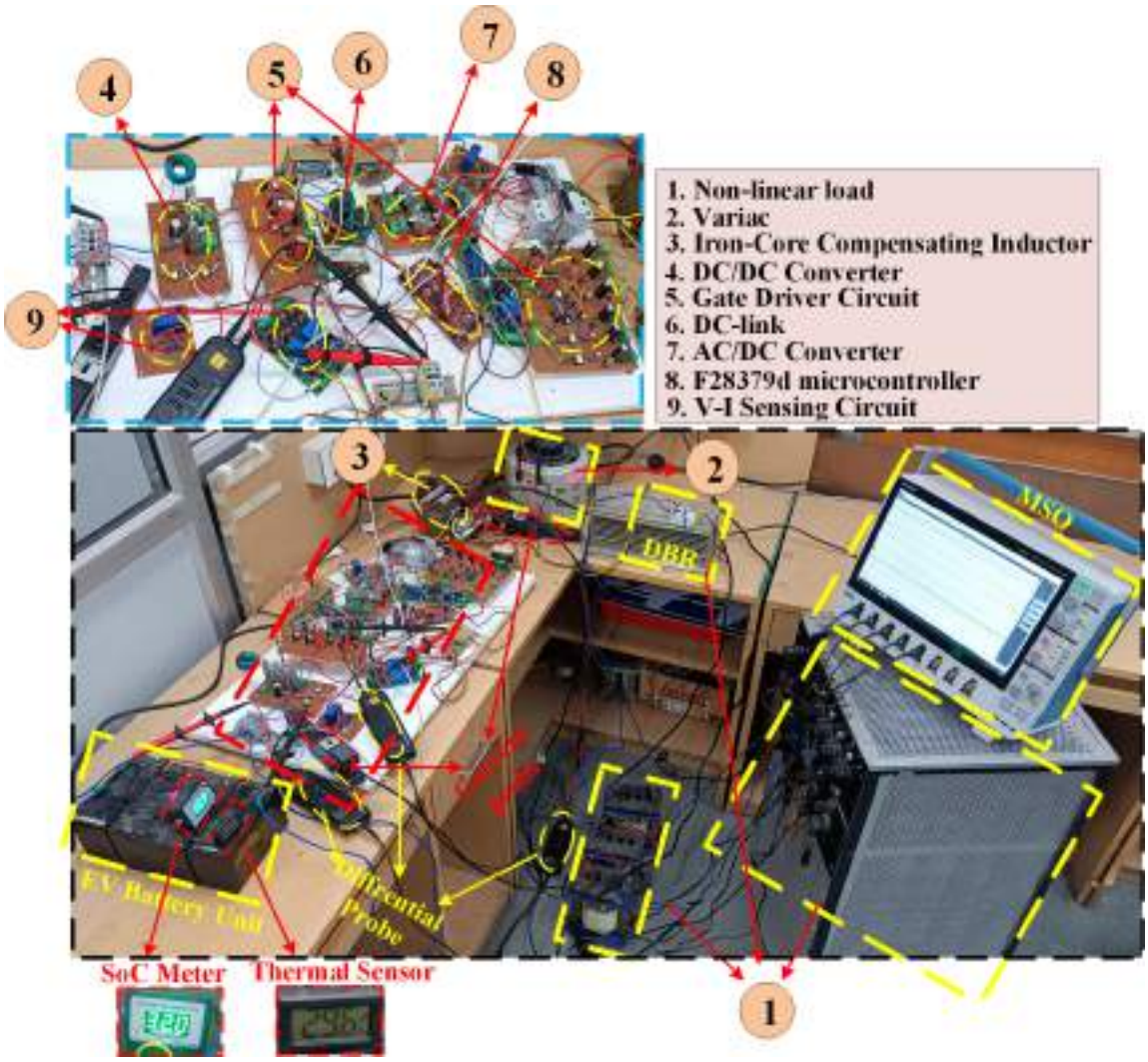

FIGURE 3.20: Laboratory setup for the single-phase GIEVC system

compliance under various operating conditions. Detailed descriptions of the hardware setup were provided, including the selection and integration of key components such as DC link voltage and current sensors, isolated gate driver circuits, and both converter stages with appropriate filter designs. Furthermore, the chapter elaborated on the use of a programmable grid simulator and battery simulator to emulate real-world grid dynamics and vehicle battery behavior, respectively. The entire system was interfaced with a TI F28379D DSP and tested through OPAL-RT-based real-time Hardware-in-the-Loop (HIL) simulation. This integrated modeling and

FIGURE 3.21: Real-time simulation setup

hardware setup lays a solid foundation for validating the proposed control strategy under practical and dynamic grid scenarios in subsequent chapters.

Based on the detailed modeling and hardware implementation presented in this chapter. Therefore, to test the developed system, various charging control strategies are studied and evaluated in Chapter 4, including conventional current control methods and advanced grid synchronization techniques. Special attention is given to the role of different types of quadrature signal generators (QSGs) and filtering methods such as LLMF, LMS, and LMF in enhancing dynamic response and grid compliance. These strategies are not only studied analytically but also validated through real-time Hardware-in-the-Loop (HIL) simulation using the OPAL-RT platform, enabling a realistic assessment of their performance under practical grid and battery conditions.

Chapter 4

Study and analysis of different charging control strategies of EVs

4.1 Introduction

The increasing penetration of Electric Vehicles (EVs) into modern transportation systems has introduced both opportunities and challenges for power grid infrastructure. While EVs offer a clean and efficient alternative to fossil-fuel-based mobility, their widespread deployment can lead to adverse impacts on grid stability, peak demand profiles, and power quality if not properly managed. As a result, the design of effective charging control strategies has become critical in ensuring the reliable operation of power systems.

Among the various control strategies, those incorporating real-time grid signal extraction and accurate load current decomposition have proven especially effective in enhancing power quality and enabling demand-side management. One such approach involves the use of Cascaded Non-Identical Second-Order Generalized Integrator (CNISOGI) structures. The CNISOGI, a fourth-order quadrature signal generator, provides superior selectivity and dynamic tracking performance compared to conventional SOGI-based methods.

System description has explained in the section 3.1

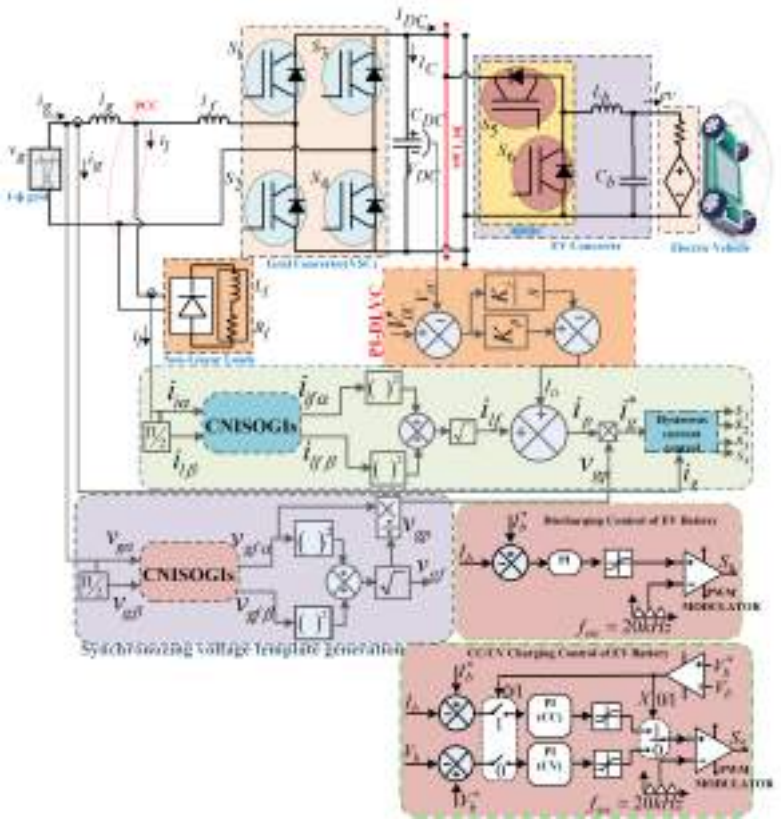

FIGURE 4.1: Circuit diagram of the first stage with control scheme

4.2 Control Techniques and Controller Design

In the framework of control techniques, front-end converter (FEC) control is covered first, then DC/DC control.

4.2.1 FEC switching strategy

The control design of the FEC under non-ideal voltage situations is of primary importance since it is the main component of OBBC that must cope with disruptions in grid-side voltage and current. The voltage sag, voltage swell, and non-sinusoidal grid voltages have been taken into account since the system is single-phase, and they have been used to assess the controller's effectiveness. Additionally, a non-linear load at PCC was employed to demonstrate how the FEC can simultaneously recharge as

well as discharge the battery while accounting for reactive power and load harmonics to maintain a sinusoidal grid current at unity power factor (UPF). Here, as previously noted, phase lock loops (PLLs) employ CNISOGI as a pre-filter to generate grid synchronizing voltage templates. To account for the reactive and harmonic components of non-linear load current, the same structure is also used to extract the fundamental component.

The Fig. 4.1 displays all aspects of the controller within the grid-connected system. Here, the grid voltage v_g and load current i_l are transformed into $\alpha\beta$-frame through transportation delays. The small residential load $i_l\alpha\beta$ comprising fundamental and harmonic current is expressed in 4.1.

$$\begin{bmatrix} i_{l\alpha} & i_{l\beta} \end{bmatrix} = \begin{bmatrix} i_{lf\alpha} + i_{lh\alpha} & i_{lf\beta} + i_{lh\beta} \end{bmatrix} \tag{4.1}$$

where $i_{lf\alpha}, i_{lf\beta}$ indicates the fundamental component and $i_{lh\alpha}, i_{lh\beta}$ represents the harmonic component of i_l in $\alpha\beta$- frame. Here, CNISOGI is utilized to separate $i_{lh\alpha}$ and $i_{lh\beta}$, from $i_{l\alpha}$ and $i_{l\beta}$ to extract $i_{lf\alpha}$ and $i_{lf\beta}$. Furthermore, the $i_{lf\alpha}$ along with its phase-shifted quadrature component $i_{lf\beta}$ are passed through the peak estimation block to calculate i_{lf} as given by 4.2.

$$i_{lf} = \sqrt{(i_{lf\alpha}^2 + i_{lf\beta}^2)} \tag{4.2}$$

Similarly, the v_g^α and v_g^β component of grid voltage is fed to CNISOGI to filter out DC offset as well as harmonics components to extract the fundamental grid voltage components $v_{gf(\alpha\beta)}$. The $v_{gf\alpha}$ along with its phase-shifted quadrature component $v_{gf\beta}$ are passed through a peak estimation block to calculate v_{gf}. Further, the in-phase component $v_{gf\alpha}$ is divided by calculated v_{gf} to obtain unit voltage template v_{gp} as given by 4.3 and 4.4.

$$v_{gf} = \sqrt{\left(v_{gf\alpha}^2 + v_{gf\beta}^2\right)} \tag{4.3}$$

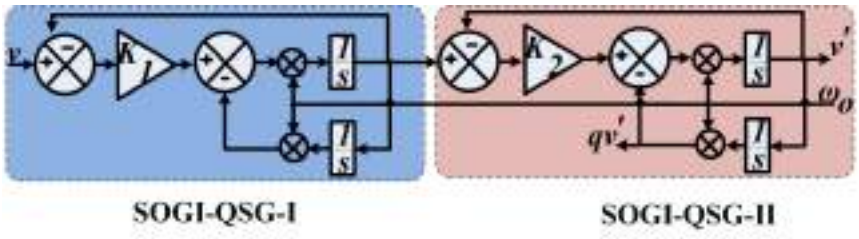

FIGURE 4.2: Block schematic of the CNISOGI-QSG

$$v_{gp} = \frac{\left(v_{gf\alpha}\right)}{\sqrt{\left(v_{gf\alpha}^2 + v_{gf\beta}^2\right)}} \tag{4.4}$$

4.2.2 Design of CNISOGI-QSG

Fig. 4.2(a) shows how a CNISOGI filter is constructed. Furthermore, 4.5 and 4.7 provide a transfer function for both the quadrature-phase element ($q\hat{v}$) along with in-phase element ($\hat{v}$) of the CNISOGI filter onto the input (v).

$$G_1(s) = \frac{v^{'}(s)}{v(s)} = \left(\frac{K_1\omega_o s}{s^2 + K_1\omega_o s + \omega_o^2}\right)\left(\frac{K_2\omega_o s}{s^2 + K_2\omega_o s + \omega_o^2}\right) \tag{4.5}$$

$$H_1(s) = \frac{qv'(s)}{v(s)} = \frac{\left(K_1\omega_o s\right)}{\left(s^2 + K_1\omega_o s + \omega_o^2\right)} \cdot \frac{\left(K_2\omega_o^2 s\right)}{\left(s^2 + K_2\omega_o s + \omega_o^2\right)} \tag{4.6}$$

where K_1 & K_2 are the function of ζ_1 & ζ_2, and they are selected to assure the element SOGI-QSGs of the NISOGIs-QSG remain continuously under-damped. Therefore, to determine the values of K_1 & K_2, a simple methodology has been adopted, where the step response of the in-phase element $(v^{'})$ & quadrature-phase element $(qv)^{'}$ have been plotted at different gain values. Further, those gain values have been considered that exhibit the least settling time. The plot of the step response of the in-phase element $(v^{'})$ at different gains is shown in Fig. 4.3(a) while the plot for the quadrature-phase element $(qv)^{'}$ is depicted in Fig. 4.3(b). Upon evaluation of these plots, it is evident that for values of K_1 = 1.452 & K_2 = 1.8, the in-phase element's $(v^{'})$ settling time is found out to be 24.4ms while the quadrature-phase $(qv)^{'})$ component settles in 22.2ms.

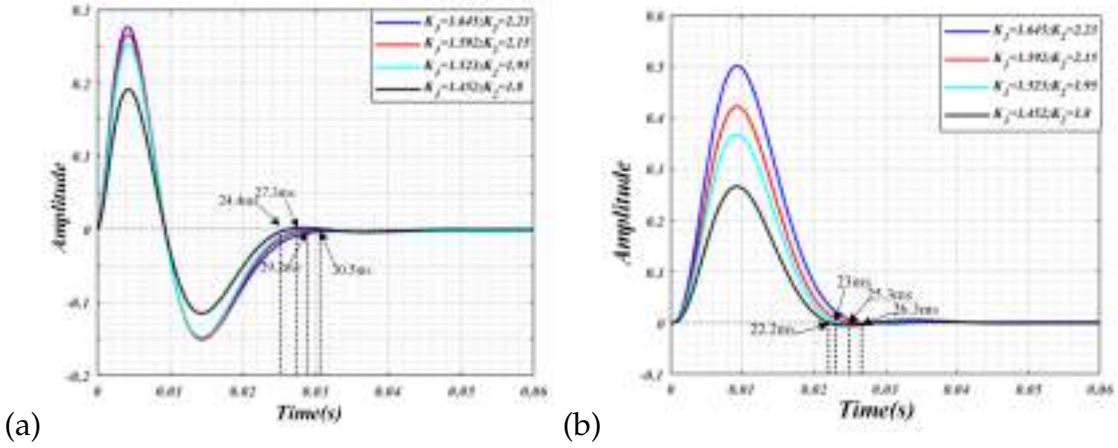

(a) (b)

FIGURE 4.3: (a) Step response of v' for different K_1 & K_2 values and (b) Step response of $qv'$for different K_1 & K_2 values

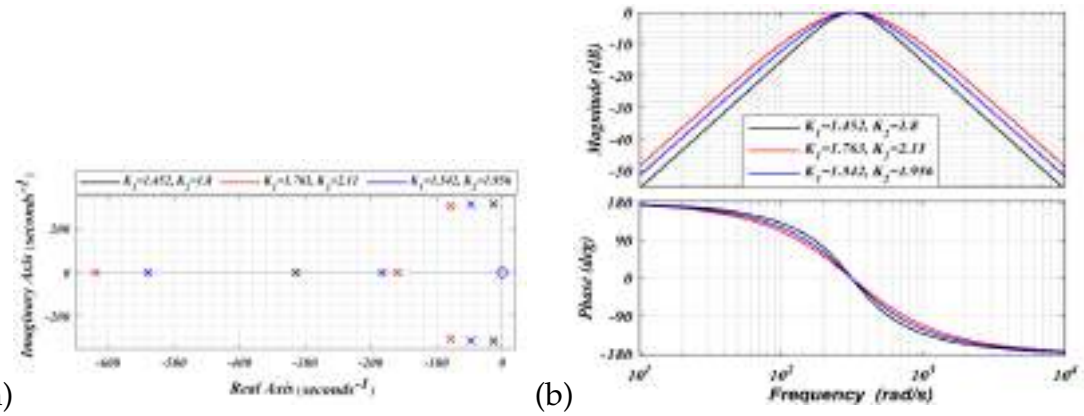

(a) (b)

FIGURE 4.4: (a) Polar plot of the CNISOGI with the different values of gains and (b) Bode plot of the suggested method

The pole-zero trace of the CNISOGI filter is seen in Fig. 4.4(a). Additionally, it is evident that every pole is located on the left side of the hypothetical axis, indicating the system's stability. Also, the Bode plot of the in-phase components of the CNISOGIs-QSG at the various values of K_1 and K_2 are related in Fig. 4.4(b). It is observed that the CNISOGIs-QSG attenuates harmonic components more strongly.

4.2.3 Comparison of the proposed method with the existing methods

Compared to existing approaches, traditional second- and third-order quasi-synchronous generators (QSGs) offered acceptable harmonic mitigation but lacked robustness against DC-offset voltages and grid disturbances. While fourth-order QSGs improved DC-offset rejection, they often resulted in slower dynamic responses, particularly when damping factors were not optimally selected. Moreover, earlier repetitive control (RC) strategies, although effective in steady-state harmonic suppression, tended to degrade under fluctuating grid conditions and transient disturbances, limiting their overall performance.

To address these shortcomings, the proposed Cascaded non-identical SOGI structure combines cascaded SOGIs with nested integration, ensuring superior DC-offset elimination and faster dynamic performance. Simultaneously, a carefully designed repetitive controller enhances both steady-state and dynamic responses under non-ideal grid conditions. Unlike conventional RC-based methods, the present approach systematically addresses steady-state and transient performances even under distorted and unbalanced grids. Consequently, the integration of cascaded non-identical SOGI and RC offers a more robust, accurate, and practical solution for Front-End Converter (FEC) control in grid-interactive electric vehicle chargers.

To further substantiate these claims, the step responses of cascaded non-identical SOGI, based on optimal gain values (K_1 = 1.452 and K_2 = 1.8) obtained through the proposed tuning method, are presented in Fig. 4.5(a) and Fig. 4.5(b) for the in-phase and quadrature components, respectively. For comparison, the step responses based on SO-SOGI and CSOGI structures are also plotted. It is evident that the proposed tuning method achieves the minimum settling times, with the in-phase and quadrature components settling at 24.4 ms and 22.2 ms, respectively, outperforming the other established approaches.

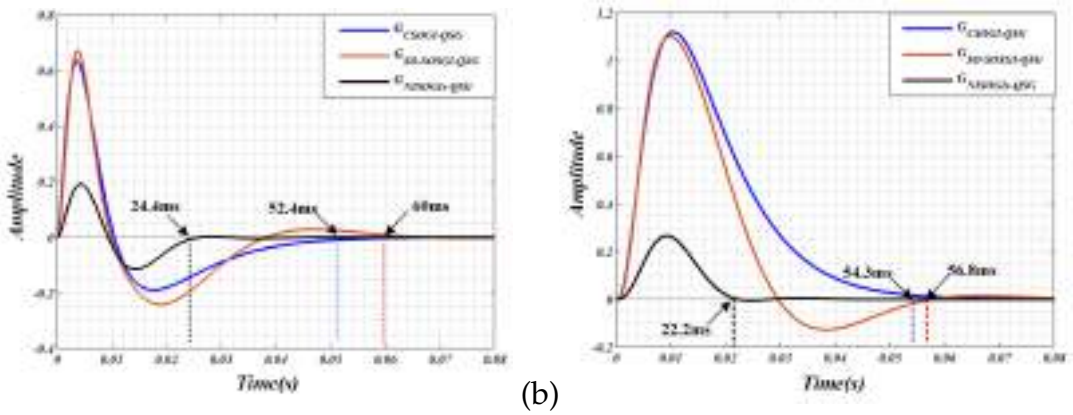

(a) (b)

FIGURE 4.5: An analysis of the step response of the in-phase components for SO-SOGI-QSG (with $K_1 = 1.56$ and $K_2 = 3.11$), CSOGI (with K = 2.66), and CNISOGIs-QSG (with $K_1 = 1.452$ and $K_2 = 1.8$)

TABLE 4.1: Comparison of Different Quadrature Signal Generators

Performance Metric	**Proposed D-QSG**	**CSOGI-QSG [132],[133]**	**SO-SOGI-QSG [134]**	**Conv. SOGI PLL [135],[136]**
Bandwidth	++++	+++	++ (lower)	+ (low)
Computation Burden	384.89ms	384.89ms	394.49ms	395ms
Steady-State Distortion	+ (Better harmonic rej.)	++ (Moderate)	++++ (Sensitive)	++++
Settling Time (In-phase) [136]	24.4ms	52.4ms	60ms	51ms
Noise Rejection [137]	++++	+++	++++	+++
Stability	++++	+++	+	+++
Harmonic Rejection	++++	+++	++	+
Dynamic Tracking	++++	+++	+	++

++++ High, +++ Moderate, ++ Low, + Poor

For the previously indicated amount of K_1 as well as K_2, a Bode diagram and Nyquist plot of a in-phase with quadrature-phase elements for CSOGI-QSG and SO-SOGI-QSG corresponding to cascaded non-identical SOGI-QSG are shown in Figs. 4.6 and 4.7 respectively. It is noticed that the cascaded non-identical SOGIs-QSG deliver stronger attenuation to harmonic components compared to the CSOGI-QSG and SO-SOGI-QSG with better dynamic response. Additionally, we observe that the stability

margin reduces when we go from Cascaded non-identical SOGI-QSG to SO-SOGI-QSG.

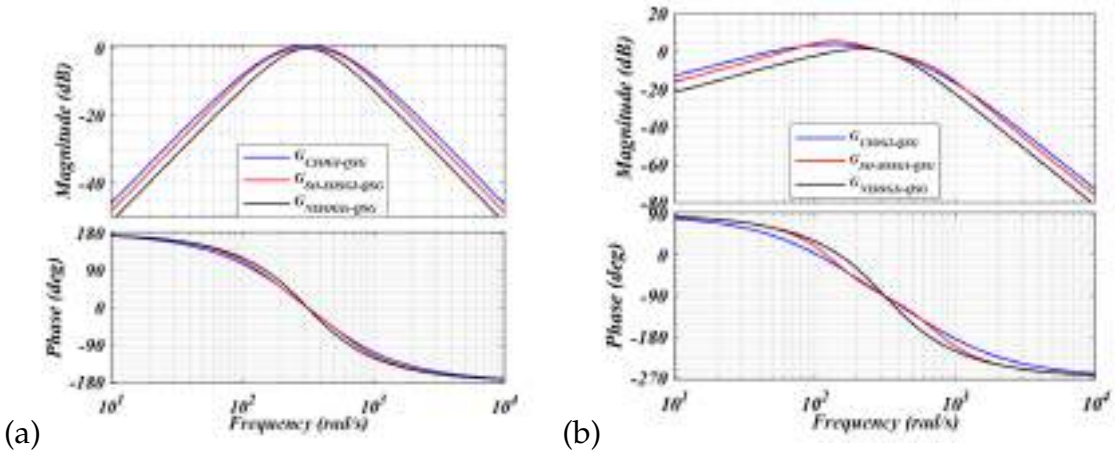

(a) (b)

FIGURE 4.6: Bode Diagram comparison of in-phase components of CNISOGI-QSG ($K_1 = 1.452$ and $K_2 = 1.8$), SO-SOGI-QSG ($K_1 = 1.56$ and $K_2 = 3.11$), and CSOGI ($K = 2.66$).

Moreover, the control performance of FEC depends on the rigid control of DC-link voltage under grid-side disturbance and dynamically changing battery charging/discharging conditions. Therefore, it is of utmost importance to regulate DC-link voltage (V_{DC}) around its reference voltage (V^*_{DC}). Being a DC quantity, a regular PI is sufficient enough to regulate V_{DC} around its reference voltage taken as 400 V. The output of the PI regulator exhibits the fundamental current component I_D required to maintain (V_{DC}) around its reference voltage and is expressed in 4.7.

$$I_D(k) = [(k_p + k_i/s)(V^*_{DC_{ref}}(k) - V_{dc}(k))] \tag{4.7}$$

Here, k_p and k_i indicate the proportional and integral gains of the PI controller. Further, to compensate for the load harmonics and reactive component, the overall active current reference (I_p) is modified by incorporating the fundamental load current component i_{lf} and expressed in 4.8.

$$I_p = I_D + I_{lf} \tag{4.8}$$

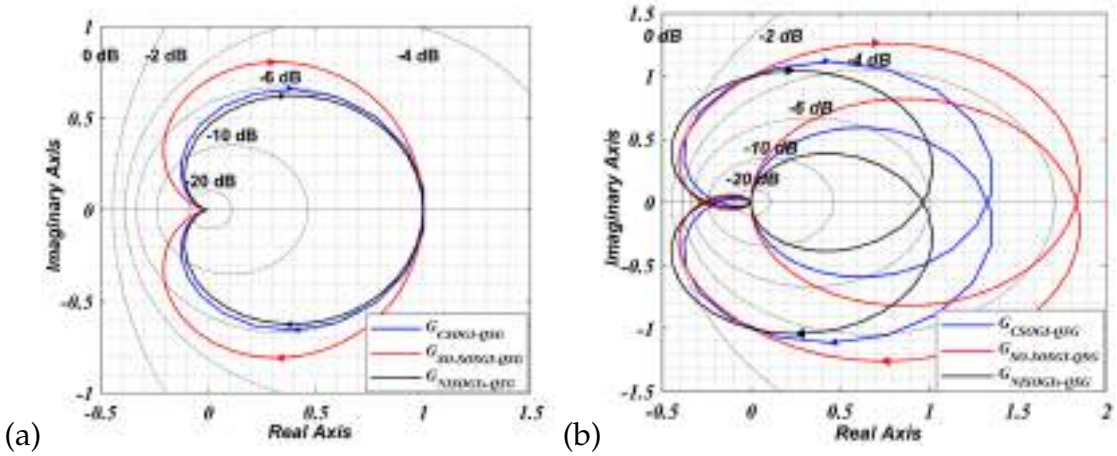

FIGURE 4.7: NYQUIST plot comparison of quadrature-phase components of CNISOGI-QSG ($K_1 = 1.452$ and $K_2 = 1.8$), SO-SOGI-QSG ($K_1 = 1.56$ and $K_2 = 3.11$), and CSOGI ($K = 2.66$).

The active current reference I_p is multiplied with unit voltage template v_{gp} to provide the reference sinusoidal current corresponding to active power as given by 4.9.

$$i_g^* = I_p * v_{gp} \tag{4.9}$$

At last, these desired reference values are, after comparison with the actual grid current i_g, fed to the Hysteresis Current Control (HCC) to compute gating signals for the Grid Side Converter (GSC) IGBT switches.

4.2.4 BDDC Control

The primary goal of BDDC control is to continue charging or draining the battery in spite of grid-side interruptions. Here, the battery is charged using both constant voltage (CV) and constant current (CC). First, CC charging is used to manage battery charging. Once the battery voltage exceeds the allowed permissible voltage level, CV charging is introduced. This technique aids in quick battery charging without going over the charger's rated voltage and current limitations. The only thing left to do is build the battery reference current such that it includes CC/CV charging, as the DC-Link voltage is almost set at the rated voltage. Furthermore, since BDDC is a bidirectional system, its operation may be managed in

both charging and discharging modes. Thus, in order to accomplish the intended goals, the controller must follow the reference current (I_b^*) for the battery, which may be developed based on the requirements. The BDDC's whole controller architecture is seen in Fig. 4.1.

4.3 RESULT AND DISCUSSION

Therefore, the efficacy of the charger is done and well presented in two subsections as follows:

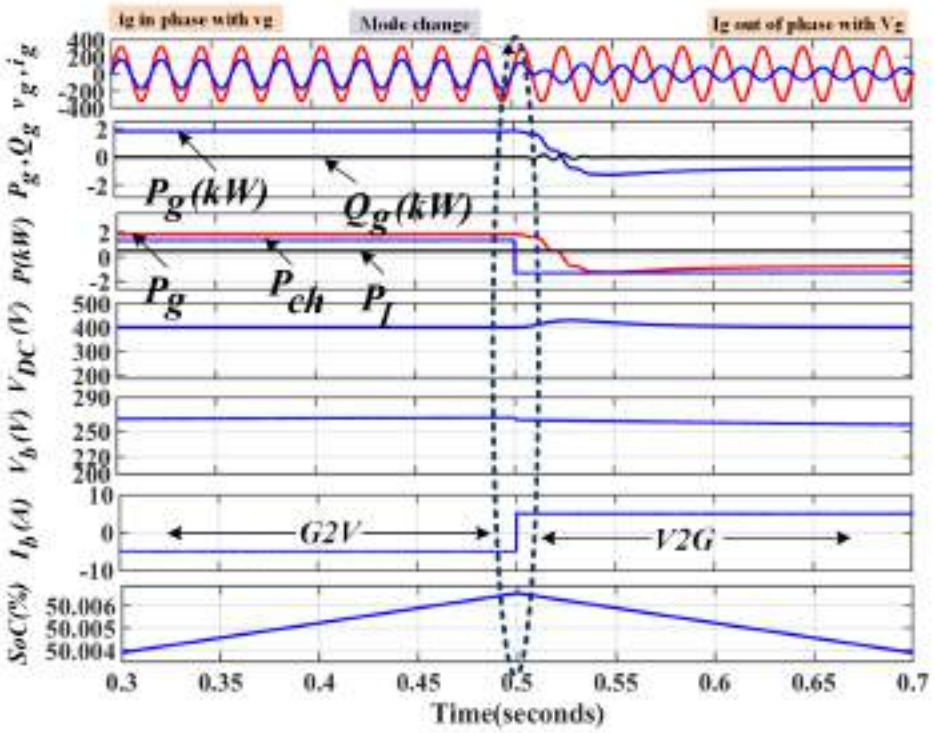

FIGURE 4.8: Steady state performance under normal operating conditions.

4.3.1 SIMULATION VALIDATION

Using a variety of Simscape library components, the system is methodically designed and simulated in MATLAB/Simulink. A 230 v_{rms}, 50 Hz

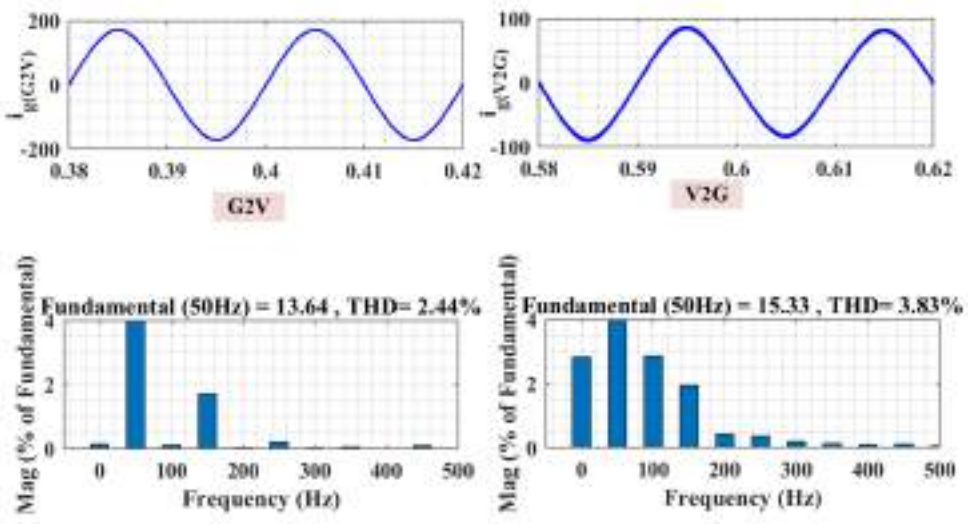

FIGURE 4.9: Keywaveforms showing the THDs for the G2V/V2G modes.

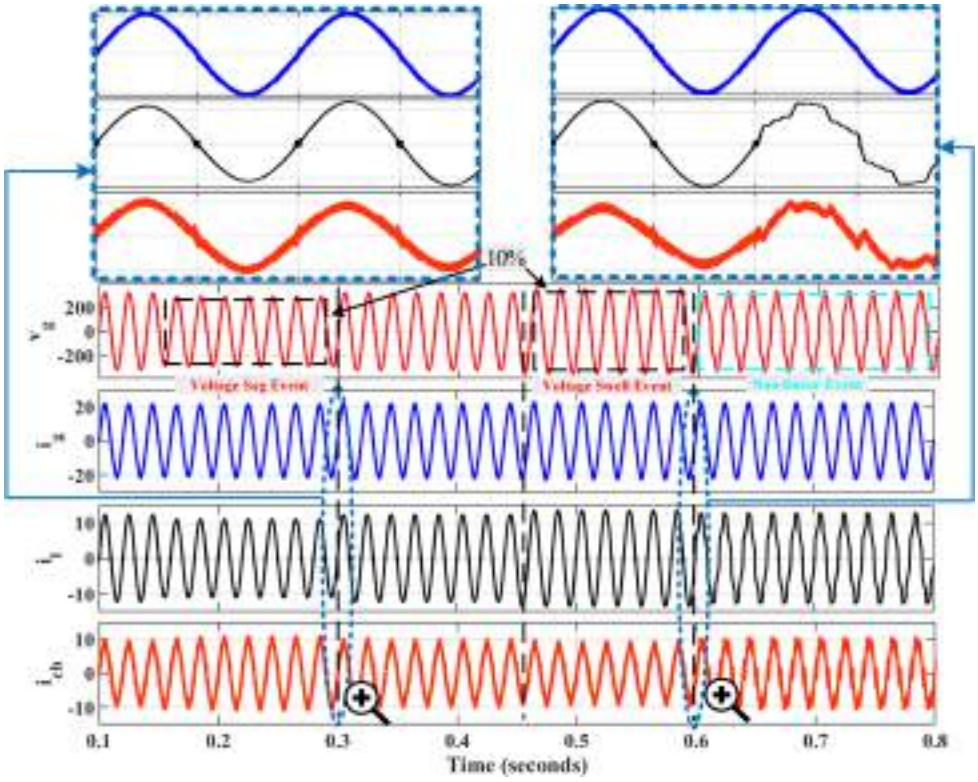

FIGURE 4.10: Trace of the currents at the point of common coupling (PCC).

single-phase supply is used as the input for the OBBC FEC. Additionally, a non-linear load that represents the normal home load has been linked to the PCC. Results from the simulation are available for two distinct periods. Fig. 4.8 illustrates the controller's performance in the first phase while operating in the G2V and V2G modes. To enable UPF grid operation, the charger initially operates in G2V mode while meeting the reactive power needs of adjacent loads. The transition from G2V to V2G mode of operation occurs at 0.5 seconds. It is important to note that the transition between the two modes of operation is quite seamless. Furthermore, since the charger side is the sole source of reactive power, the grid always runs at UPF even when reactive power demand is at PCC. As the grid's present profile makes clear, the grid must only ever interact with active electricity. While the grid current operates in phase with the grid voltage in the G2V mode, it is out of phase with the grid voltage in the V2G mode. Furthermore, THDs for the cases such that G2V/V2G modes are depicted in Fig. 4.9. It can be noted that in G2V mode THD of the grid current is 2.44% while 3.83% in V2G mode.

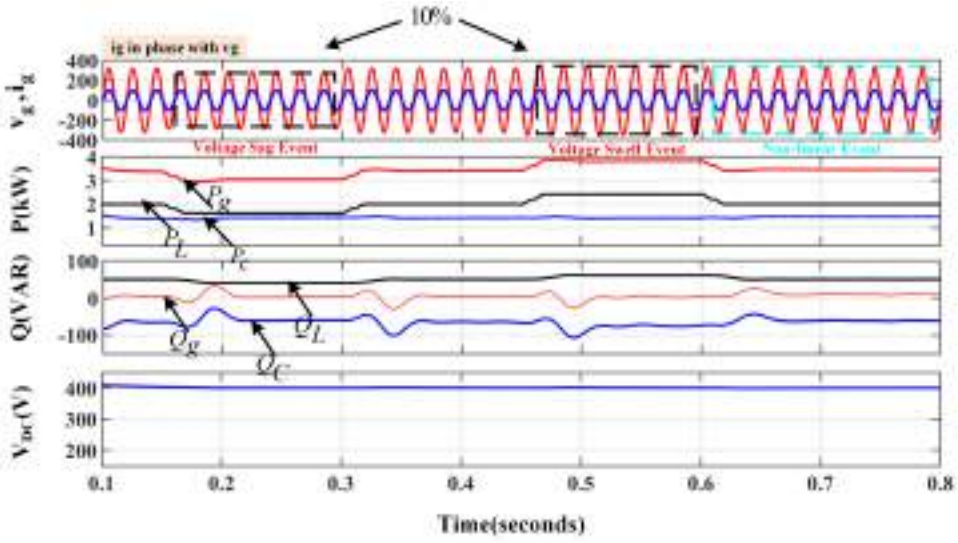

FIGURE 4.11: Steady state performance when harmonics are injected (weak grid operating condition).

During the second operating phase, various grid-side voltage disturbances are taken into consideration for system functioning. Here, as shown in Figs.

4.10 and 4.11, the voltage sag as well as swell of 10% with voltage THDs of 15% have been taken to examine the control performance of the charger. At first, as was previously said, the charger operates under typical grid circumstances. There is a voltage drop that occurs in 0.15 to 0.3 seconds. The voltage returns to normal between 0.3 and 0.45. Finally, from 0.6 to 0.8, the non-linear grid voltage with 15% THDs is taken into consideration. A voltage swell is inserted between 0.45 and 0.6. The waveforms for load current, FEC current, grid voltage, and grid current are shown in Fig. 4.10. Here, the FEC is set up to readily correct for both load harmonics and reactive power while concurrently charging the battery under various grid voltage disruptions. The grid voltage, current, active/reactive power of the FEC, load, and grid along the DC-Link voltage are all shown in Fig. 4.11, which further supports this claim. Here, grid voltage and grid current at UPF are always sinusoidal. This is further shown by the almost negligible reactive power on the grid side, which is a complement to the reactive power on the load from the charger.

The 10% sag and swell event at the source side is depicted in Figure 4.12. As a result, it is evident that while reactive power fluctuates somewhat, active power does not. On the PCC side, there is also an active power balancing shown. Moreover, V_{DC} (145V), V_b (56V), and I_b(-5A) all show almost constant values. Moreover, Figure 4.13 displays the THDs of the corresponding occurrences. For i_g, 2.68% THD is achieved during the sag event, whereas 3.83% THD happened for the i_g during the swell event.

The initial reaction of the system to a dynamic loading situation is shown in Figure 4.14. The majority of domestic loads are non-linear loads linked to the PCC; these loads' increments and decreases cause the system to behave dynamically while it is charging. such that there is propotional change in the i_g with these increments of non-linear load. Furthermore, it is noted that %SoC is found to be virtually linearly growing and that the stiffness of the V_{DC} (145V), V_b (56V), and I_b(-5A) is maintained during the whole operation.

From this point forward, changes in the non-linear demand at the PCC cause changes in the Active Power (P) and Reactive Power (Q) that the grid supplies in the charging mode. It is noteworthy that reducing load

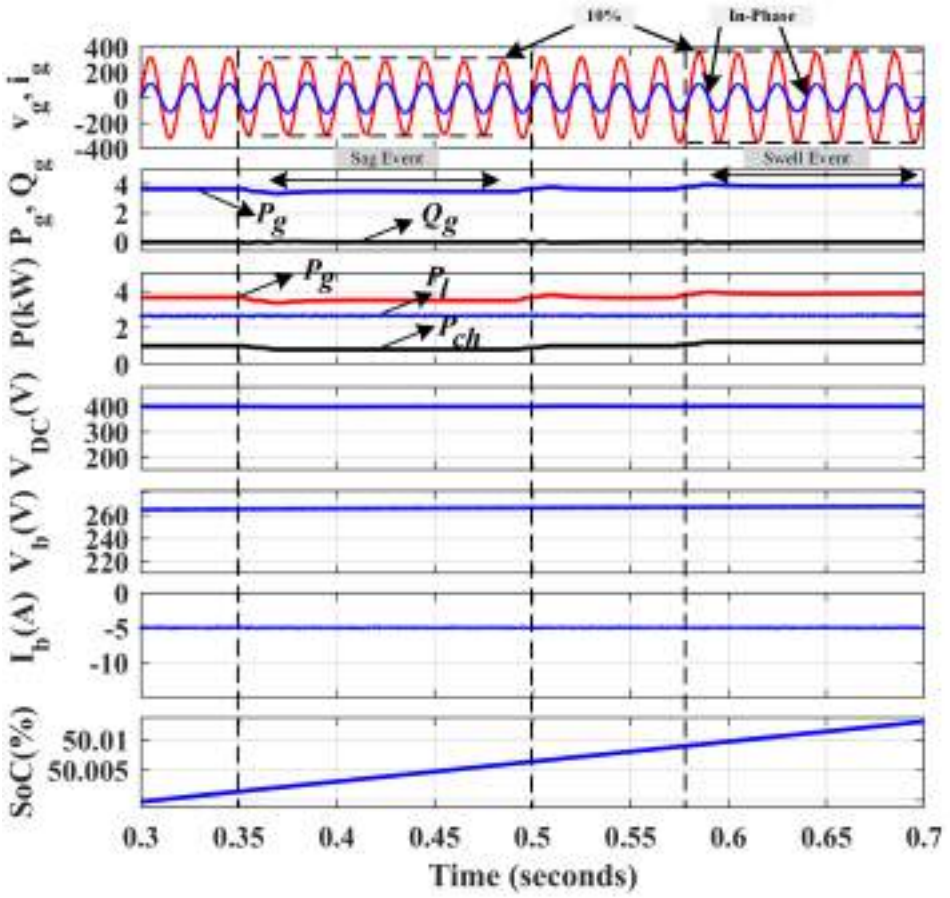

FIGURE 4.12: Simulated waveform for the sag and swell event.

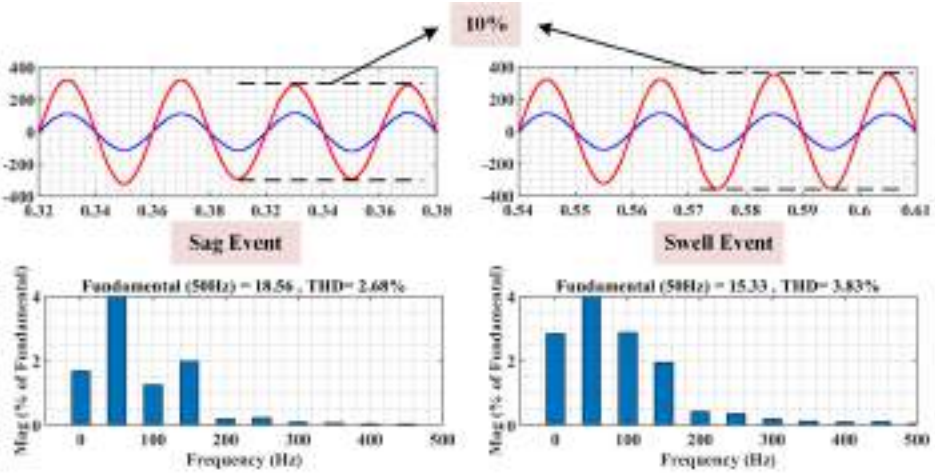

FIGURE 4.13: Simulated waveform for the sag and swell event.

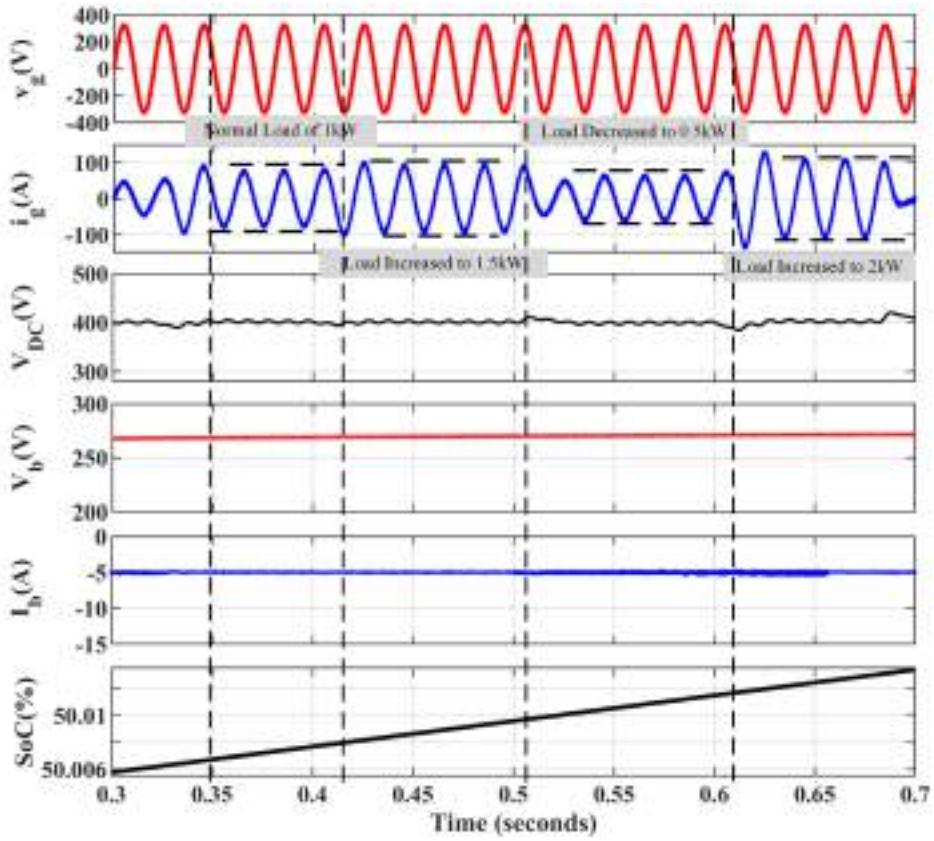

FIGURE 4.14: Dynamics behaviour of the system.

harmonics and reactive power consumption at PCC is one of the goals of the proposed charger's FEC. Here, the grid side current control reference only contains the fundamental component; the reactive and harmonic components must come from the converter side. This is an example of an indirect control strategy for DC link control. So, an almost negligible amount of reactive power is supplied from the grid while FEC acts as reactive power support at the PCC. Also, Q_g, Q_l, and Q_{ch} are grid, load, charger reactive power respectively. Similarly, irrespective of dynamics at the PCC balance of active power is maintained as shown in Figure 4.15.

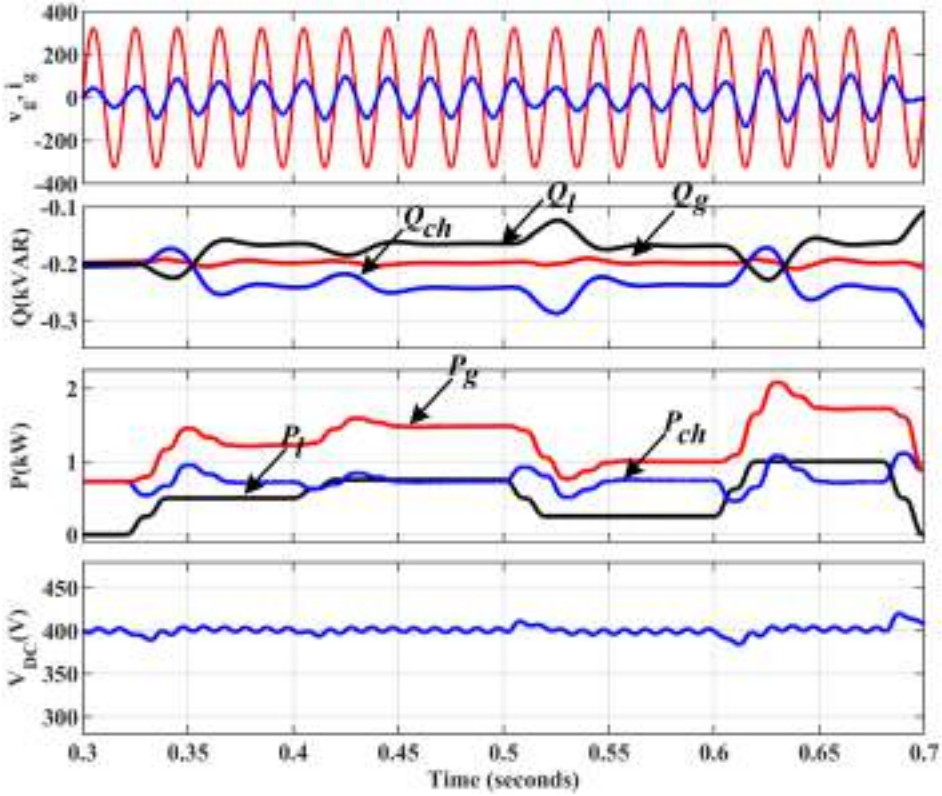

FIGURE 4.15: Power balance when the dynamics occur.

4.4 CONCLUSION

This chapter presented a comprehensive study of various control strategies for grid-interactive EV charging systems, with a particular focus on a fourth-order Cascaded Non-Identical Second-Order Generalized Integrator (CNISOGI)-based control scheme. A comprehensive comparison of CNISOGI with the other existing techniques like SO-SOGI and CSOGI in terms of step response, which was found to be 24.4 ms, Bode plot, Nyquist plots, etc. Also, the CNISOGI technique proved effective in handling grid disturbances such as voltage sag, swell, and harmonics by precisely estimating synchronizing voltage templates and maintaining sinusoidal grid current even under distorted conditions. Additionally, the method was utilized for load compensation, enabling reactive power support and harmonic mitigation while regulating active and reactive power in both G2V and V2G modes. The performance of the proposed control strategy is

validated through MATLAB/Simulink simulations, demonstrating dynamic robustness and grid compliance.

A comprehension study of various control strategies for grid-interactive EV chargers has been done. Also, simulation validation of the system under different scenarios is obtained. Now, to have more practical realization of the system, a real-time simulation has been performed and discussed in Chapter 5. Chapter 5 is another level of testing of the developed charger. OPAL-rt technologies make real-time simulator is used for the real-time implementation.

Chapter 5

Real-Time Investigation of Grid-Interactive EV Charger under Wide Voltage Range Scenarios

5.1 INTRODUCTION

In this chapter, a real-time investigation is carried out to evaluate the performance of the proposed grid-interactive bidirectional EV charger under a wide range of voltage conditions, including sags, swells, harmonics, and transient disturbances. As electric vehicles evolve from passive loads to active grid-support assets, it becomes essential to validate their behavior in dynamic grid environments to ensure compliance, stability, and responsiveness. The focus of this chapter is on analyzing the system's capability to operate reliably during voltage abnormalities while maintaining active and reactive power exchange, voltage regulation, and unity power factor. Using the OPAL-RT real-time simulation platform, the developed control algorithm incorporating CNISOGI-based signal processing and dynamic reference generation is tested in Hardware-in-the-Loop (HIL) mode to closely replicate real-world grid behavior. The chapter also includes coordinated testing with a laboratory hardware prototype, ensuring that both software and hardware elements of the charger respond effectively to sudden grid disturbances. This

investigation demonstrates the robustness and adaptability of the proposed control architecture under practical voltage fluctuation scenarios.

5.2 Control Technique used for the Real-time simulation

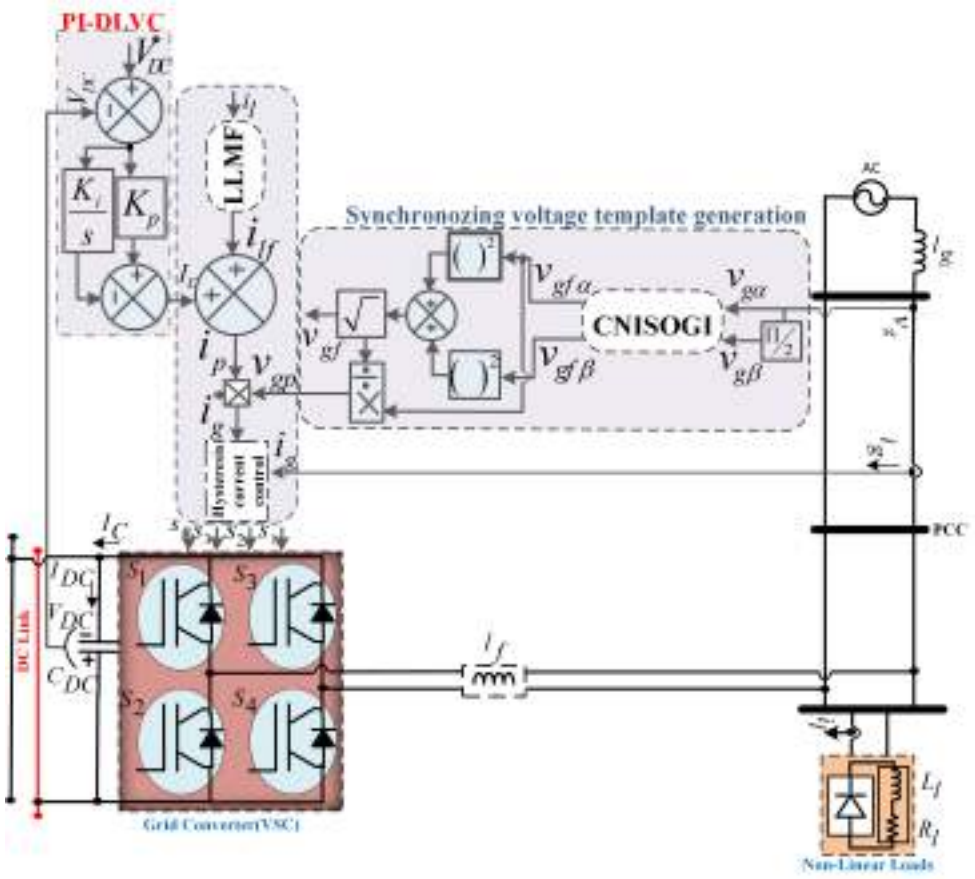

FIGURE 5.1: Control schematic for grid connected EV charger

Fig. 5.1 shows the control logic used for AC/DC converter stage. The system description is already discussed in Section 3.1. Also, the controller description is given in Section 4.2.2. The only difference is the use of the LLMF filter used to extract the fundamental from the load current. The unit template generation from the grid voltage v_g is carried out through

CNISOGI. Architecture block diagram, polar and bode plots of the CNISOGI is depicted in Fig. 5.2.

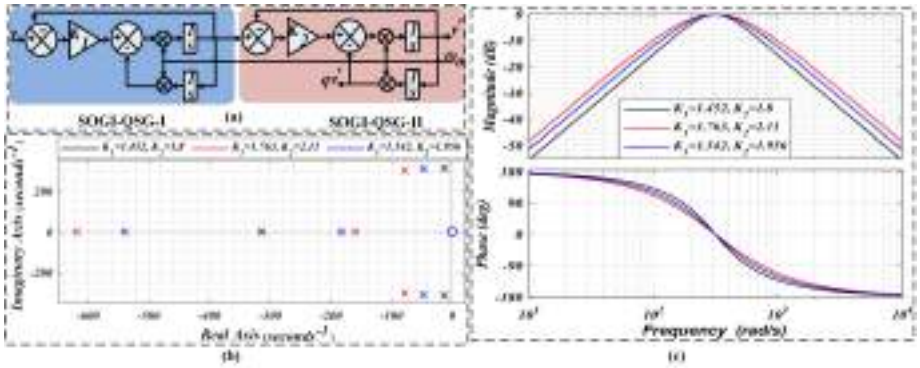

FIGURE 5.2: Block schematic of the CNISOGI-QSG, (b) Polar plot of suggested CNISOGI-QSG, (c) Bode Plot of suggested CNISOGI-QSG

Henceforth, to validate the effectiveness of the proposed method in extracting the in-phase and quadrature components out of a non-ideal voltage signal, an input supply comprising 5^{th}, 7^{th}, 11^{th}, and 13^{th} harmonics and a dc offset, with overall THD of 15% has been considered as shown in Fig.5.3. The extracted values of in-phase and quadrature components utilizing and CNISOGI can be observed. On analyzing these waveforms, it can be observed that CSOGI and SO-SOGI are not immune to grid side disturbances as they introduce DC-Offset and ripples in extracted components. However, the CNISOGIs approach tackles the grid side THDs effortlessly and extracts the fundamental component without any DC offset and ripples. Henceforth, comparison in terms of computational burden of proposed method (CNISOGI) with the other methods i.e CSOGI, SO-SOGI were performed on the real-time simulator using d-Space-1104s. So, the proposed filter takes 3.7365E-05 while CSOGI takes 3.8489E-05 and SO-SOGI takes 3.94496E-05 turnaround time on the sample time of 5E-05. Therefore, it can be concluded that CNISOGI is 3.008% and 5.579% efficient than CSOGI and SO-SOGI respectively.

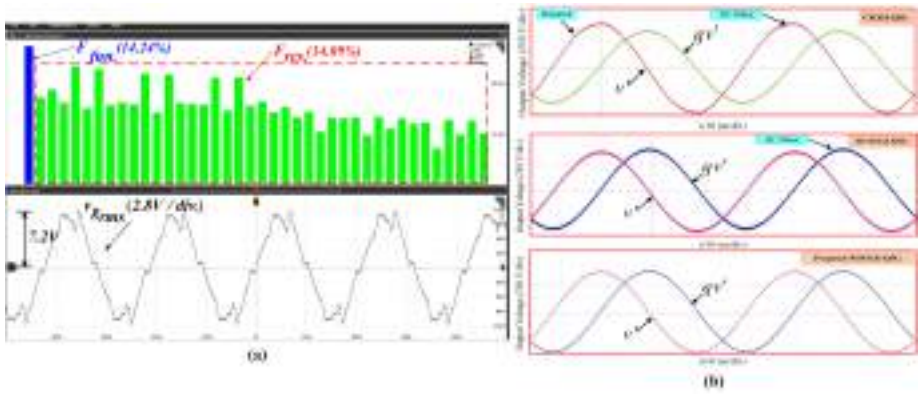

FIGURE 5.3: (a) With an overall THD of 15%, the grid voltage consists of 5^{th}, 7^{th}, 11^{th}, and 13^{th} harmonics plus a DC offset, (b) Waveforms of the simulated output, $v^{'}$ spectrums, and $qv^{'}$ spectrums for various QSG with respect to output waveform

5.2.1 Estimation of the Active Weight Loss Component of load current

To calculate the switching loss within the shunt compensator, V_{DC}^{*}, V_{DC} is passed through a low-pass filter (LPF). Given the inaccuracy of V_{DC} for feedback, a proportional-integral (PI) controller estimates the active component of the DC-link voltage regulation and the losses generated by the PI-DC link voltage controller (DLVC). A stable $V_{DC} = 400$V is maintained.

$$\omega_{\text{loss}}(n+1) = \omega_p(n) + \left[k_p\{V_{dce}(n+1) - V_{dce}(n)\} + k_i\{V_{dce}(n+1)\}\right] \quad (5.1)$$

where, the constants for integral & proportional controller gains are represented by the letters k_i and k_p.

5.2.2 Generation of Grid reference Current & Gating Pulses

About getting the pulse load current is fed to the LLMF filter as shown in Fig. 5.4 (for Eqn (59) explained in Section V) which gives the $\omega_p(n) = i_{lf}$. Also. it illustrates an advanced adaptive algorithm tailored for real-time parameter estimation in signal processing systems. It begins with the error

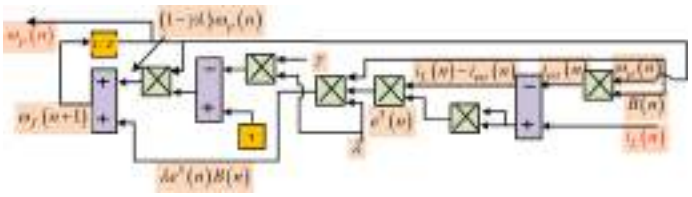

FIGURE 5.4: Circuit Diagram of LLMF Control Architecture

signal, derived from the difference between the input current ($i_L(n)$) and its estimate ($i_{est}(n)$), which is further processed through a cubic error term ($e^3(n)$) scaled by the adaptation constant (λ). This contributes to updating the estimated frequency ($\omega_f(n+1)$) via a summation block. The feedback loop, involving the proportional gain (γ) and a modulation factor $(1-\gamma\lambda)$, ensures stable dynamic performance and fast convergence. A recursive delay element ($1/Z$) synchronizes the frequency update with real-time input, while dynamic coefficients $B(n)$ adaptively adjust corrections to minimize error under varying conditions. By combining third-order error correction and adaptive feedback, this algorithm achieves exceptional precision and robustness, making it highly effective for applications requiring reliable real-time parameter tracking, such as power systems and grid synchronization.

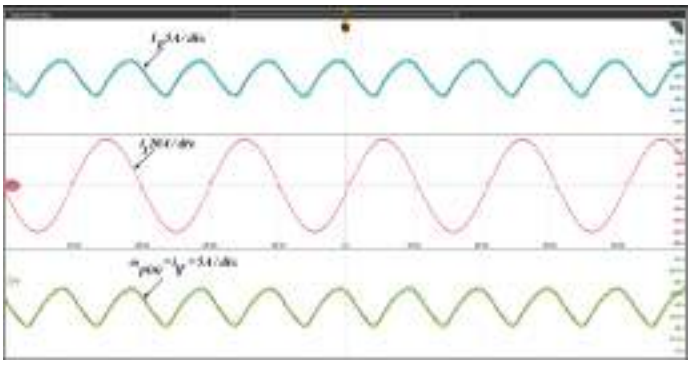

FIGURE 5.5: Active fundamental weight (ω_p) and active current reference (I_p)

Henceforth, Fig. 5.5 validates about the active fundamental weight (ω_p) and active current reference (I_p). As discussed earlier, that (ω_p) is the filtered part of the load current generated by the LLMF.

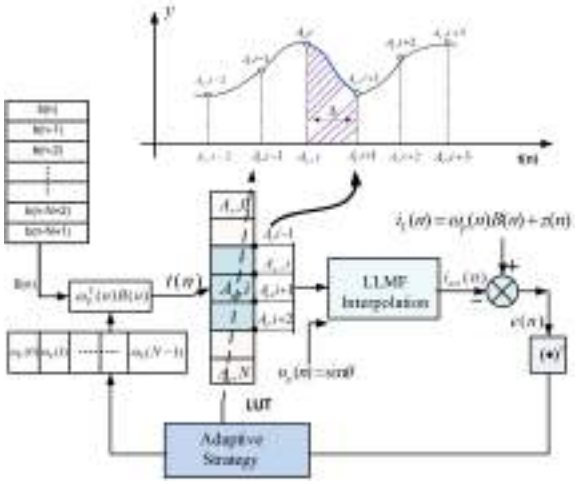

FIGURE 5.6: Weight updating structure of LLMF adaptive algorithm

5.3 Mathematical Modeling of Leaky Least Mean Fourth algorithm

LLMF algorithm is a member of an entirely novel category of stochastic gradient descent-based algorithms that aims to reduce mean fourth error, has become convex function for weight vector that is adaptable. Compared to the LMF method, the LLMF algorithm has a smaller steady-state error and quicker initial convergence, which is its main strength. As depicted in Fig. 5.6, N symbolizes the overall amount of matrix vectors.

The initial stages of interpolation involve identifying the interval index i that aligns with the input signal t(n) and allocating the interpolation intervals, which are pivotal steps in the process. The control points for the look-up table (LUT) are given as follows:

$$\mathbf{A}_N \in \mathbb{R}^{A\times 1} = \begin{bmatrix} A_1 & A_2 & A_3 & \cdots & A_N \end{bmatrix}^T \tag{5.2}$$

where the i-th control point denotes the A_i and $\mathbf{A}_N \in \mathbb{R}^{4\times 1} = \begin{bmatrix} A_{i-1} & A_i & A_{i+1} & A_{i+2} \end{bmatrix}$ for the i-th span. Additionally, by deducting the LLMF interpolation output from the actual load current $i_L(n)$, an error, $e(n)$, is derived. Once load dynamics are achieved, this adaptive progression is maintained until a stable condition is attained.

Let us presume that the system receives the signal $B(n)$ together with a new weight coefficient vector:

$$\boldsymbol{\omega}_p(n) = \begin{bmatrix} \omega_p(0) & \omega_p(1) & \omega_p(2) & \dots & \omega_p(N-1) \end{bmatrix}^T; \tag{5.3}$$

and that the observed output signal $i_L(n)$ is given by 5.4.

$$i_L(n) = \boldsymbol{\omega}_p(n) \times \mathbf{B}(n) + z(n) \tag{5.4}$$

where,

$$\mathbf{B}(n) = \begin{bmatrix} b(n) & b(n-1) & \cdots & b(n-N+1) \end{bmatrix}^T \tag{5.5}$$

$z(n)$ represents the discovered noise, where is considered to be independent of $\mathbf{B}(n)$, and shows the vector of the input signal $\mathbf{B}(n)$.

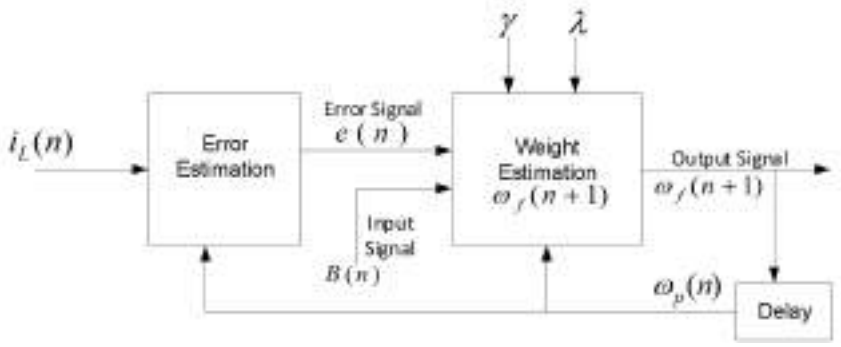

FIGURE 5.7: Block diagram of LLMF control algorithm

The objective is to use the input signal $B(n)$ and the measured output signal $i_L(n)$ to adaptively estimate the undefined channel coefficient vector $\boldsymbol{\omega}_p(n)$. In Fig. 5.7, the LLMF block diagram is shown. Utilizing this block allows for the real-time estimation of the load current's basic weight and variations in weight. Comparing the LLMF control approach to the LMF method, it has been shown that the latter rapidly decreases the error to zero.

In any AC system, the nonlinear load comprises the total of the fundamental and harmonic components, shown as:

$$i_L(t) = i_{L1}\sin(\omega t + \theta) + i_{L2}\sin(2\omega t + \theta) + \cdots \mathrm{Y} \tag{5.6}$$

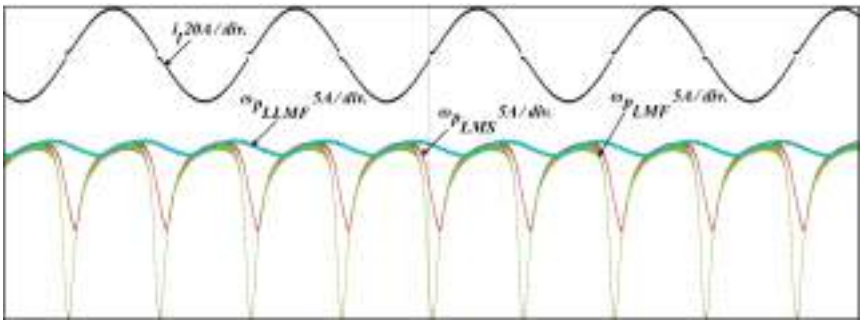

FIGURE 5.8: Fundamental Active weight of load current

$$i_L(t) = i_{L1}\sin(\omega t + \theta) + \sum_{r=2}^{\infty} i_{Lr}\sin(r\omega t + \theta_r) \tag{5.7}$$

where r denotes the order of harmonics; θ_r represents the harmonic phase angle; ω is the angular frequency for the fundamental harmonics; i_{L1} is the fundamental component, and i_{Lr} is the r-th harmonic component for the current. The equation follows as:

$$i_L(t) = i_{L1}[\sin(\omega t)\cos(\theta) + \sin(\theta)\cos(\omega t)] + \sum_{r=2}^{\infty} i_{Lr}[\sin(r\omega t)\cos(\theta_r) + \cos(r\omega t)\sin(\theta_r)] \tag{5.8}$$

$$i_L(t) = i_{L1}[\sin(\omega t)\cos(\theta) + \sin(\theta)\cos(\omega t)] + \sum_{r=2}^{\infty} i_{Lr}[\sin(r\omega t)\cos(\theta_r) + \cos(r\omega t)\sin(\theta_r)] \tag{5.9}$$

Substitute $i_{L1}\cos(\theta), i_{L1}\sin(\theta), i_{Lr}\cos(\theta_r), i_{Lr}\sin(\theta_r)$ with $\omega_p(0), \omega_p(1), \omega_p(2), \omega_p(3)$ respectively, and neglect even-numbered harmonics:

$$i_L(t) = [\omega_p(0)\sin(\omega t) + \omega_p(1)\cos(\omega t)] + \sum_{r=3,5,\ldots}^{\infty} [\omega_p(2)\sin(r\omega t) + \omega_p(3)\cos(r\omega t)] \tag{5.10}$$

In matrix form,

$$\begin{bmatrix}\omega_p(0) & \omega_p(1) & \omega_p(2) & \omega_p(3) & \cdots & \cdots\end{bmatrix}\begin{bmatrix}\sin(\omega t)\\ \cos(\omega t)\\ \sin(3\omega t)\\ \cos(3\omega t)\\ \vdots\\ \vdots\end{bmatrix} \tag{5.11}$$

where,

$\mathbf{B}(n) = \begin{bmatrix}\sin(\omega t) & \cos(\omega t) & \sin(3\omega t) & \cos(3\omega t) & \cdots & \infty\end{bmatrix}^T$

$\boldsymbol{\omega}_p(n) = \begin{bmatrix}\omega_p(0) & \omega_p(1) & \omega_p(2) & \omega_p(3) & \cdots & \cdots\end{bmatrix}$

Further, these are used to calculate the load current presented as:

$$i_{\text{est}}(n) = \boldsymbol{\omega}_p(n) \times \mathbf{B}(n) \tag{5.12}$$

Let the actual nonlinear load current and rough current be $i_L(n)$ and $i_{\text{est}}(n)$ respectively, used to assess the error signal $e(n)$:

$$e(n) = i_L(n) - \boldsymbol{\omega}_p(n) \times \mathbf{B}(n) \tag{5.13}$$

With the LMF method, the cost function that has to be reduced is given by:

$$C_{\text{LMF}}(n) = \frac{1}{4}e^4(n) = \frac{1}{4}\left[i_L(n) - \boldsymbol{\omega}_p(n)\mathbf{B}(n)\right]^4 \tag{5.14}$$

The LLMF algorithm, together with the leakage parameter (γ), introduces the modified LMF cost function. Consequently, the LLMF's minimal cost function is:

$$C_{\text{LLMF}}(n) = \frac{1}{4}e^4(n) + 2\gamma\|\boldsymbol{\omega}_p(n)\|^2 \tag{5.15}$$

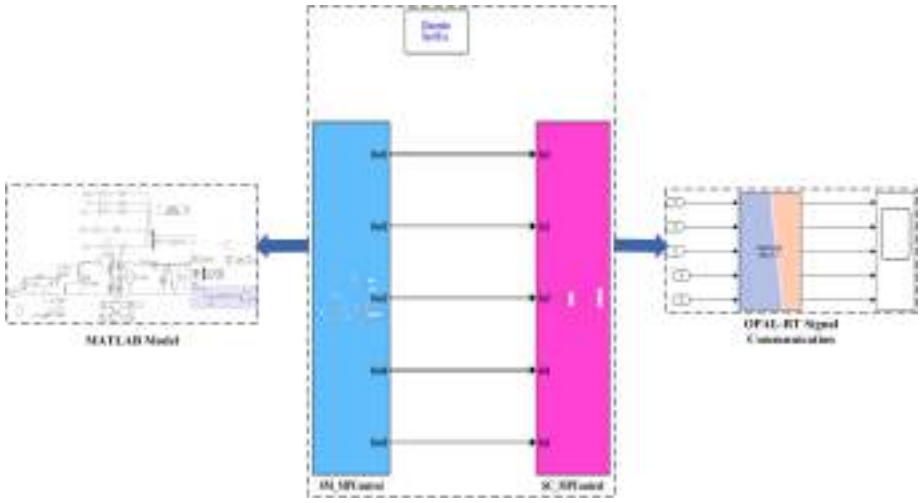

FIGURE 5.9: OPAL-RT Simulator Model.

To get the partial derivative for the cost function in relation to the weight vector, the gradient estimate is defined as:

$$\frac{\partial C(n)}{\partial \boldsymbol{\omega}_p(n)} = \Big(\gamma \boldsymbol{\omega}_p(n) - e^3(n)\mathbf{B}(n)\Big) \tag{5.16}$$

The gradient approach, sometimes referred to as the weight update equation of the LLMF, may be used iteratively to find the minimum of $C(n)$:

$$\boldsymbol{\omega}_f(n+1) = \boldsymbol{\omega}_p(n) - \lambda \frac{\partial C(n)}{\partial \boldsymbol{\omega}_p(n)} \tag{5.17}$$

$$= \boldsymbol{\omega}_p(n) - \lambda \Big(\gamma \boldsymbol{\omega}_p(n) - e^3(n)\mathbf{B}(n)\Big) \tag{5.18}$$

$$\boldsymbol{\omega}_f(n+1) = \boldsymbol{\omega}_p(n)(1-\lambda\gamma) + \lambda e^3(n)\mathbf{B}(n) \tag{5.19}$$

where λ denotes the adaptation constant, γ is the learning rate, and its value ranges between 0 and 1.

Henceforth, the precision of LLMF is shown in Fig. 5.8 where, for a load current of 20A/div, the active fundamental weight of different filter

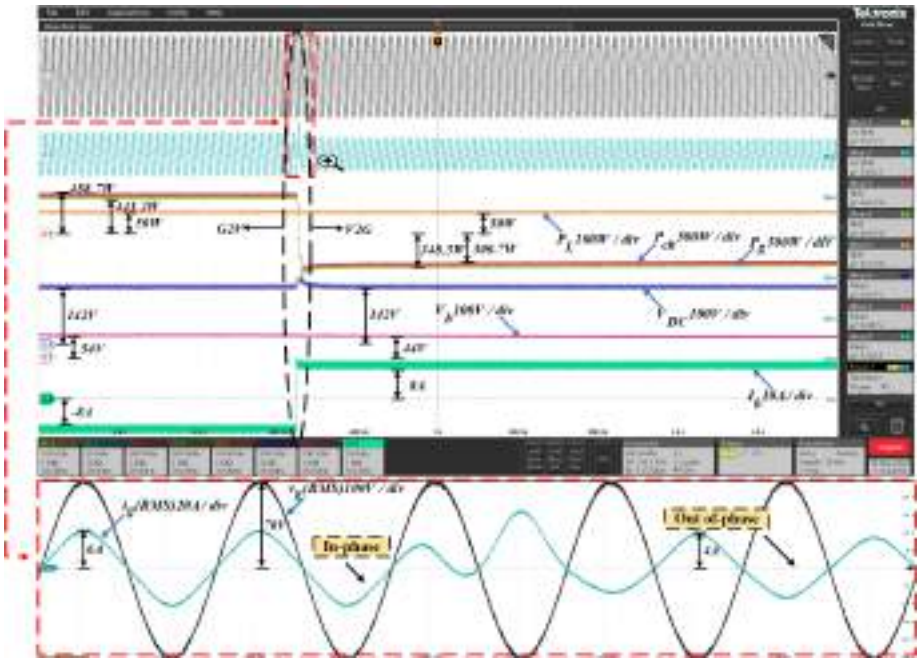

FIGURE 5.10: Real-time HIL of Steady-state performance under normal operating conditions

methods is compared, and it can be observed that among LMS and LMF, LLMF gives a better result.

5.4 Real-time Simulation Results and Discussion

The Real-time simulation setup has been discussed in section 3.1. In addition, OPAL-RT ensures smooth integration and accurate control by combining hardware and software synchronization options in a synergistic manner. In particular, the software synchronized mode is used for analysis in order to carefully assess the control method's effectiveness. The system performance is validated using MATLAB 2018a and the OP4510 model of RT-Lab 2019.2.3. Additionally, this part provides a comprehensive exhibition of the platform-obtained example test results depicted in 5.9., which serve to successfully reinforce the resilience and usefulness of the designed controller.

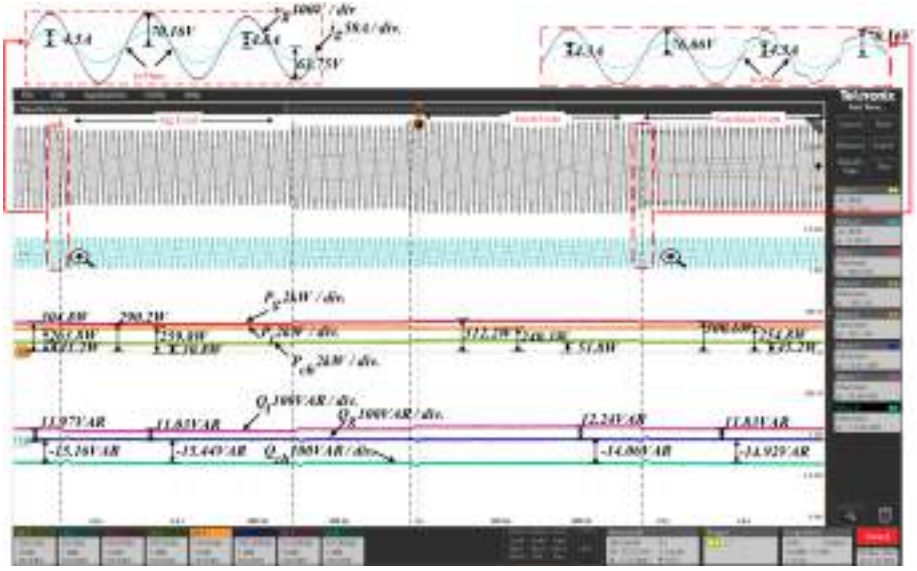

FIGURE 5.11: Real-time validation of Steady-state performance when harmonics are injected (weak grid operating condition)

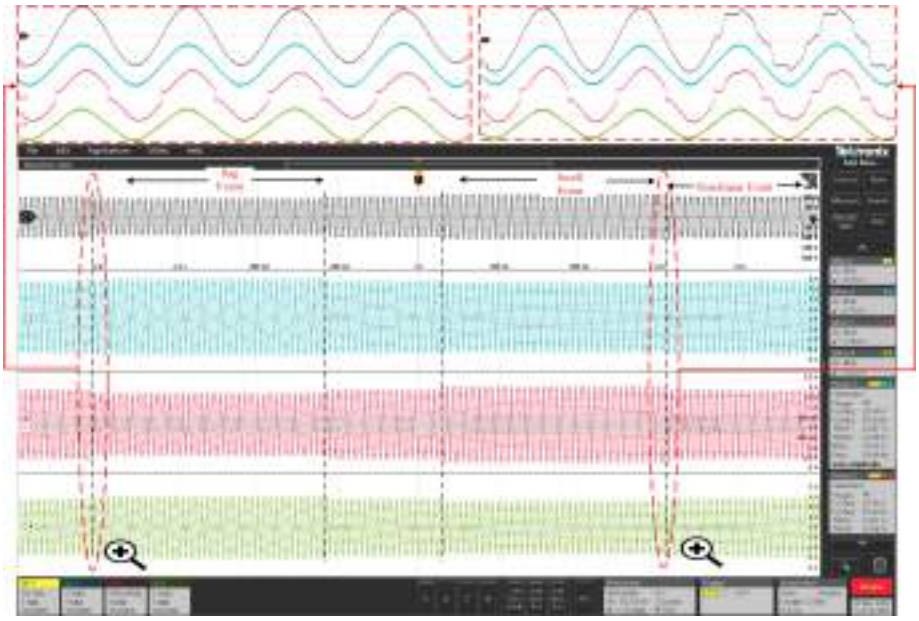

FIGURE 5.12: Real-time HIL of Grid voltage (v_g), Grid current (i_g), load current (i_l), and FEC current (i_{ch}).

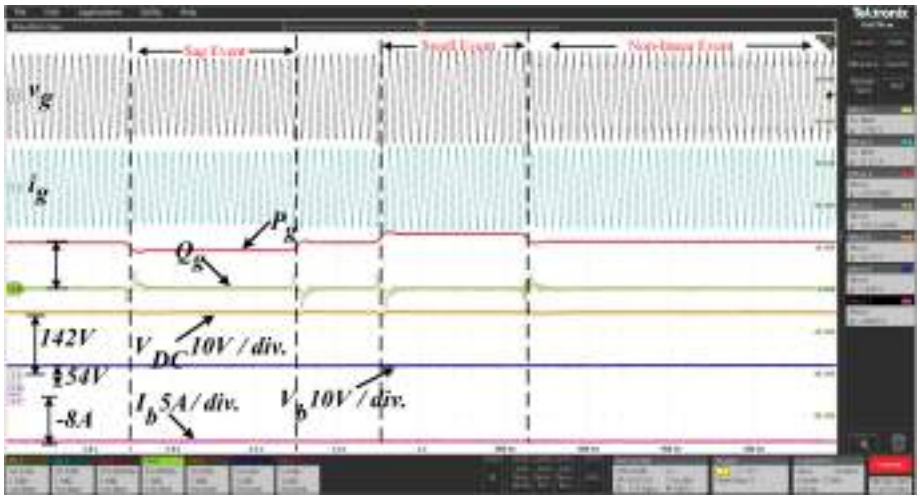

FIGURE 5.13: Real-time validation of Steady-state performance when sag & swell in grid voltage

Fig. 5.10 illustrates the Grid Voltage $v_g = 70v_{rms}$ at 100V/div. on Channel 1, and the real-time HIL results of the mode change from G2V to V2G. Channel 2 is devoted to Grid Current i_g. In charging mode (G2V), it draws a current of 6A (20A/div), and in discharging mode (G2V to V2G), it injects a current of 4A. The seamless transition from G2V to V2G with guaranteed UPF grid functioning while providing the load reactive demand from the FEC side alone is seen in the magnified version of v_g and i_g below. The power used by the load (50W) and charger (440W) in the presence of a non-linear load connected at PCC may be determined to be provided by the grid (500W) during G2V. After that, a reversal of power flow is seen as soon as the transition takes place. This is because the load (50W) is receiving the required power from the charger (350W), and the excess power (290W) is being delivered into the grid, creating an out-of-phase grid current. Throughout all modes of operation, the DC-link voltage and battery voltage, which are 140V at 100V/div and 54V at 100V/div, respectively, are kept constant. Indicating the G2V and V2G modes of operation, the battery current may also follow the reference current change from -8A to 8A at 10A/div.

Figs. 5.11, 5.12, and 5.13 show how the system might behave dynamically under non-ideal voltage settings. Initially, the optimal voltage is applied in

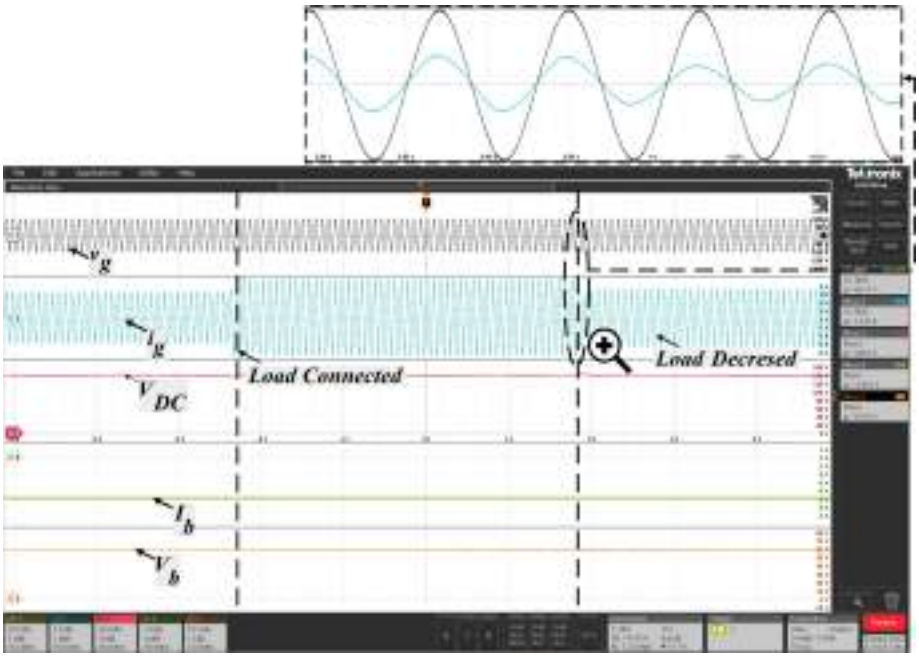

FIGURE 5.14: Experimental results when load is decreased

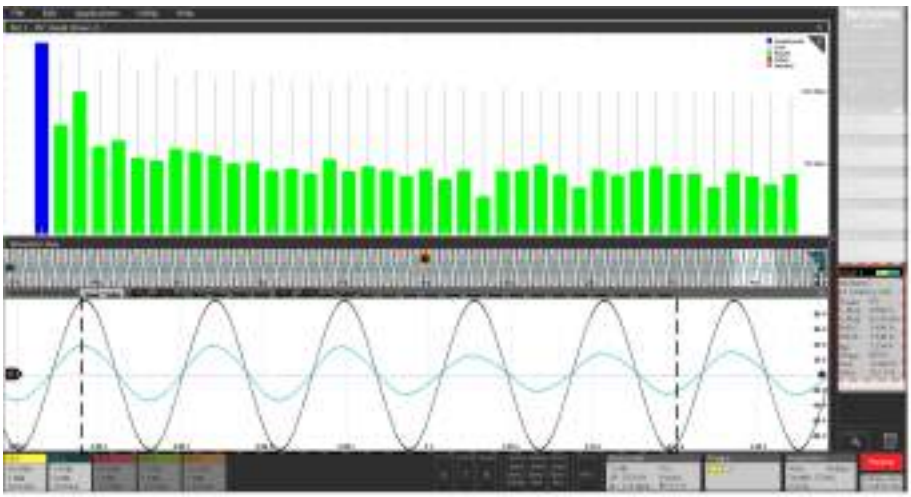

FIGURE 5.15: Experimental results when load is decreased

this case. However, over time, voltage sag and swell of 10% and voltage THDs of 15% have been added to analyze the control performance. The charger is completely capable of responding to control instructions without being impacted by grid-side disruption, as can be shown by carefully examining the different waveforms. The battery current follows the reference current instruction with ease, the DC-link is almost always kept almost constant, and the FEC may concurrently charge and discharge the battery and correct for reactive power and load harmonics. The grid current at UPF consistently maintains a sinusoidal pattern despite non-ideal voltage and non-linear load at PCC, as can be seen from the magnified version of the grid voltage, grid current, load current, and FEC current shown in Fig. 5.12. Additionally, the reactive power profile of the grid, load, and FEC may be used to verify this fact. It shows that the UPF grid operates as shown in Figs. 5.11 and 5.13 when the FEC is able to fulfill the reactive power load requirement, keeping grid reactive power consistently around zero.

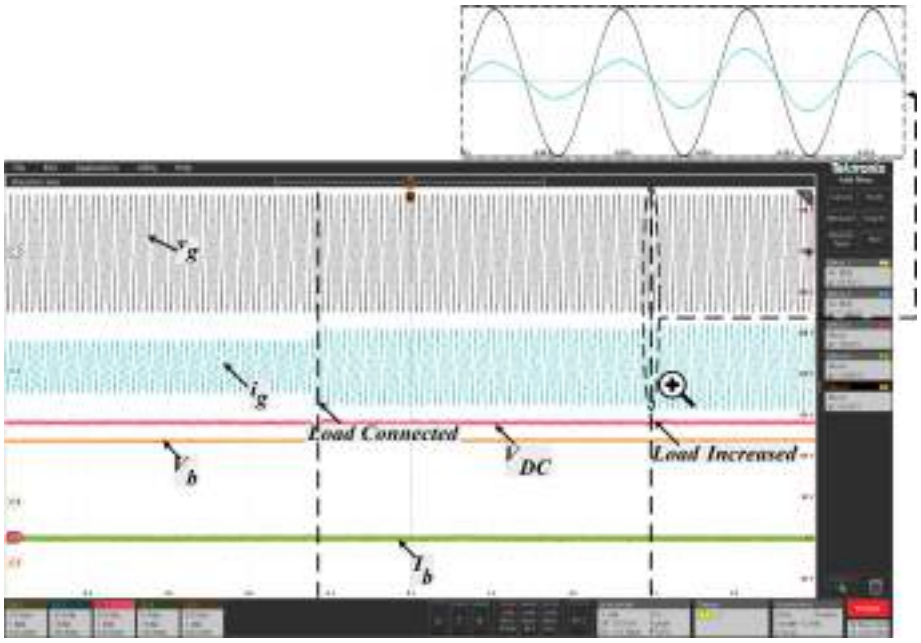

FIGURE 5.16: Experimental results when load is increased

Fig. 6.13 shows the behavior of the system at the time of load decrement. After certain point of time non-linear load has been connected and to show

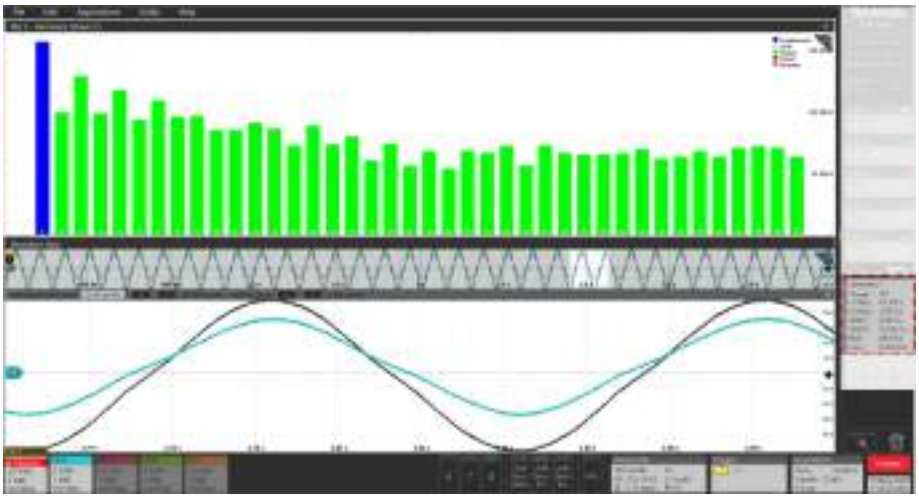

FIGURE 5.17: Experimental results when load is increased

the dynamics resistive load of 0.5kW has been removed suddenly. Due to which small deviation in DLVC voltage can be seen. Also, at the time of load removal zoomed part of v_g and i_g is shown.

In addition, to analyse the distortion in grid current occurred, THD of $\approx 2\%$ is obtained as observed from From Fig. 5.15[!h]

Fig. 5.16 illustrates the performance of the system under increasing load, whereas Fig. 5.17 shows the THD $\approx$ 4.5% of grid current. The system is now operating with no load attached to the PCC as well as the battery is charging in CC mode with a fixed current of -5A (1A/div.). After a while, a load is attached, causing the voltage V_{DC} to slightly drop. Additionally, a 0.5kW resistor has been attached to verify the dynamics in the operating system.

The prototype's sag and swell events are analyzed to determine the system's efficacy, as illustrated by the Figs. 5.18 and 5.20. Grid voltage (v_g) and grid current (i_g) with about 10% sag and swell events are displayed on channels 1 and 2. It is evident from closely inspecting the distinct waveform that the charger is fully capable of responding to control inputs without being influenced by grid-side disturbance. The DLVC is nearly always maintained at a constant level, the battery current easily complies with reference current instructions, and the battery may be charged and discharged simultaneously

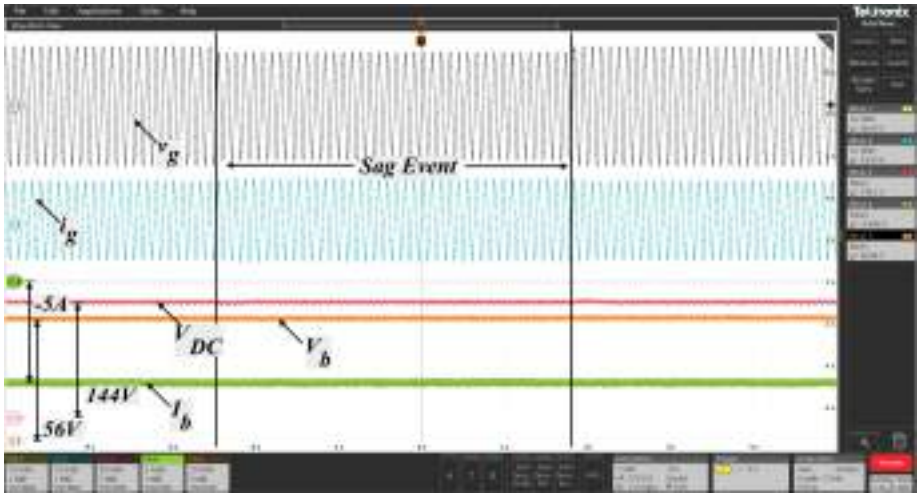

FIGURE 5.18: Experimental results when Sag event occurs

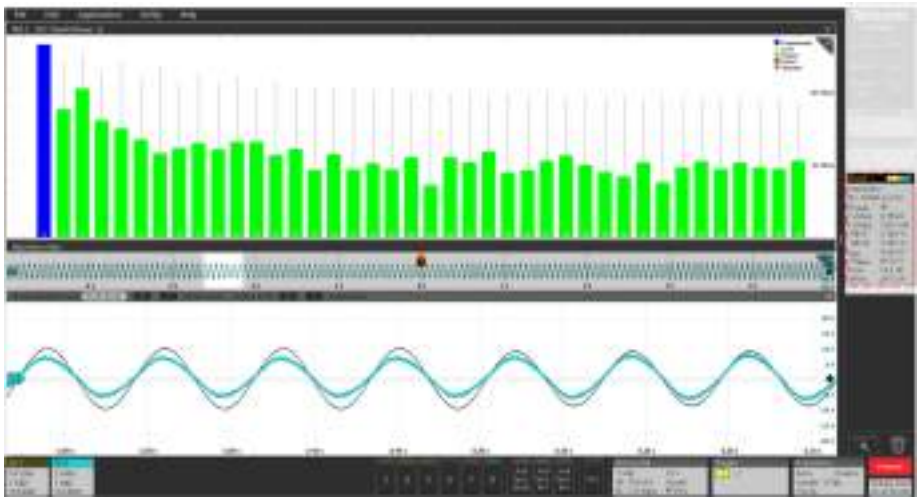

FIGURE 5.19: THD results when Sag event occurs

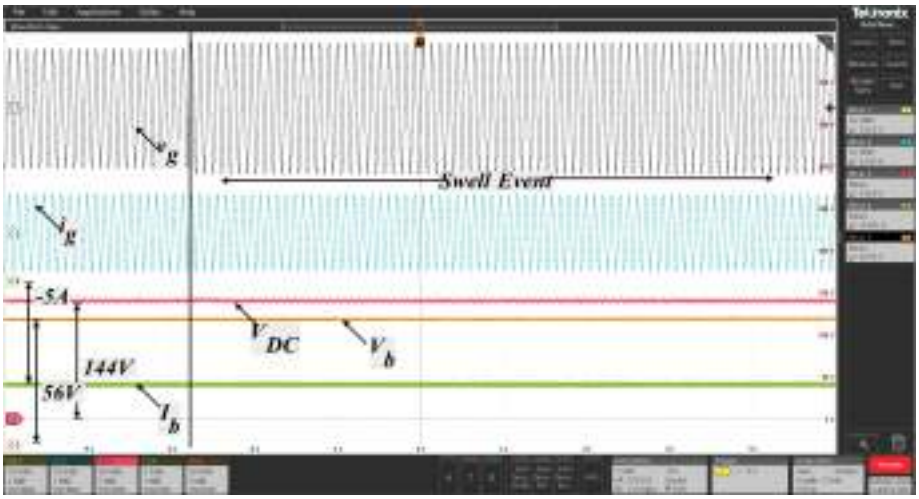

FIGURE 5.20: Experimental results when Swell event occurs

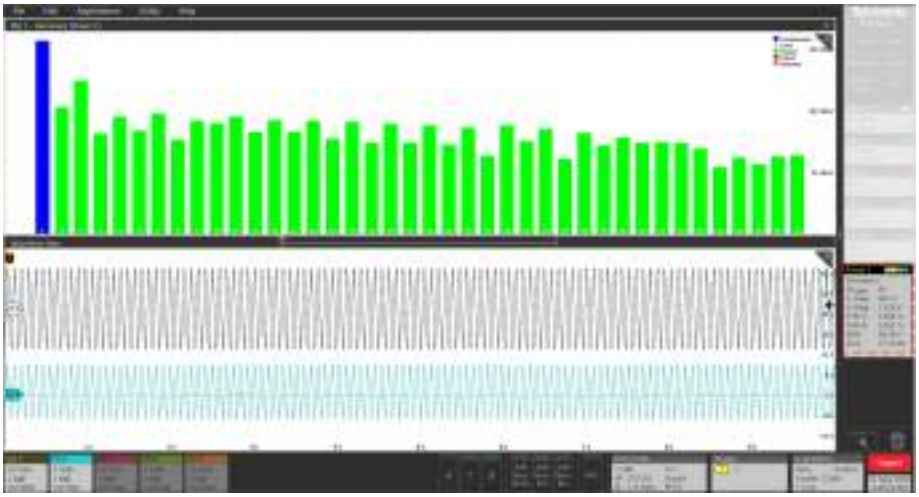

FIGURE 5.21: THD behaviour when Swell event occurs

by the FEC. It is also noteworthy that during the event, the battery voltage V_b, battery current I_b, and DLVC voltage V_{DC} all stay constant.

Battery voltage V_{DC} of 144V (at 50V/div.) is represented by Channel 3, battery current of -5A (at 2A/div.) is represented by Channel 4, as well as battery voltage of 56V (20V/div.) is represented by Channel 5. In addition, THDs of grid current in sag event $\approx$ 3.2% and swell event $\approx$ 2.5% which is $\leq$ 5% as shown in Fig. 5.19 and 5.21.

5.5 Conclusion

In this chapter, the control framework for the Grid-Interactive Electric Vehicle Charger (GIEVC) was validated using a Simulation-in-the-Loop (SIL) setup on the OP4510 real-time simulator from OPAL-RT Technologies. The voltage synchronization was carried out using a fourth-order CNISOGI, which effectively extracted clean unit voltage templates even under distorted grid conditions, demonstrating excellent immunity to harmonics, voltage sag, and swell events. For power quality enhancement and load compensation, advanced filtering techniques were explored in detail. A Leaky Least Mean Fourth (Leaky-LMF) filter was mathematically modeled and implemented, offering improved convergence stability and noise resilience compared to traditional filters. Its performance was critically evaluated against the conventional Least Mean Square (LMS) algorithm and the Linear Line Matching Filter (LLMF). The comparative analysis revealed that while LMS provided faster convergence under ideal conditions, it struggled under non-stationary disturbances. The LLMF and Leaky-LMF filters, on the other hand, showed superior robustness and adaptability, with the Leaky-LMF offering enhanced control over stability via its leakage factor. The integration of these advanced filtering techniques into the GIEVC control structure allowed for effective mitigation of harmonics and accurate compensation of reactive power. Real-time simulation results under both G2V and V2G modes confirmed that the proposed filter-assisted CNISOGI-based control scheme ensured stable

operation, reliable power exchange, and full grid code compliance even under dynamically varying grid scenarios.

So far, the Grid-Interactive Electric Vehicle Charger (GIEVC) system has demonstrated reliable performance in both MATLAB/Simulink simulations and real-time Simulation-in-the-Loop (SIL) environments using the OP4510 platform. These validations confirmed the effectiveness of the proposed control strategy under a wide range of grid disturbances. To further evaluate the robustness and practical viability of the system, the control algorithms have now been implemented on a laboratory-scale hardware prototype. The next chapter presents the experimental validation of the GIEVC under real-world non-ideal conditions, including voltage sag, swell, harmonic distortion, and dynamic load changes. A detailed discussion on the advanced control techniques employed and their performance on the hardware setup is provided to establish the feasibility of the proposed system for practical deployment.

Chapter 6

Design of a simple and robust control technique for improving system response

6.1 INTRODUCTION

Bidirectional power flow in grid-interactive electric vehicle (EV) chargers, also known as vehicle-to-grid (V2G) systems, is fundamental to enabling EVs to operate as dynamic grid assets. A critical aspect of such systems is the stability of the DC-link voltage, which ensures efficient energy transfer between the AC grid and the DC battery. However, under non-ideal grid conditions such as voltage sag, swell, harmonics, and sudden load changes, maintaining this stability becomes significantly more challenging. Conventional PI controllers, although commonly used, often fail to provide robust performance under such dynamic conditions due to their limited adaptability and tuning complexity.

Building upon the advanced control strategies discussed in previous chapters, this chapter introduces artificial intelligence (AI)-based controllers, including artificial neural networks (ANNs) and reinforcement learning (RL), for real-time, adaptive DC-link voltage control. Furthermore, the CNISOGI structure previously employed for unit voltage template generation and load harmonic filtering is integrated alongside a Leaky Least Mean Fourth (Leaky-LMF) filter to enhance power quality and

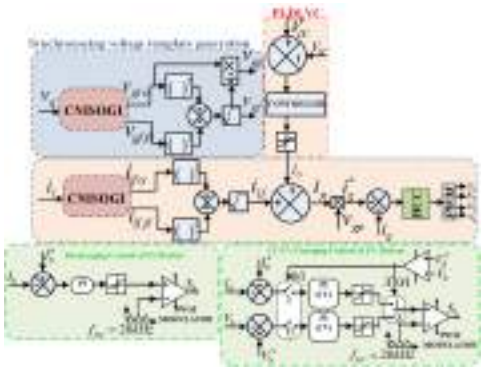

FIGURE 6.1: Controller design for the GIEVC

dynamic system response. The performance of these techniques is validated through hardware setup. The chapter details control design and experimental evaluation of the proposed system under realistic grid disturbances, demonstrating the superior performance of AI-driven and CNISOGI-based control approaches.

6.2 Controller Design of the GIEVC

Fig. 6.1 shows the control logic of the grid-interactive EV charger. The system description of GIEVC is discussed in Section 3.1. Further, as far as the controller design is concern, the only difference with the the controller discussed in Chapter 4 and 5 is the controller used for the control of DC-Link voltage (DLVC).

6.2.1 AI based DLVC

Decision trees are a widely used AI/ML technique, particularly well-suited for both classification and regression tasks. As nonlinear models, they offer the unique advantage of being computationally efficient while also being easy to interpret. These models work by recursively splitting data based on feature values, with internal nodes representing conditions or decisions and leaf nodes representing the final outcomes or predictions. For classification tasks, the splitting criteria are often based on metrics like Gini

impurity or information gain, while in regression tasks, decision trees focus on minimizing prediction errors such as mean squared error (MSE). One of the primary reasons decision trees are favored is their interpretability, which allows users to visualize the decision-making process and understand how the model arrives at its predictions.

Versatility and Strengths of Decision Trees

Decision trees exhibit significant versatility, making them suitable for various types of data. They can handle both categorical and continuous data, and they do not require any assumptions about the underlying data distribution. Their non-parametric nature enables them to capture complex relationships within the data, which makes them highly effective for a wide range of datasets. Specifically, decision trees often outperform deep learning models when working with tabular datasets, where features are individually meaningful and do not exhibit strong multi-scale temporal-spatial dependencies. This makes decision trees a go-to algorithm for supervised prediction tasks in many real-world applications, particularly when computational efficiency and model interpretability are of paramount importance.

Entropy and Information Gain

A foundational concept in decision tree learning is entropy, which measures the disorder or uncertainty within a dataset. In decision trees, entropy is used to compute information gain, which helps determine how well a feature splits the data. A feature with high information gain is one that effectively reduces the uncertainty, leading to more homogeneous subsets. The goal of the decision tree is to maximize information gain at each step of the tree's construction, thereby improving classification accuracy. Information gain measures how much a feature f reduces uncertainty or entropy in a dataset before and after it's divided based on f. It indicates the effectiveness of f in separating the dataset L into subsets $|L^v|$, where each subset represents data with a distinct value of f. A higher information gain suggests a feature is better at improving classification clarity. The best feature for splitting is the one with the highest information gain, implying it offers the most significant reduction in uncertainty.

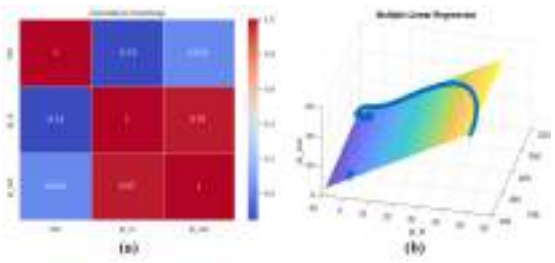

FIGURE 6.2: (a) Decision Tree correlation heatmap, (b) Decision Tree

$$\text{Entropy}(L) = -\sum_{i=1}^{j} p_i \log_2(p_i) \tag{6.1}$$

$$IG(L, f) = \text{Entropy}(L) - \sum_{v=1}^{V} \frac{|L^v|}{|L|} \text{Entropy}(L^v) \tag{6.2}$$

Gini Index and Fitness Functions

Another essential splitting criterion is the Gini index, which measures the purity of a dataset. A lower Gini index indicates that the data is more homogeneous after the split, making it a desirable property for decision trees. The Gini index is calculated for each potential split, and the one that maximizes purity (or minimizes impurity) is chosen. For regression tasks, other fitness functions, such as MSE, Mean Absolute Error (MAE), and the coefficient of determination (R^2), are used to evaluate the quality of the splits. These metrics help optimize the decision tree by reducing prediction errors and improving overall model performance.

$$\text{GINI}(L) = 1 - \sum_{i=1}^{j} p_i^2 \tag{6.3}$$

where pi is relative frequency if class $i$in L. If the dataset is split on attribute A into two subsets L_1 and L_2 with sizes N_1 and N_2 respectively, GINI is calculated as [138]

$$GINI_A(L) = \frac{N_1}{N} GINI(L_1) + \frac{N_2}{N} GINI(L_2) \tag{6.4}$$

Reduction in impurity is calculated as [138]

$$\Delta GINI(A) = GINI(L) - GINI_A(L) \tag{6.5}$$

Pruning Techniques to Prevent Overfitting

Despite their flexibility, decision trees are prone to overfitting, especially when they grow too deep and model the noise in the data. To combat overfitting, two main pruning techniques are used: pre-pruning and post-pruning. Pre-pruning involves stopping the tree's growth early based on predefined constraints such as maximum depth or minimum samples per leaf. Post-pruning, on the other hand, allows the tree to grow fully and then prunes back branches that do not contribute significantly to the model's predictive power. By simplifying the tree, pruning helps improve its generalization ability and reduces the risk of overfitting.

$$\text{MSE} = \frac{1}{n}\sum_{i\in n}(Y_i - \bar{Y}_t)^2 \tag{6.6}$$

$$\text{MAE} = \frac{1}{n}\sum_{i\in n}|Y_i - \bar{Y}_t| \tag{6.7}$$

$$R^2 = 1 - \frac{\sum_{i\in n}(Y_i - \bar{Y}_t)^2}{\sum_{i\in n}(Y_i - \tilde{Y})^2} \tag{6.8}$$

Implementation of Decision Trees in MATLAB

Decision trees can be implemented using various programming tools, and one popular platform is MATLAB. MATLAB provides a range of functions for creating, visualizing, and training decision tree models. For example, the fitrtree function is used for regression tasks and takes both independent and dependent variables as input. In this work, continuous variables are involved as reference DC-Link voltage (V_{DC}) and error (P_{in}), the decision tree is used to predict the current component ($I_D(k)$) denoted as pi_{out}. The fitrtree function automatically handles the splitting process, and the depth of the tree can be controlled by adjusting parameters like maximum depth to prevent overfitting. In this case, a tree with a maximum depth of 3 was implemented, ensuring a balance between complexity and accuracy.

Moreover, the correlation heatmap in Figure 6.2(a) reveals a strong positive correlation (0.97) between pi_{in} and pi_{out}, indicating that these two variables are closely related, while (V_{DC}) shows little to no correlation with either variable. This suggests that it pi_{in} is a critical factor in predicting pi_{out}. The decision tree in Figure 6.2(b) further explores this relationship by splitting the data based on thresholds pi_{in} to minimize squared error. The model shows that as pi_{in} increases, the predicted output value also increases, confirming the strong influence of pi_{in} on the system's performance. Together, these visualizations highlight the importance of pi_{in} as a key predictor in the system. In addition, the workflow in Figure 6.4(a) outlines the process of constructing a decision tree model, starting with data import, variable definition, and dataset splitting into training and testing sets. The model iteratively identifies the best split points that minimize prediction error, continuing until a stopping criterion such as maximum depth or minimum sample size is met. At this point, leaf nodes are generated to represent the average outcome. In Figure 6.4(b), the model's performance is illustrated, showing a sharp decline in mean squared error (MSE) across training, validation, and test datasets. By epoch 22, the model achieves its best validation performance with an exceptionally low MSE of 2.0506e-08, demonstrating high accuracy and strong generalization capabilities with no signs of overfitting.

6.2.2 Comparison with other techniques

Linear regression is a widely-used statistical method that models the relationship between a dependent variable and one or more independent variables through a linear equation. While its simplicity makes it effective for basic, linear relationships, it struggles with complex, non-linear datasets and is sensitive to outliers. Decision trees, in contrast, offer more flexibility, as they can handle non-linear relationships and are more robust against outliers by constructing decision paths based on splits in the data. Similarly, artificial Neural Networks (ANNs) are powerful models capable of capturing non-linear patterns due to their layered structure and ability to process data through weighted connections. However, ANNs come with

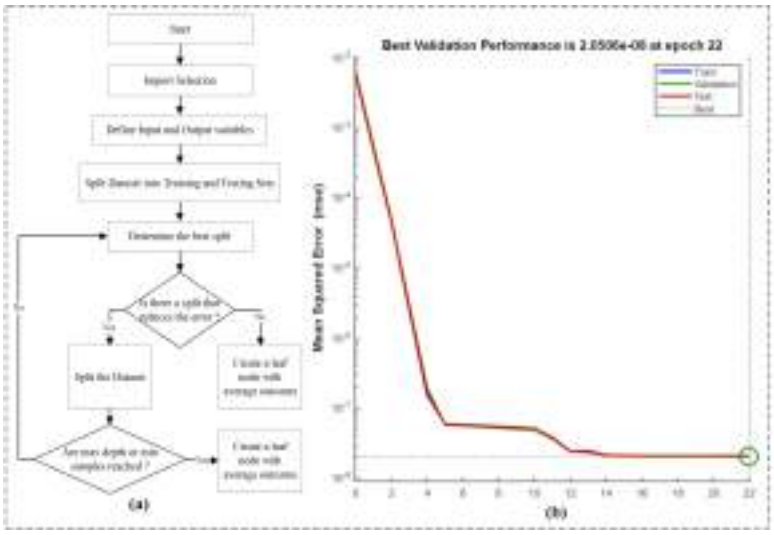

FIGURE 6.3: (a) Decision Tree Flowchart, (b) Performance analysis at epoch 22

drawbacks, such as high computational costs, long training times, and a lack of interpretability. In comparison, decision trees provide clearer interpretability and require less computational power. The performance of these models is visually demonstrated in the figures, where the Decision tree in Figure 6.4(a) yields the most accurate predictions, showing the closest alignment between actual and predicted values. Meanwhile, the linear regression in Figure 6.4(b) exhibits greater dispersion, indicating lower predictive accuracy, and the third model in Figure 6.4(c) falls between the two. Overall, the Decision Tree model demonstrates superior predictive capability, particularly in handling complex relationships, as illustrated by the higher concentration of data points along the diagonal in Figure 6.4(a). In addition, the Decision Tree model (Figure 6.5(a)) exhibits a sharp peak with approximately 1000 values tightly concentrated around zero, reflecting a significant number of highly accurate predictions. However, this central peak is accompanied by wide tails, suggesting that the model may suffer from overfitting, capturing noise in the dataset that leads to high variance in predictions for other samples. On the other hand, Linear Regression (Figure 6.5(b)) shows a broader, skewed error distribution with around 600 samples near zero and a tendency for negative errors, indicating underfitting. The skewness suggests that the

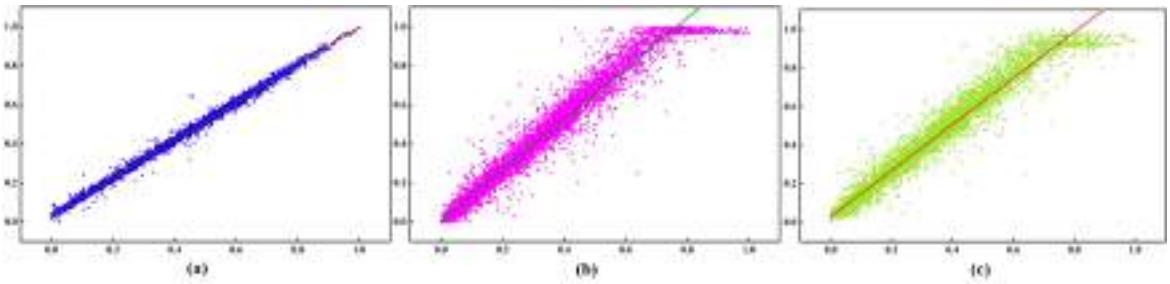

FIGURE 6.4: Actual vs Predicted Values of (a) Decision Tree, (b) Linear Regression and (c) ANN

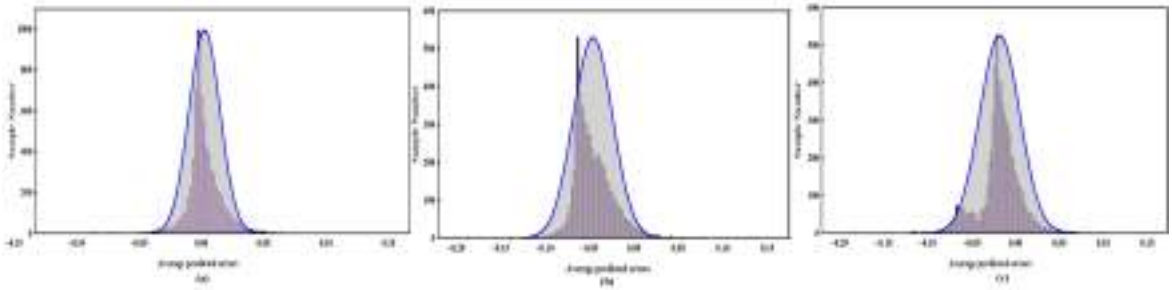

FIGURE 6.5: Residual Histogram of (a) Decision Tree, (b) Linear Regression and (c) ANN

model struggles to capture complex relationships, leading to systematic bias, particularly towards underprediction. The ANN (Figure 6.5(c)) presents a more balanced distribution with around 600 values near zero, similar to Linear Regression, but with a tighter, more symmetrical spread of errors. This indicates that ANN generalizes the data better, reducing both bias and variance. These findings suggest that while the Decision tree can excel in fitting data closely, its tendency to overfit may limit its generalizability. In contrast, ANN strikes a more favorable balance between predictive accuracy and robustness, making it the most promising model for achieving consistent performance across diverse datasets. Future research should further investigate hyperparameter optimization and regularization techniques to enhance the predictive capacities of these models. Also, a comparison between the proposed method with ANN and LR is gievn in table 6.1.

Henceforth, a validation of these techniques on the sysytem and response of AI based DLVC is presented in the Figure 6.6. The results achieved by

TABLE 6.1: Comparison of Proposed method with ANN and LR

S.No.	Parameters	ANN Technique	LR Technique	Proposed method
1	Pridiction	++	+	+++
2	THD of source current (%)	5%	4.96%	4.90%
3	Sampling time (T_s)	50μ sec	50μ sec	50μ sec
4	No. of samples	600	600	1000

$+++ = verygood, ++ = good, + = moderate$

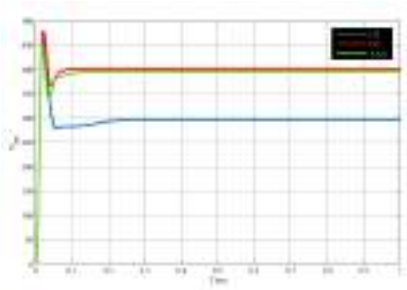

FIGURE 6.6: Performance analysis of V_{DC} for (a) Decision Tree, (b) Linear Regression and (c) ANN

the Decision Tree Regressor have notably surpassed those attained by both Linear Regression and ANNs within the regression scenario. The Decision Tree Regressor demonstrated superior performance, particularly in its ability to view non-linear relationships and complex patterns that are present in the data, such that maintains itself which the Linear Regression model struggles with due to its integral linearity.

6.2.3 Hardware-based Validation

These error metrics are important for the performance evaluation of our models on both training and testing datasets. They help in identifying areas where the model performs well and where it may need improvements. By analyzing these metrics , we can gain deeper insights into the efficacy of the controllers and make data-driven decisions to enhance our predictive models.

Table 6.2 and Table 6.3 shows the expression of the prediction accuracies of the ML models on the training and testing data,respectively. These results

show that the developed ML- based Decision Tree model exhibit high accuracy compared to others.

TABLE 6.2: Training Performance

Model Number	Model Type	MSE	RSquared	MAE
1	Tree	0.0039	0.999	0.03
2	Neural Network	0.076	0.997	0.16
3	Linear Regression	0.84	0.97	0.55

TABLE 6.3: Testing Performance

Model Number	Model Type	MSE	RSquared	MAE
1	Tree	0.003	0.999	0.0379
2	Neural Network	0.171	0.994	0.29
3	Linear Regression	0.844	0.974	0.557

In order to thoroughly assess the robustness & effectiveness of the developed controller, a scaled hardware prototype have been developed for real-time implementation purpose. The experimental configuration, visually depicted in Fig. 3.19, provides a comprehensive overview of the essential components comprising the Laboratory prototype system. The hardware implementation of the system includes a NHR make 9410 series regenerative grid simulator which is capable of generating desired sag, swell in supply voltage. Chroma make 62060D-600 series Bidirectional DC power supply is used as battery simulator, Tektronix 5 series mixed signal oscilloscope to observe the waveform, CP1104 series dSPACE control box for the real time implementation of control algorithm which handled smoothly the system dynamics effectively while maintaining power quality with minimum oscillations in the grid and battery currents. A non-linear load is a combination of 70mH inductor and 2kW resistor with 0.25kW tapping's for the dynamic behaviour of the system. LEM make LV-25P, LA25-P VI sensing elements are used to measure the voltage and current. Tektronix make P5200A series 50MHz, High voltage Differential Probes are also used to capture and analyse the voltages.

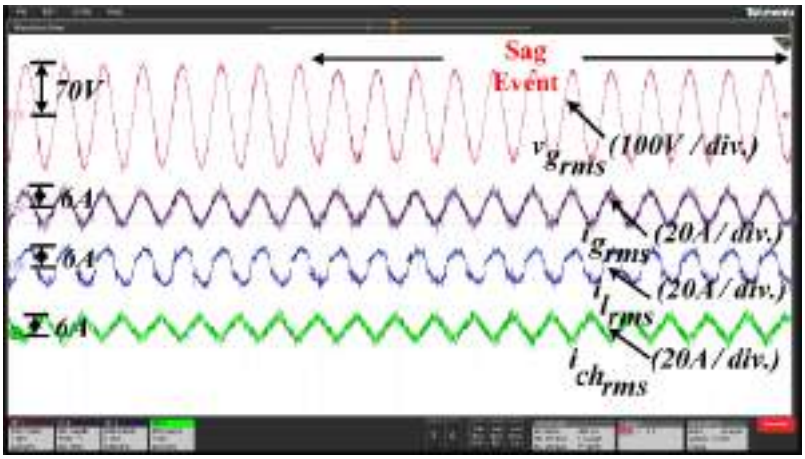

FIGURE 6.7: Experimental waveform of (v_g), (i_g), (i_l), and (i_{ch}) under sag condition

Fig. 6.7-6.8 shows the performance of system under 10% sag in the grid voltage v_g. Amid the sag event, the ststem is able to perform smoothly as evident from the waveform of Grid current i_g, load current i_l, and FEC current i_{ch}. Similarly, the undisturbed DC-Link voltage and regulated battery voltage & current proves the efficacy of the control.

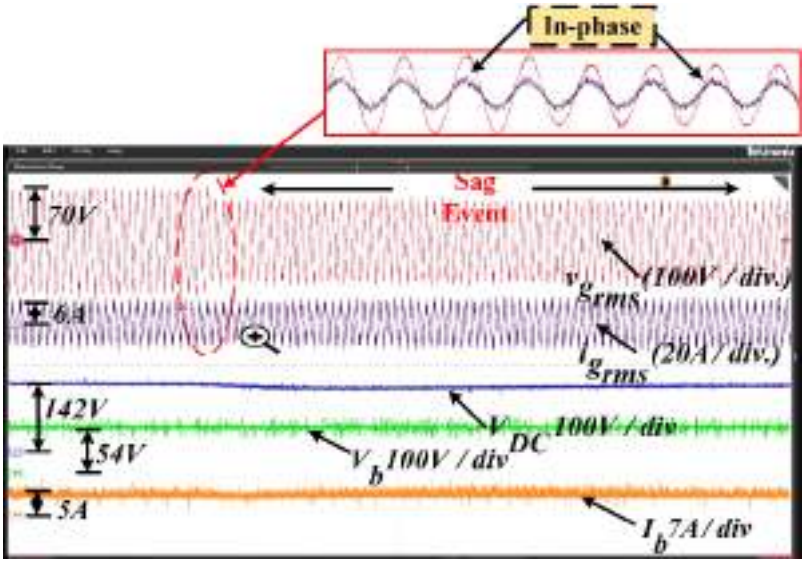

FIGURE 6.8: Key waveform of the system during sag event

Fig. 6.9-6.10 shows the experimental results with 10% swell in grid voltage. Here also the system is able to sail of smoothly as indicated by the various

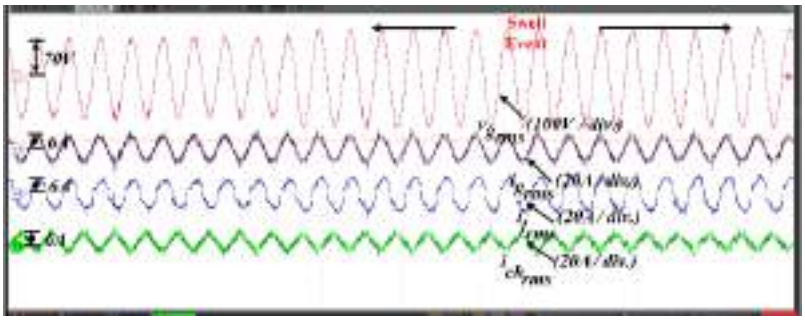

FIGURE 6.9: Experimental waveform of (v_g), (i_g), (i_l), and (i_{ch}) under swell condition

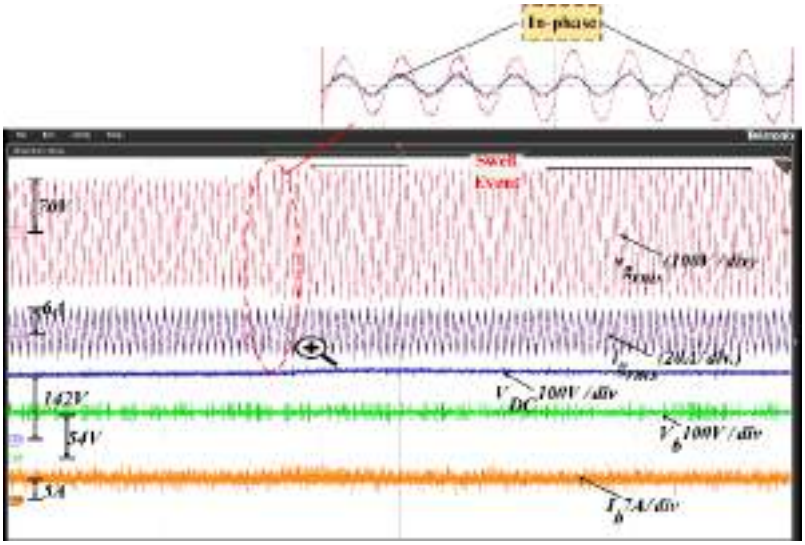

FIGURE 6.10: Experimental analysis of the system performance during swell event

waveforms. This can also be seen in the zoomed part of v_g and i_g which maintains the UPF operation. On DC side, the V_{DC} is perfectly regulated without having any significant disturbance in battery voltage, V_b and current, I_b.

Further, to demonstrate the capabilities of proposed controller under distorted grid voltage, the 15% THD's have been considered as shown in Fig 6.11-6.12. Here also it can be observed that grid side current is perfectly maintained smooth while ensuring the smooth regulation of various parameters on DC-side.

Finally, the Fig. 6.13 provides the reults under dynamic loading conditions.

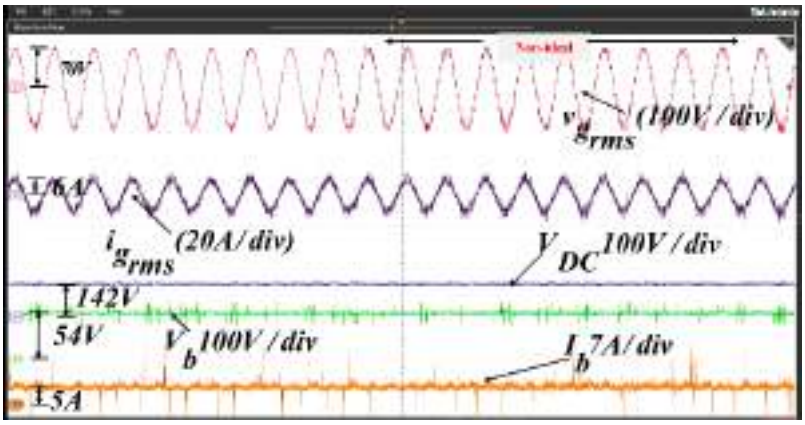

FIGURE 6.11: Key waveform of the (v_g), (i_g), (i_l), and (i_{ch}) for the non-ideal condition

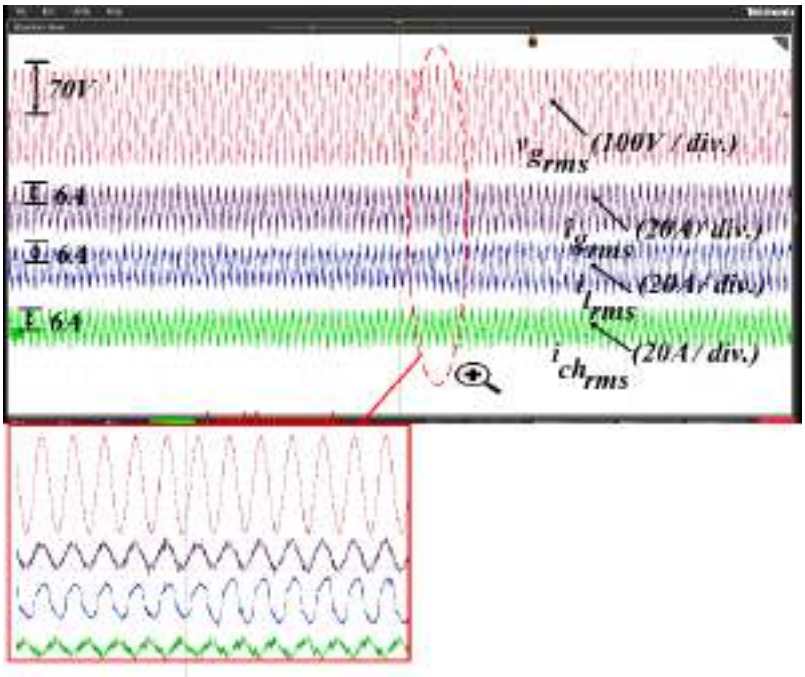

FIGURE 6.12: Experimental analysis of the system performance during non-ideal event

On analyzing the various waveform, it could be easily understood that the charger is fully able to respond to control commands without getting affected by load-side disturbance. Further, the DC-link is maintained almost constant, the battery current easily follows the reference current command and FEC can compensate for the load harmonics as well as reactive power while in charging mode. From the zoomed version of grid voltage, grid current, load current, and FEC current, it can be observed that the grid current always remains sinusoidal at UPF despite non-linear load at PCC.

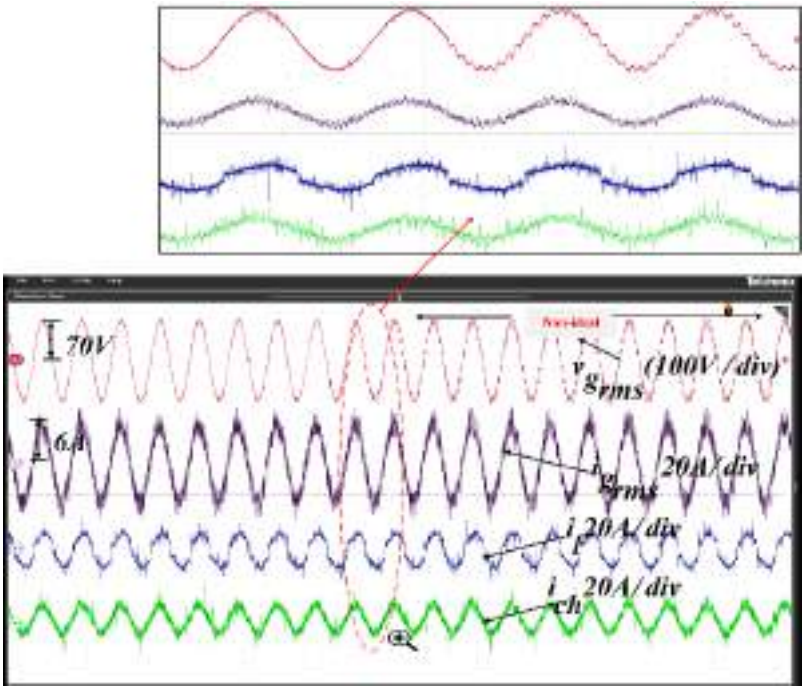

FIGURE 6.13: Key result of the system during dynamic condition

6.3 Conclusions

This chapter demonstrated the effective implementation of AI-based control strategies on a hardware prototype of a grid-interactive electric vehicle charger (GIEVC) for robust DC-link voltage regulation under real-world grid disturbances. Among the evaluated methods, the Decision

Tree Regressor outperformed both Linear Regression and Artificial Neural Networks (ANNs) by accurately modeling non-linear behaviors and ensuring faster dynamic response. Furthermore, the integration of fourth-order quadrature signal generators, particularly the CNISOGI, enabled accurate unit template generation and harmonic compensation, while the Leaky Least Mean Fourth (LLMF) filter further enhanced system performance in terms of harmonic attenuation and settling time. Experimental validation under non-ideal conditions such as voltage sag, swell, harmonics, and load dynamics confirmed that the proposed AI and filtering approaches significantly reduced total harmonic distortion (THD) and improved grid stability compared to traditional PI control. These results support the adoption of intelligent control and advanced signal processing techniques in modern EV charging systems to enhance their resilience and efficiency.

Chapter 7

Conclusions and Future Scopes

This chapter encapsulates the notable outcomes derived from the research, offering overarching conclusions and discussions on the main findings, alongside recommendations for potential future research extensions.

7.1 Conclusions

This thesis presented a detailed exploration into the modeling, control, and experimental validation of a Grid-Interactive Electric Vehicle Charger (GIEVC) system capable of bidirectional power flow for both Grid-to-Vehicle (G2V) and Vehicle-to-Grid (V2G) operations. With increasing electric vehicle (EV) penetration and demand for smart grid interfacing, the developed system addresses the challenges of power quality degradation, grid instability, and inefficient control under non-ideal conditions. The work is structured into six coherent chapters, each systematically contributing toward the realization of a robust, efficient, and intelligent EV charging infrastructure.

Chapter 1 provided a basic introduction and motivation for the work. It outlined the growing importance of electric vehicles in the context of modern smart grids, and how bidirectional EV chargers play a key role in energy flexibility and grid support. The chapter highlighted the need for intelligent, robust, and efficient control methods in GIEVC systems.

Chapter 2 reviewed existing literature on EV charging technologies. It discussed key trends, conventional charging strategies, and recent

innovations in control techniques. It also identified major research gaps, including challenges in harmonic mitigation, voltage regulation under disturbances, and the need for adaptive and intelligent control schemes.

Chapter 3 focused on the design and development of a two-stage bidirectional charger prototype, consisting of a front-end Voltage Source Converter (VSC) and an isolated back-end DC-DC converter using a high-frequency transformer. The system was modeled to support up to 1.5 kW of bidirectional power flow with a DC-link voltage regulated at 400 V. Hardware components, which include isolated gate drivers, Hall-effect-based current sensors, resistive-capacitive voltage sensors, a grid simulator, and a battery simulator, were discussed in detail. At last, three different configurations that were developed in the laboratory are discussed.

Chapter 4 presented the modeling and simulation of a fourth-order Cascaded Non-Identical Second-Order Generalized Integrator (CNISOGI) for generating clean unit voltage templates, even under distorted grid conditions. When benchmarked against traditional methods like SOGI, CSOGI, and SO-SOGI, the CNISOGI showed better Total Harmonic Distortion (THD) performance, reducing grid current THD from 7.45% to 2.68% under polluted grid voltage conditions. Its ability to extract clean quadrature signals allowed not only for accurate phase detection but also improved current control and reference signal generation, leading to more precise reactive power compensation and harmonic mitigation. Validation through MATLAB/Simulink simulations confirmed the robustness of the approach during voltage sag/swell conditions and nonlinear load disturbances.

Chapter 5 expanded the signal processing framework by introducing a Leaky Least Mean Fourth (LLMF) adaptive filter for estimating distorted load currents. The LLMF algorithm was mathematically modeled and validated against conventional Least Mean Square (LMS) and Least Mean Fourth (LMF) techniques. Simulation and real-time results showed that the LLMF filter achieved up to 48% faster convergence and reduced harmonic content in the current signal by 25% more than LMS and 18% more than

LMF. The LLMF-based system was tested on OPAL-RT under realistic grid disturbances, where it maintained sinusoidal source currents even with up to 25% total harmonic injection and handled transient events with <5% overshoot and <30 ms settling time, thereby validating its practical effectiveness.

Chapter 6 implemented Artificial Intelligence (AI) and Machine Learning (ML) algorithms to enhance DC-link voltage control. The performance of Linear Regression, Artificial Neural Networks (ANN), and Decision Tree Regressor (DTR) was evaluated using hardware-level testing. Results indicated that the DTR model reduced DC-link voltage settling time by 40% compared to PI control and achieved 98.3% prediction accuracy in maintaining voltage regulation under fluctuating loads. ANN and DTR also demonstrated improved resilience to grid anomalies, with THD reduction of up to 2.4% more than PI and significantly better handling of voltage sag/swell conditions. This chapter also leveraged the CNISOGI for clean unit template generation and LLMF for load current reconstruction, thereby combining advanced filtering and intelligent control on the hardware platform. The hardware testbed, developed in Chapter 3, was used for experimental validation of AI/ML-based control strategies, demonstrating practical robustness, power quality improvement, and bidirectional energy flow compliance.

In conclusion, the thesis successfully developed a comprehensive and scalable solution for grid-interactive EV charging by integrating advanced signal processing techniques like CNISOGI and LLMF filters, AI/ML-based intelligent control, and robust hardware implementation. Simulation results using MATLAB and real-time testing on OPAL-RT and physical hardware underlined the charger's capability to maintain THD below 3%, ensure <50 ms voltage recovery time, and adapt dynamically to grid changes and load fluctuations. The findings support the deployment of smart, reliable, and future-ready EV charging infrastructure and offer a solid foundation for subsequent research in adaptive control, reinforcement learning, and predictive energy management in grid-interactive systems.

7.2 Contributions

The key contributions arising from the research outlined in this thesis include:

1. A comprehensive design and hardware development of a two-stage Grid-Interactive Electric Vehicle Charger (GIEVC), consisting of a front-end AC/DC converter and an isolated DC/DC converter, capable of bidirectional power flow for both G2V and V2G operations.
2. Implementation of a novel fourth-order Cascaded Non-Identical Second Order Generalized Integrator (CNISOGI) structure for accurate unit template generation. The CNISOGI demonstrated a superior step response time of 24.4 ms and improved performance over conventional filters like SOGI and CSOGI in handling harmonics and grid disturbances.
3. Modeling and validation of a Leaky Least Mean Fourth (LLMF) filter for load current harmonic compensation. The LLMF filter was compared against conventional LMS and LMF techniques, showing better convergence and improved performance in filtering non-ideal load conditions.
4. Study and comparison of advanced charging control strategies, including Model Predictive Control (MPC), and their effectiveness in dynamic grid scenarios using both simulation and real-time platforms.
5. Integration of Artificial Intelligence/Machine Learning-based control strategies, such as Decision Tree Regressors, for robust DC-link voltage regulation. The AI-based controllers showed improved transient response and better adaptability compared to PI and ANN controllers.
6. Real-time simulation and hardware validation of the developed control schemes using OPAL-RT OP4510 and a TI F28379D-based laboratory prototype, ensuring practical feasibility and robustness of the proposed GIEVC system under sag, swell, harmonic pollution, and load dynamics.

7.3 Future Scopes

Based on the research conducted in this thesis, outlined below are key considerations and prospective areas for future exploration and development.

1. The CNISOGI structure can be extended to handle unbalanced grid conditions and frequency variations more effectively by integrating adaptive parameter tuning mechanisms or combining it with phase-locked loop (PLL)-free control strategies.
2. The AI/ML-based controllers, especially Decision Tree Regressors, can be further optimized using advanced ensemble methods such as Gradient Boosting or Random Forests to improve their generalization capability in highly dynamic grid environments.
3. The existing LLMF filter can be adapted for real-time parameter adjustment based on grid dynamics using reinforcement learning techniques, potentially improving filter convergence speed and adaptability.
4. Expansion of the control system to support integration with renewable energy sources like PV or wind turbines for forming a hybrid energy management system (HEMS), allowing better energy balancing in microgrids.
5. Real-time communication protocols (such as IEC 61850) and cybersecurity aspects can be integrated into the hardware prototype to ensure secure and intelligent EV-grid interaction in smart grid deployments.
6. Future work may also involve the miniaturization and cost optimization of the hardware setup for commercial deployment and interoperability with existing EV charging infrastructures.

Bibliography

[1] P. Luo, T. J. Liang, K. H. Chen, and S. M. Chen, "Design and implementation of a high step-up dc-dc converter with active switched inductor and coupled inductor," *IEEE Transactions on Industry Applications*, vol. 59, no. 3, pp. 3470–3480, May-June 2023.

[2] A. Bassa de los Mozos, G. R. Chandra Mouli, and P. Bauer, "Evaluation of topologies for a solar powered bidirectional electric vehicle charger," *IET Power Electronics*, vol. 12, no. 14, pp. 3675–3687, 2019.

[3] T. J. Liang, T. A. A. Tran, K. K. N. Huynh, and K. H. Chen, "Soft-switching three-port converter with a three-winding coupled inductor," *IEEE Journal of Emerging and Selected Topics in Power Electronics*, vol. 11, no. 5, pp. 5470–5485, Oct. 2023.

[4] M. A. Akhtar and S. Saha, "An adaptive frequency-fixed second-order generalized integrator-quadrature signal generator using fractional-order conformal mapping based approach," *IEEE Transactions on Power Electronics*, vol. 35, no. 6, pp. 5548–5552, 2019.

[5] Akshay, G. Yadav, and M. Singh, "Validation of a parameter design methodology for air-core two-coil wpt system with multi-resonant lc compensation," in *2023 IEEE International Conference on Power Electronics, Smart Grid, and Renewable Energy (PESGRE)*, 2023, pp. 1–6.

[6] M. Ansari, G. Yadav, and M. Singh, "A 3.3kw modified llc resonant converter for grid-tied ev system under wide voltage range," in *2023 3rd International Conference on Intelligent Technologies (CONIT)*, 2023, pp. 1–6.

[7] G. Yadav and M. Singh, "Unveiling the superiority: Comparative analysis of anfis, fopid, and pi controllers in grid-connected ev systems for g2v/v2g applications," in *2023 International Conference on Electrical, Electronics, Communication and Computers (ELEXCOM)*, Roorkee, India, 2023, pp. 1–6.

[8] M. Israr and P. Samuel, "High-performance front end pfc controller design for light electric vehicle charger application," *Computers and Electrical Engineering*, vol. 120, p. 109822, 2024.

[9] M. Ansari, G. Yadav, and M. Singh, "Modified bidirectional llc converter for electric vehicle application," in *2023 Second International Conference on Electrical, Electronics, Information and Communication Technologies (ICEEICT)*, Trichirappalli, India, 2023, pp. 1–7.

[10] F. de Paula García-López, M. Barragán-Villarejo, and J. M. Maza-Ortega, "Grid-friendly integration of electric vehicle fast charging station based on multiterminal dc link," *International Journal of Electrical Power & Energy Systems*, vol. 114, p. 105341, 2020.

[11] G. Yadav and M. Singh, "Robust control design for grid-tied ev system with sogi-based architecture in wide voltage range scenarios," in *2023 International Conference on Electrical, Electronics, Communication and Computers (ELEXCOM)*, Roorkee, India, 2023, pp. 1–6.

[12] A. K. Seth and M. Singh, "Plant integrated proportional integrating based control design for electric vehicle charger," *Computers and Electrical Engineering*, vol. 105, p. 108522, 2023.

[13] A. A. Ghani, V. K. Ramachandaramurthy, and J. Y. Yong, "Design of a master power factor controller for an industrial plant with solar photovoltaic and electric vehicle chargers," *Electrical Engineering*, vol. 104, no. 1, pp. 13–25, 2022.

[14] C. Ke, A. Wu, C. Bing, and L. Yi, "Measuring and reconstruction algorithm based on improved second-order generalised integrator configured as a quadrature signal generator and phase locked loop for

the three-phase ac signals of independent power generation systems," *IET Power Electronics*, vol. 9, no. 11, pp. 2155–2161, 2016.

[15] V. Shah and S. Payami, "Integrated converter with g2v, v2g, and dc/v2v charging capabilities for switched reluctance motor drive-train based ev application," *IEEE Transactions on Industry Applications*, vol. 59, no. 3, pp. 3837–3850, May-June 2023.

[16] G. Yadav and M. Singh, "Robust control design for grid-tied ev system with sogi-based architecture in wide voltage range scenarios," in *2023 International Conference on Electrical, Electronics, Communication and Computers (ELEXCOM)*, Roorkee, India, 2023, pp. 1–6.

[17] J. Saroha, M. Singh, and D. K. Jain, "Anfis-based add-on controller for unbalance voltage compensation in a low-voltage microgrid," *IEEE Transactions on Industrial Informatics*, vol. 14, no. 12, pp. 5338–5345, Dec. 2018.

[18] M. E. Şahİn, F. Blaabjerg, and A. SangwongwanİCh, "Modelling of supercapacitors based on simplified equivalent circuit," *CPSS Transactions on Power Electronics and Applications*, vol. 6, no. 1, pp. 31–39, March 2021.

[19] V. Sumanasena, L. Gunasekara, S. Kahawala, N. Mills, D. D. Silva, M. Jalili, S. Sierla, and A. Jennings, "Artificial intelligence for electric vehicle infrastructure: Demand profiling, data augmentation, demand forecasting, demand explainability and charge optimisation," *Energies*, 2023.

[20] G. Ramanathan, G. Ramanathan, and J. L. Munda, "Pv-assisted grid connected multi output electric vehicle charger with pv2v, g2v and pv2g functions," *PLOS ONE*, 2024.

[21] P. Singla, S. Boora, P. Singhal, N. Mittal, V. Mittal, and F. Gared, "Design and simulation of 4 kw solar power-based hybrid ev charging station," *Dental science reports*, 2024.

[22] P. Aduama, Z. Zhang, and A. S. Al-Sumaiti, "Multi feature data fusion-based load forecasting of electric vehicle charging stations using a deep learning model," *Energies*, 2023.

[23] L. Zeng, S. Z. Chen, and Z. H. Tang, "An electric vehicle charging method considering multiple power exchange modes' coordination," *Sustainability*, 2023.

[24] "Smart online charging algorithm for electric vehicles via customized actor–critic learning," *IEEE Internet of Things Journal*, 2022.

[25] T. Mao, X. Zhang, and B. Zhou, "Intelligent energy management algorithms for ev-charging scheduling with consideration of multiple ev charging modes," *Energies*, 2019.

[26] S. R. Sarangi, P. Dutta, and K. Jalan, "It infrastructure for providing energy-as-a-service to electric vehicles," *IEEE Transactions on Smart Grid*, 2012.

[27] "Review of electric vehicle charging technologies, standards, architectures, and converter configurations," *IEEE Access*, 2023.

[28] S. Hemavathi and A. Shinisha, "A study on trends and developments in electric vehicle charging technologies," *Journal of energy storage*, 2022.

[29] A. Rachid, H. E. Fadil, K. Gaouzi, K. Rachid, A. Lassioui, Z. E. Idrissi, and M. Koundi, "Electric vehicle charging systems: Comprehensive review," *Energies*, 2022.

[30] A. Ali, H. H. H. Mousa, M. Shaaban, M. A. Azzouz, and A. S. A. Awad, "A comprehensive review on charging topologies and power electronic converter solutions for electric vehicles," *Journal of modern power systems and clean energy*, 2024.

[31] H. Kilicoglu and P. Tricoli, "Technical review and survey of future trends of power converters for fast-charging stations of electric vehicles," *Energies*, 2023.

[32] Y. Yasa, "A system efficiency improvement of dc fast-chargers in electric vehicle applications: Bypassing second-stage full-bridge dc-dc converter in high-voltage charging levels," *Ain Shams Engineering Journal*, 2023.

[33] S. Mateen, M. Amir, A. Haque, and F. I. Bakhsh, "Ultra-fast charging of electric vehicles: A review of power electronics converter, grid stability and optimal battery consideration in multi-energy systems," *Sustainable Energy, Grids and Networks*, 2023.

[34] S. M. Rao, R. J. Satputaley, R. K. Keshri, V. B. Borghate, and A. Khergade, "Improving dc-bus voltage regulation in grid fed ev fast charging station using mli based dvr," *IEEE Transactions on Power Delivery*, 2024.

[35] H. Yu, J. Tu, X. Lei, Z. Shao, and L. Jian, "A cost-effective and high-efficient ev shared fast charging scheme with hierarchical coordinated operation strategy for addressing difficult-to-charge issue in old residential communities," *Sustainable Cities and Society*, 2024.

[36] D.-S. Zhang, J. E. Huber, and J. W. Kolar, "A three-phase synergetically controlled buck–boost current dc-link ev charger," *IEEE Transactions on Power Electronics*, 2023.

[37] M. Kim, K. Park, S. Yu, J. Lee, Y.-H. Park, L. Sang-Woo, and B.-H. Chung, "A secure charging system for electric vehicles based on blockchain." *Sensors*, 2019.

[38] P. Tauš, M. Taušová, P. Sivák, M. S. Muchová, and E. Mihaliková, "Parameter optimization model photovoltaic battery system for charging electric cars," *Energies*, 2020.

[39] P. Singla, S. Boora, P. Singhal, N. Mittal, V. Mittal, and F. Gared, "Design and simulation of 4 kw solar power-based hybrid ev charging station," *Dental science reports*, 2024.

[40] J. Gao, T. Wong, C. Wang, and J. Y. Yu, "A price-based iterative double auction for charger sharing markets," *IEEE Transactions on Intelligent Transportation Systems*, 2022.

[41] Z. Niu, K. An, and W. Ma, "Vehicle-to-grid enabled charging infrastructure planning and operations considering demand uncertainties," *Transportation Research Part D-transport and Environment*, 2024.

[42] A. M. D. Correia, P. Moura, and A. T. D. Almeida, "Technical and economic assessment of battery storage and vehicle-to-grid systems in building microgrids," *Energies*, 2022.

[43] S. Sagaria, M. van der Kam, and T. Boström, "The influence of socio-technical variables on vehicle-to-grid technology," *Energy*, 2024.

[44] D. Borge-Diez, D. Icaza, E. Açıkkalp, and H. Amaris, "Combined vehicle to building (v2b) and vehicle to home (v2h) strategy to increase electric vehicle market share," *Energy*, 2021.

[45] J. Chen, J. Qing, and Q. Cai, "Impact of bi-directional electric vehicle and demand response on residential distributed pv capacity planning based on tou pricing." *Journal of Environmental Management*, 2024.

[46] J. Li and A. Li, "Optimizing electric vehicle integration with vehicle-to-grid technology: The influence of price difference and battery costs on adoption, profits, and green energy utilization," *Sustainability*, 2024.

[47] M. Fresia and S. Bracco, "Electric vehicle fleet management for a prosumer building with renewable generation," *Energies*, 2023.

[48] S. Hossain, K. S. Rahman, A. K. M. A. Habib, W.-S. Tan, M. Mahmud, S. Chowdhury, and S. Channumsin, "Grid-vehicle-grid (g2v2g) efficient power transmission: An overview of concept, operations, benefits, concerns, and future challenges," *Sustainability*, 2023.

[49] S. Alyami, "Ensuring sustainable grid stability through effective ev charging management: A time and energy-based approach," *Sustainability*, 2024.

[50] N. Jin, J. Wang, Y. Li, L. He, X. Wu, H. Wang, and L. Lu, "A bidirectional grid-friendly charger design for electric vehicle operated under pulse-current heating and variable-current charging," *Sustainability*, 2023.

[51] G. Erdogan and W. F. Hassen, "Charging scheduling of hybrid energy storage systems for ev charging stations," *Energies*, 2023.

[52] V. K. Manickam and K. Dhayalini, "Hybrid optimized control of bidirectional off-board electric vehicle battery charger integrated with vehicle-to-grid," *Journal of energy storage*, 2024.

[53] H. Long, Z. Guo, and C. Zhou, "A charge-discharge optimization strategy considering the spatiotemporal distribution of electric vehicles and the operational safety of the power distribution network in the power-transportation coupling network," *Journal of Cleaner Production*, 2024.

[54] Z. Kang, Z. Ye, C.-M. Lam, and S.-C. Hsu, "Sustainable electric vehicle charging coordination: Balancing co2 emission reduction and peak power demand shaving," *Applied Energy*, 2023.

[55] M. Khalid, J. Thakur, S. M. Bhagavathy, and M. Topel, "Impact of public and residential smart ev charging on distribution power grid equipped with storage," *Sustainable Cities and Society*, 2024.

[56] C. Korkas, C. Tsaknakis, A. C. Kapoutsis, and E. B. Kosmatopoulos, "Distributed and multi-agent reinforcement learning framework for optimal electric vehicle charging scheduling," *Energies*, 2024.

[57] T.-T. LE, R. M. Hakim, and S. Choi, "A high-efficiency bidirectional single-stage ac-dc converter under wide voltage range for fast chargers," *IEEE Transactions on Power Electronics*, vol. 38, no. 4, pp. 4945–4956, 2023.

[58] A. Ali, H. H. H. Mousa, M. Shaaban, M. A. Azzouz, and A. S. A. Awad, "A comprehensive review on charging topologies and power electronic converter solutions for electric vehicles," *Journal of modern power systems and clean energy*, vol. 12, no. 3, pp. 675–694, 2024.

[59] "Bidirectional acâ€"dc modular multilevel converter with electric spring functions for stabilizing renewable ac power grid at the distribution voltage level," *IEEE Journal of Emerging and Selected Topics in Power Electronics*, vol. 10, no. 6, pp. 7589–7600, 2022.

[60] D. Kumar, F. Zare, and F. Blaabjerg, "Special issue on modeling and analysis of interaction between grids and grid-connected power electronics converters in distribution networks," *IEEE Journal of Emerging and Selected Topics in Power Electronics*, vol. 10, no. 3, pp. 2658–2661, 2022.

[61] E. Monmasson, "Paving the path toward the use of power electronics building blocks [editorâ€™s column]," *IEEE Industrial Electronics Magazine*, vol. 17, no. 1, pp. 2–3, 2023. [Online]. Available: https://ieeexplore.ieee.org/ielx7/4154573/10081121/10081174.pdf

[62] F. Blaabjerg, Y. Yang, K. Kim, and J. Rodriguez, "Power electronics technology for large-scale renewable energy generation," *Proceedings of the IEEE*, vol. 111, pp. 335–355, 2023. [Online]. Available: https://ieeexplore.ieee.org/ielx7/5/4357935/10070105.pdf

[63] H. S. Lam, H. Yuan, S.-C. Tan, C. C. Mi, J. Pou, and S. Y. R. Hui, "Bidirectional acâ€“dc modular multilevel converter with electric spring functions for stabilizing renewable ac power grid at the distribution voltage level," pp. 7589–7600, 2022.

[64] R. Palaniappan, O. Molodchyk, M. S. Sarcheshmeh, M. W. Asmah, J. yun Liu, T. Schlichtherle, F.-D. Richter, E. A. Kwofie, D. R. Festner, G. Blanco, A. Mutule, O. Borscevskis, S. S. Rafaat, Y. Lei, U. HÃ¤ger, and C. Rehtanz, "Experimental verification of smart grid control functions on international grids using a realâ€ time simulator," *Iet Generation Transmission Distribution*, vol. 16, no. 13, pp. 2747–2760, 2022.

[65] S. Kumar, L. N. Patel, B. Singh, and A. L. Vyas, "Self-adjustable step-based control algorithm for grid-interactive multifunctional single-phase pv-battery system under abnormal grid conditions," *IEEE Transactions on Industry Applications*, vol. 56, no. 3, pp. 2978–2987, 2020.

[66] K. Pal, S. Kumar, B. Singh, and T. C. Kandpal, "Sigmoidal and gaussian functions based neural neuron technique for grid interactive solar energy system enabling power quality improvement," *Iet Generation Transmission Distribution*, vol. 14, no. 23, pp. 5471–5479, 2020.

[Online]. Available: https://ietresearch.onlinelibrary.wiley.com/doi/pdf/10.1049/iet-gtd.2020.0790

[67] B. Singh, "Resilient control algorithm for wind-hydro based distributed generation system with grid synchronization capability," pp. 4687–4699, 2023.

[68] D. Stanelyte and V. Radziukynas, "Review of voltage and reactive power control algorithms in electrical distribution networks," *Energies*, vol. 13, no. 1, 2019.

[69] S. Ghosh and S. Chattopadhyay, "Three-loop-based universal control architecture for decentralized operation of multiple inverters in an autonomous grid-interactive microgrid," *IEEE Transactions on Industry Applications*, vol. 56, no. 2, pp. 1966–1979, 2020.

[70] M. GwÃ³Åºdź and Åukasz CiepliÅ„ski, "An algorithm for calculation and extraction of the grid voltage component," *Energies*, vol. 14, no. 16, 2021. [Online]. Available: https://www.mdpi.com/1996-1073/14/16/4842/pdf

[71] E. Espina, J. Llanos, C. Burgos-Mellado, R. Cardenas-Dobson, M. Martinez-Gomez, and D. Saez, "Distributed control strategies for microgrids: An overview," *IEEE Access*, vol. 8, pp. 193 412–193 448, 2020.

[72] F. Blaabjerg, R. Teodorescu, M. Liserre, and A. V. Timbus, "Overview of control and grid synchronization for distributed power generation systems," *IEEE Transactions on Industrial Electronics*, vol. 53, no. 5, pp. 1398–1409, 2006.

[73] R. Teodorescu, M. Liserre, and P. Rodriguez, *Grid Converters for Photovoltaic and Wind Power Systems*. John Wiley & Sons, 2011.

[74] M. Karimi-Ghartemani and R. Iravani, "A nonlinear control method for synchronous d-q frame control of power converters," *IEEE Transactions on Power Delivery*, vol. 18, no. 4, pp. 1355–1364, 2003.

[75] V. Aviña-Corral, O. Martínez-Fuentes, and J. de Jesus Rangel-Magdaleno, "Fast orthogonal signal generator for sine amplitude and phase estimation using two sampled points," *IEEE Transactions on Instrumentation and Measurement*, 2024.

[76] U. Sharma and B. Singh, "An adaptive lyapunov's quadrature signal generator-based frequency-locked-loop technique for a two-stage non-isolated bidirectional charger," *Journal of Energy Storage*, vol. 88, p. 111612, 2024.

[77] J. Wei, Z. Cai, L. Zhang, J. Yu, Z. Zhang, and B. Zhou, "The quadrature signals synchronous demodulation method for rotor position estimation of three-stage synchronous machine," *IEEE Transactions on Power Electronics*, 2024.

[78] L. Gou, C. Wang, X. You, M. Zhou, and S. Dong, "Ipmsm sensorless control for zero- and low-speed regions under low switching frequency condition based on fundamental model," *IEEE Transactions on Transportation Electrification*, vol. 8, no. 1, pp. 1182–1193, March 2022.

[79] P. Tripathy, B. Misra, B. Nayak, P. Tripathy, and L. Nanda, "Performance investigation of modified second order generalized integrator based phase locked loops for a dc offset perturbed grid," in *2024 IEEE 4th International Conference on Applied Electromagnetics, Signal Processing, & Communication (AESPC)*. IEEE, 2024, pp. 1–6.

[80] M. Mansouri, D. Westwick, and A. M. Knight, "The on-line estimation of multi-mode electromechanical oscillations using the cascade structure of damped-sogi," *IEEE Access*, 2024.

[81] S. Khan, K. Sudhakar, M. H. Yusof, and S. Sundaram, "Review of building integrated photovoltaics system for electric vehicle charging." pp. e202 300 308–e202 300 308, 2024.

[82] Y. Chen, Z. Jiang, L. Wei, Y. Zhang, and J. Jiang, "An asymmetric full-bridge bidirectional dc-ac converter with power decoupling and common-mode current suppression for v2g application," *IEEE Journal of Emerging and Selected Topics in Power Electronics*, pp. 1–1, 2024.

[83] C. Cai, M. Saeedifard, J. Wang, P. Zhang, J. Zhao, and Y. Hong, "A cost-effective segmented dynamic wireless charging system with stable efficiency and output power," *IEEE Transactions on Power Electronics*, vol. 37, no. 7, pp. 8682–8700, 2022.

[84] N. Mohamed, F. Aymen, M. Alqarni, R. A. Turky, B. Alamri, Z. M. Ali, and S. H. Abdel Aleem, "A new wireless charging system for electric vehicles using two receiver coils," *Ain Shams Engineering Journal*, vol. 13, no. 2, pp. 101 569–101 569, 2022.

[85] Y. Shanmugam, N. R, P. Vishnuram, M. Bajaj, K. M. AboRas, P. Thakur, and Kitmo, "A systematic review of dynamic wireless charging system for electric transportation," *IEEE Access*, vol. 10, pp. 133 617–133 642, 2022.

[86] C. Jiang, W. Chen, J. Wang, Z. Wang, and W. Xiao, "An improved deep q-network approach for charging sequence scheduling with optimal mobile charging cost and charging efficiency in wireless rechargeable sensor networks," *Ad hoc networks*, vol. 157, pp. 103 458–103 458, 2024.

[87] K. O. Momoh, S. A. Zulkifli, P. Korba, F. R. S. Sevilla, A. N. Afandi, and A. Velazquez-IbaÃ±ez, "State-of-the-art grid stability improvement techniques for electric vehicle fast-charging stations for future outlooks," *Energies*, vol. 16, no. 9, pp. 3956–3956, 2023. [Online]. Available: https://www.mdpi.com/1996-1073/16/9/3956/pdf?version=1683550383

[88] S. Chapaloglou, A. Nesiadis, K. Atsonios, N. Nikolopoulos, P. Grammelis, A. Carrera, and O. Camara, "Microgrid energy management strategies assessment through coupled thermal-electric considerations," *Energy Conversion and Management*, vol. 228, 2021.

[89] "Enhanced grid frequency and dc-link voltage regulation in hybrid ac/dc microgrids through bidirectional virtual inertia support," *IEEE transactions on industrial electronics*, vol. 70, no. 7, pp. 6931–6940, 2023.

[90] M. Cossutta, S. Pholboon, J. McKechnie, and M. Sumner, "Techno-economic and environmental analysis of community energy

management for peak shaving," *Energy Conversion and Management*, vol. 251, 2022.

[91] A. Kazemtarghi, S. Dey, and A. Mallik, "Optimal utilization of bidirectional evs for grid frequency support in power systems," *IEEE Transactions on Power Delivery*, vol. 38, no. 2, pp. 998–1010, 2023.

[92] D. Kumar, F. Zare, and F. Blaabjerg, "Special issue on modeling and analysis of interaction between grids and grid-connected power electronics converters in distribution networks," *IEEE Journal of Emerging and Selected Topics in Power Electronics*, vol. 10, no. 3, pp. 2658–2661, 2022.

[93] A. R. Abbasi and D. Baleanu, "Recent developments of energy management strategies in microgrids: An updated and comprehensive review and classification," *Energy Conversion and Management*, 2023.

[94] J. Chen, W. Si, M. Liu, and F. Milano, "On the impact of the grid on the synchronization stability of grid-following converters," *IEEE Transactions on Power Systems*, pp. 1–4, 2023.

[95] "Techno-economic and environmental analysis of community energy management for peak shaving," *Energy Conversion and Management*, vol. 251, pp. 114 900–114 900, 2022.

[96] A. Kazemtarghi, S. Dey, and A. Mallik, "Optimal utilization of bidirectional evs for grid frequency support in power systems," pp. 998–1010, 2023.

[97] X. Wang and Q. Liang, "Energy management strategy for plug-in hybrid electric vehicles via bidirectional vehicle-to-grid," *IEEE Systems Journal*, vol. 11, no. 3, pp. 1789–1798, 2017.

[98] D. V. Quang, D. Milani, and M. R. M. A. Zahra, "A review of potential routes to zero and negative emission technologies via the integration of renewable energies with co2 capture processes," *International Journal of Greenhouse Gas Control*, vol. 124, pp. 103 862–103 862, 2023.

[99] A. C. Lazaroiu, C. Panait, G. SeriÈ›an, C. Popescu, and M. Roscia, "Maximizing renewable energy and storage integration in university campuses," *Renewable Energy*, pp. 120 871–120 871, 2024.

[100] C.-H. Chou, S. L. Ngo, and P. P. Tran, "Renewable energy integration for sustainable economic growth: Insights and challenges via bibliometric analysis," *Sustainability*, 2023.

[101] G. Grazioli, S. Chlela, S. Selosse, and N. MaÃ¯zi, "The multi-facets of increasing the renewable energy integration in power systems," *Energies*, vol. 15, no. 18, pp. 6795–6795, 2022. [Online]. Available: https://www.mdpi.com/1996-1073/15/18/6795/pdf?version=1663667241

[102] A. Q. Al-Shetwi, "Sustainable development of renewable energy integrated power sector: Trends, environmental impacts, and recent challenges." *Science of The Total Environment*, vol. 822, pp. 153 645 – 153 645, 2022.

[103] A. Zakariazadeh, R. Ahshan, R. A. Abri, and M. Al-Abri, "Renewable energy integration in sustainable water systems: A review," *Cleaner engineering and technology*, 2024.

[104] C. Alcaraz, J. Lopez, and S. D. Wolthusen, "Ocpp protocol: Security threats and challenges," *IEEE Transactions on Smart Grid*, vol. 8, no. 5, pp. 2452–2459, 2017. [Online]. Available: https://www.nics.uma.es/sites/default/files/papers/AlcarazLopezWolthusen2017.pdf

[105] Z. Garofalaki, D. Kosmanos, S. Moschoyiannis, D. Kallergis, and C. Douligeris, "Electric vehicle charging: A survey on the security issues and challenges of the open charge point protocol (ocpp)," *IEEE Communications Surveys Tutorials*, vol. 24, no. 3, pp. 1504–1533, 2022.

[106] G. Percivall, T. Idol, N. Alameh, and J. Harrison, "Innovation in ogc: The interoperability program," *ISPRS international journal of geo-information*, vol. 4, no. 4, pp. 2362–2378, 2015. [Online]. Available: https://www.mdpi.com/2220-9964/4/4/2362/pdf

[107] J. A. Oliveira-Lima, V. Delgado-Gomes, J. Martins, and C. Lima, "Standard-based service-oriented infrastructure to integrate intelligent buildings in distributed generation and smart grids," *Energy and Buildings*, vol. 76, pp. 450–458, 2014.

[108] O. Noran, "Achieving a sustainable interoperability of standards," *Annual Reviews in Control*, vol. 36, no. 2, pp. 327–337, 2012.

[109] X. Costa-Perez, A. Festag, H.-J. Kolbe, J. Quittek, S. Schmid, M. Stiemerling, J. Swetina, and H. van der Veen, "Latest trends in telecommunication standards," vol. 43, no. 2, pp. 64–71, 2013. [Online]. Available: http://sigcomm.org/sites/default/files/ccr/papers/2013/April/2479957-2479968.pdf

[110] A. Mariscotti, "Power quality phenomena, standards, and proposed metrics for dc grids," *Energies*, vol. 14, no. 20, 2021.

[111] M. E. Reis, A. Bettencourt, and H. Ribeiro, "The regulatory challenges of innovative customized combination products," *Frontiers in Medicine*, vol. 9, 2022. [Online]. Available: https://www.frontiersin.org/articles/10.3389/fmed.2022.821094/pdf

[112] N. Schelte, S. Severengiz, S. Finke, and J. Stommel, "Analysis on user acceptance for light electric vehicles and novel charging infrastructure," in *2022 IEEE European Technology and Engineering Management Summit (E-TEMS)*, 2022, pp. 103–108.

[113] D. J. Heal, J. Gosden, and S. L. Smith, "Regulatory challenges for new drugs to treat obesity and comorbid metabolic disorders." *British Journal of Clinical Pharmacology*, vol. 68, no. 6, pp. 861–874, 2009. [Online]. Available: https://bpspubs.onlinelibrary.wiley.com/doi/pdf/10.1111/j.1365-2125.2009.03549.x

[114] D. Thilmany and C. B. Barrett, "Regulatory barriers in an integrating world food market," *Applied Economic Perspectives and Policy*, vol. 19, no. 1, pp. 91–107, 1997. [Online]. Available: https://www.jstor.org/stable/1349680

[115] J. Cohen, "Overcoming regulatory and economic challenges facing pharmacogenomics." *New Biotechnology*, vol. 29, no. 6, pp. 751–756, 2012.

[116] M. Plebanski, E. Lopez, O. Proudfoot, B. M. Cooke, M. von Itzstein, and R. L. Coppel, "Economic and practical challenges to the formulation of vaccines against endemic infectious diseases such as malaria," *Methods*, vol. 40, no. 1, pp. 77–85, 2006.

[117] S. Lester and I. Barbee, "The challenge of cooperation: Regulatory trade barriers in the transatlantic trade and investment partnership," *Journal of International Economic Law*, vol. 16, no. 4, pp. 847–867, 2013.

[118] A. Alavi, "Review of technology acceptance and use behavior," *Kuwait chapter of Arabian Journal of Business Management Review*, vol. 4, no. 7, pp. 9–14, 2015. [Online]. Available: https://www.arabianjbmr.com/pdfs/KD_VOL_4_7/2.pdf

[119] E. S. Vorm and D. J. Y. Combs, "Integrating transparency, trust, and acceptance: The intelligent systems technology acceptance model (istam)," *International Journal of Human-computer Interaction*, vol. 38, no. 18-20, pp. 1828–1845, 2022.

[120] L. Mlekus, D. Bentler, A. Paruzel, A.-L. Kato-Beiderwieden, and G. W. Maier, "How to raise technology acceptance: user experience characteristics as technology-inherent determinants," vol. 51, no. 3, pp. 273–283, 2020. [Online]. Available: https://link.springer.com/content/pdf/10.1007/s11612-020-00529-7.pdf

[121] M. Rajak and K. Shaw, "An extension of technology acceptance model for mhealth user adoption," *Technology in Society*, vol. 67, 2021.

[122] D. Ressi, R. Romanello, C. Piazza, and S. Rossi, "Ai-enhanced blockchain technology: A review of advancements and opportunities," *Journal of Network and Computer Applications*, 2024.

[123] A. Alanazi, F. K. Karim, S. A. A. Ghorashi, G. Amoudi, and S. H. A. Hamza, "Blockchain with optimal deep learning assisted secure data

sharing and classification on future healthcare systems," *alexandria engineering journal*, 2024.

[124] I. Fedorko, R. BaÄÃk, and B. Gavurova, "Analysis of selected technology acceptance model constructs and their impact on user behavior," *Innovative marketing*, vol. 18, no. 3, pp. 72–83, 2022. [Online]. Available: https://www.businessperspectives.org/images/pdf/applications/publishing/templates/article/assets/16850/IM_2022_03_Fedorko.pdf

[125] S. Xia, X. Wu, Z. Zhang, Y. Cui, Y. Cui, and W. Liu, "Practical challenges and future perspectives of all-solid-state lithium-metal batteries," *Chem*, vol. 5, no. 4, pp. 753–785, 2019.

[126] A. Aceti, I. Beghetti, L. Maggio, S. Martini, G. Faldella, and L. Corvaglia, "Filling the gaps: Current research directions for a rational use of probiotics in preterm infants," *Nutrients*, vol. 10, no. 10, 2018. [Online]. Available: https://www.mdpi.com/2072-6643/10/10/1472/pdf

[127] "Lack of consensus identifies important areas for future clinical research: Advanced prostate cancer consensus conference (apccc) 2019 findings," *European journal of cancer*, vol. 160, pp. 24–60, 2022. [Online]. Available: https://discovery.ucl.ac.uk/id/eprint/10142515/1/Vogl_2021.pdf

[128] W. Xiao, C. Liu, H. Wang, M. Zhou, M. S. Hossain, M. Alrashoud, and G. Muhammad, "Blockchain for secure-gas: Blockchain-powered secure natural gas iot system with ai-enabled gas prediction and transaction in smart city," *IEEE Internet of Things Journal*, vol. 8, no. 8, pp. 6305–6312, 2021.

[129] R. J. Valentino and N. D. Volkow, "Cannabis and cannabinoid signaling: Research gaps and opportunities." *Journal of Pharmacology and Experimental Therapeutics*, 2024.

[130] Y. Zhang, X. Liu, L. Yang, and L. Zou, "Current researches, rationale, plausibility, and evidence gaps on metformin for the management of

hypertensive disorders of pregnancy." *Frontiers in Pharmacology*, vol. 11, 2020.

[131] S. Rivera, S. M. Goetz, S. Kouro, P. W. Lehn, M. Pathmanathan, P. Bauer, and R. A. Mastromauro, "Charging infrastructure and grid integration for electromobility," *Proceedings of the IEEE*, vol. 111, no. 4, pp. 371–396, 2023.

[132] Z. Xin, X. Wang, Z. Qin, M. Lu, P. C. Loh, and F. Blaabjerg, "An improved second-order generalized integrator based quadrature signal generator," *IEEE Transactions on Power Electronics*, vol. 31, no. 12, pp. 8068–8073, 2016.

[133] M. Xie, H. Wen, C. Zhu, and Y. Yang, "Dc offset rejection improvement in single-phase sogi-pll algorithms: Methods review and experimental evaluation," *IEEE Access*, vol. 5, pp. 12 810–12 819, 2017.

[134] J. Matas, M. Castilla, J. Miret, L. García de Vicuña, and R. Guzman, "An adaptive prefiltering method to improve the speed/accuracy tradeoff of voltage sequence detection methods under adverse grid conditions," *IEEE Transactions on Industrial Electronics*, vol. 61, no. 5, pp. 2139–2151, 2014.

[135] M. Ciobotaru, R. Teodorescu, and F. Blaabjerg, "A new single-phase pll structure based on second order generalized integrator," in *2006 37th IEEE Power Electronics Specialists Conference*, Jeju, South Korea, 2006, pp. 1–6.

[136] Zunaib, N. Ali, N. Christofides, L. Hadjidemetriou, and E. Kyriakides, "Design of an advanced pll for accurate phase angle extraction under grid voltage hihs and dc offset," *IET Power Electronics*, 2018.

[137] H. Ahmed, "Low-order measurement offset rejection methods in single-phase sogi-pll," *IEEE Sensors Letters*, vol. 8, no. 1, pp. 1–4, 2024.

[138] S. Tangirala, "Evaluating the impact of gini index and information gain on classification using decision tree classifier algorithm,"

International Journal of Advanced Computer Science and Applications (IJACSA), vol. 11, no. 2, 2020.

Appendix A

Calculation of the parameters used

To calculate the source inductance which helps in removing the switching frequency harmonics and also it functions as the energy storing element while boost operation.

$$l_g = \left(1 - \frac{v_g}{V_{dc}}\right) \cdot \frac{v_g}{a \times f_{sw}} \tag{A.1}$$

$$\left(1 - \frac{230}{400}\right) \cdot \frac{230}{1.2 \times 50000} = 1.629\,\text{mH} \approx 1.5\,\text{mH} \tag{A.2}$$

The interfacing inductor helps in reducing the noises of the switching frequency from the grid current

$$l_f = \frac{mV_{DC}}{4af_{sw}\Delta I_{L\,\max}} \tag{A.3}$$

$$= (0.9400)/(41.2500001) = 1.5mH \approx 2mH. \tag{A.4}$$

Where, V_{DC} is the DC-Link voltage, f_{sw} is the switching frequency of FEC and $\Delta I_{L\,\max}$ is the grid current ripple.

In two stage OBBC charger DC-link capacitor is the common point between them. Therefore,

$$C_{DC} = \frac{P/V_{DC}}{2 \times \omega_g \times \Delta V_{DC}} = \frac{1100/400}{2 \times 2\pi \times 50 \times 5} \tag{A.5}$$

$$875.35\,\mu\text{F} \approx 1100\,\mu\text{F} \tag{A.6}$$

Where, P is the rated power, ω_g is the grid frequency and, ΔV_{DC} is the allowable ripple current content in DC-link.

TABLE A.1: Parameters used for simulation

Parameters	Values
Grid voltage, v_g	230 v_{rms}
Source inductance, l_g	1.5mH
Interfacing inductor, l_f	2mH
DC-Link Capacitor, C_{DC}	1100µF
DC-Link voltage, V_{DC}	400V
Non-Linear load (R_l & L_l)	100Ω, 85mH
Battery voltage	260V Li-Fe, 14Ah, 50% SoC
DC Filter inductor	4mH
DC Filter Capacitor	200 µF

TABLE A.2: Parameters used for hardware setup

Parameters	Values
Grid voltage, v_g	70 v_{rms}
Source inductance, l_g	Iron Core 0.5mH
Interfacing inductor, l_f	Iron Core 2mH
DC-Link Capacitor, C_{DC}	1000µF, 550V
DC-Link voltage, V_{DC}	140V
Non-Linear load (R_l & L_l)	1.5kW, 60mH
Battery voltage	48V Lead Acid, 7Ah
DC Filter inductor	Ferrite Core 2mH
DC Filter Capacitor	56 µF, 250V
IGBT Switches	1B32CJ FGA25N120 ANTD

Code used for the algorithms

1. The code reads data from an Excel file and performs linear regression on the predictors (X and Y) to model the response variable (Z). It then performs an ANOVA test on the linear model and plots the linear fit with a title and labeled axes.

```
% Read the data from the Excel file
data = readtable('/MATLAB Drive/Copy of pi_in_out_$V_{DC}$(1).xlsx');
X = data.pi_in;
Z = data.pi_out;
Y = data.$V_{DC}$;
```

```

% Create a table with the predictors
predictors = [X, Y];

% Perform linear regression
mdl = fitlm(predictors, Z);

% Perform robust linear regression
mdlr = fitlm(predictors, Z);

% Perform ANOVA and display summary
anovaSummary = anova(mdl, 'summary');
disp(anovaSummary);

% Plot the robust fit and set the title
figure;
plot(mdl);
title('Linear Fit');
xlabel('Predictors');
ylabel('Response Variable');
legend('Data', 'Linear Fit', 'Location', 'Best');
```

2. The code reads data from an Excel file, performs linear regression, and finds which data points have significant residuals. It then plots a scatter plot highlighting these significant points.

```
data = readtable('/MATLAB Drive/Copy of pi_in_out_VDC(1).xlsx');
X = data.pi_in;
Z = data.pi_out;
Y = data.Vdc;

y = Z;
X = [ones(size(data(:,1))) X Y];
[~,~,r,rint] = regress(y,X,0.01);
contain0 = (rint(:,1)<0 & rint(:,2)>0);
idx = find(contain0==false)

% Assume y and r are your complete datasets
% idx is the index of the specific points you want to highlight

% Select the first 100 values
y_first100 = y(400:500);
r_first100 = r(400:500);

% If idx is not already limited to the first 100 values, you can do it
idx_first100 = idx(idx <= 100);

% Plot the first 100 values
figure;
hold on;
```

```
scatter(y_first100, r_first100); % Scatter plot of the first 100 values
scatter(y_first100(idx_first100), r_first100(idx_first100), 'b', 'filled');
% Highlight specific points within the first 100 values
xlabel("Predictors");
ylabel("Residuals");
hold off;
```

3. The code reads data from an Excel file and creates a 3D scatter plot to visualize the relationship between the predictors (X and Y) and the response variable (Z). It also fits a linear regression model to the data and overlays the fitted surface on the plot.

```
fl_data = readtable('/MATLAB Drive/Copy of pi_in_out_VDC(1).xlsx');
X = fl_data.pi_in;
Z = fl_data.pi_out;
Y = fl_data.Vdc;

% Plot the data and the model
figure;
scatter3(X, Y, Z, 'filled');
hold on;
x_axis_fit1 = linspace(min(X), max(X), 100);
x_axis_fit2 = linspace(min(Y), max(Y), 100);
[X_axis_fit1, X_axis_fit2] = meshgrid(x_axis_fit1, x_axis_fit2);
Y_axis_fit = mdl.Coefficients.Estimate(1) + ...
       mdl.Coefficients.Estimate(2) * X_axis_fit1 + ...
       mdl.Coefficients.Estimate(3) * X_axis_fit2 ;

mesh(X_axis_fit1, X_axis_fit2, Y_axis_fit);
xlabel('pi\_in');
ylabel('Vdc');
zlabel('pi\_out');
title('Multiple Linear Regression with Interaction Term');
view(50, 10);
hold off;
```

4. The code imports necessary libraries and loads data from an Excel file, then builds and trains an Artificial Neural Network (ANN) model to predict the 'pi_{out}' values based on 'V_{dc}' and 'pi_in'. It evaluates the model, predicts values, and generates plots for the learning curve, actual vs. predicted values, and residuals.

```
!pip install tensorflow
import pandas as pd
import numpy as np
import matplotlib.pyplot as mplt
import seaborn as seab
```

```
from sklearn.model_selection import train_test_split as D_split
from sklearn.preprocessing import StandardScaler as std_scl
from tensorflow.keras.models import Sequential
from tensorflow.keras.layers import Dense

# Load the data
file_path = '/content/pi_in_out_VDC.xlsx'
data = pd.read_excel(f"ile_path)

# Separate features and target
X = data[['Vdc', 'pi_in']].values
y = data['pi_out'].values

# Splitting the data into Training and Testing dataset
Tr_X, Te_X, Tr_y, Te_y = D_split(X, y, test_size=0.2, random_state=42)

# Standardize the data
Mdl_Scl = std_scl()
Tr_X = Mdl_Scl.fit_transform(Tr_X)
Te_X = Mdl_Scl.transform(Te_X)

# Build the ANN model
sq_md = Sequential()
sq_md.add(Dense(64, input_dim=Tr_X.shape[1], activation='relu'))
sq_md.add(Dense(32, activation='relu'))
sq_md.add(Dense(1))  # Output layer for regression

# Model Compilation
sq_md.compile(optimizer='adam', loss='mean_squared_error')

# Train the model
history = sq_md.fit(Tr_X, Tr_y, epochs=3, batch_size=10, validation_split=0.2, verbose
    =1)

# Evaluate the model
loss = sq_md.evaluate(Te_X, Te_y)
print(f'Mean Squared Error: {loss}')

# Predict values
pre_y = sq_md.predict(Te_X)

# Print the first 5 predictions
print('First 5 predictions:', pre_y[:5])
print('First 5 actual values:', Te_y[:5])

# Generate and analyze plots

# 1. Learning Curve
mplt.figure(figsize=(10, 6))
mplt.plot(history.history['loss'], label='Training Loss')
mplt.plot(history.history['val_loss'], label='Validation Loss')
```

```
mplt.xlabel('Epochs')
mplt.ylabel('Loss')
mplt.title('Learning Curve')
mplt.legend()
mplt.show()

# 2. Scatter Plot: Actual vs Predicted Values
mplt.figure(figsize=(10, 6))
mplt.scatter(Te_y, pre_y)
mplt.plot([min(Te_y), max(Te_y)], [min(Te_y), max(Te_y)], 'r--')
mplt.xlabel('Actual Values')
mplt.ylabel('Predicted Values')
mplt.title('Actual vs Predicted pi_out')
mplt.show()

# 4. Histogram of Residuals
mplt.figure(figsize=(10, 6))
seab.histplot(residuals, kde=True)
mplt.xlabel('Residual')
mplt.ylabel('Frequency')
mplt.title('Histogram of Residuals')
mplt.show()
```

5. The code reads data from an Excel file, splits it into training and testing sets, and trains a Decision Tree Regressor to predict 'pi_{out}' based on 'V_{DC}' and 'pi_{in}'. It then plots a scatter plot of actual vs. predicted values for both training and testing data to visualize prediction errors.

```
import numpy as np
import matplotlib.pyplot as mplt
from sklearn.tree import DecisionTreeRegressor
from sklearn.model_selection import train_test_split as split_data
from sklearn.metrics import mean_squared_error

# Generating random data
np.random.seed(0)
data = pd.read_excel('/content/pi_in_out_VDC.xlsx')
X, y = data[['Vdc','pi_in']], data.pi_out

# Split the data for testing and training
X_tr, X_te, y_tr, y_te = split_data(X, y, test_size=0.21, random_state=1)

# Train the Decision Tree Regressor
reg = DecisionTreeRegressor(max_depth=5)
reg.fit(X_tr, y_tr)

# Predict on testing and training data
y_tr_pred = reg.predict(X_tr)
y_te_pred = reg.predict(X_te)

```

```
# Plotting the prediction error
mplt.figure(figsize=(10, 6))
mplt.scatter(y_tr, y_tr_pred, color='blue', label='Train Data', alpha=0.6)
mplt.scatter(y_te, y_te_pred, color='yellow', label='Test Data', alpha=0.6)
mplt.plot([min(y), max(y)], [min(y), max(y)], color='red', lw=2, label='Perfect Fit')
mplt.ylabel('Predicted Values')
mplt.xlabel('Actual Values')
mplt.title('Prediction Error Plot')
mplt.legend()
mplt.show()
```

List of Publications

Papers in Refereed Journals

[1] G. Yadav and M. Singh, "Real-time investigation of grid-interactive EV charger with two-stage bidirectional converter under wide voltage range scenarios," *Electrical Engineering*, pp. 1–17, 2024, Springer. DOI: 10.1007/s00202-024-02609-z.

[2] G. Yadav and M. Singh, "Optimizing power quality in EV chargers using advanced quadrature signal generators and AI-driven adaptive filtering," *International Journal of Circuit Theory and Applications*, pp. 1–22, 2025, Wiley. DOI: 10.1002/cta.4424.

[3] G. Yadav and M. Singh, "A Fourth Order D–QSG Based Control for Grid-Interactive EV Chargers Under Non-Ideal Conditions," *IEEE Transactions on Transportation Electrification*, 2025. (Manuscript in second revision).

[4] G. Yadav and M. Singh, "A Robust Parameter Selection Technique for 4th-Order D-QSG Based Controller in Grid-Interactive EV Chargers Under Wide Voltage Range Scenarios," *IEEE Transactions on Power Electronics*, 2025. (Manuscript under review).

[5] G. Yadav, "Efficient response enhancement under nonideal grid voltage conditions using fourth-order d-qsg based control grid-interactive EV chargers," *International Journal of Circuit Theory and Applications*, pp. 1–15, 2025, Wiley. DOI: 10.1002/cta.70059.

[6] G. Yadav, "Enhancing Power Quality and Stability in Grid-Interactive Electric Vehicle Chargers Using Advanced Control Strategies and Disturbance Compensation," *Engineering Research Express*, vol. 7, no. 3, pp. 1–17, 2025, IOP Publishing. DOI: 10.1088/2631-8695/adf038.

[7] G. Yadav and P. Dhaka, "Stabilizing DC Bus Voltage Using CEEMDAN-XGBOOST Based Adaptive Filtering Technique in EV Chargers," *Computers and Electrical Engineering*, vol. 127, pp. 1–19, 2025, Elsevier. DOI: 10.1016/j.compeleceng.2025.110547.

[8] G. Yadav and P. Yegon, "ML-Based Grid-Interactive EV Chargers Under Nongrid Conditions," *Applied Computational Intelligence and Soft Computing*, pp. 1–16, 2025, Hindawi. DOI: 10.1155/acis/1731177.

National and International Conference Proceedings

[1] Akshay, Gaurav Yadav, and Mukhtiar Singh. Validation of a parameter design methodology for air-core two-coil wpt system with multi-resonant lc compensation. In *2023 IEEE International Conference on Power Electronics, Smart Grid, and Renewable Energy (PESGRE)*, pages 1–6, 2023. doi: 10.1109/PESGRE58662.2023.10404443.

[2] Monish Ansari, Gaurav Yadav, and Mukhtiar Singh. A 3.3kw modified llc resonant converter for grid-tied ev system under wide voltage range. In *2023 3rd International Conference on Intelligent Technologies (CONIT)*, pages 1–6, 2023. doi: 10.1109/CONIT59222.2023.10205690.

[3] Monish Ansari, Gaurav Yadav, and Mukhtiar Singh. Modified bidirectional llc converter for electric vehicle application. In *2023 Second International Conference on Electrical, Electronics, Information and Communication Technologies (ICEEICT)*, pages 1–7, 2023. doi: 10.1109/ICEEICT56924.2023.10157520.

[4] Ghanmohan Dangi, Himanshu Chhabra, Ishan Gandhi, Gaurav Yadav, and Mukhtiar Singh. Design of buck converters and integration of electrical with software subsystem for interplanetary rovers. In *2024 IEEE Third International Conference on Power Electronics, Intelligent Control and Energy Systems (ICPEICES)*, pages 211–216, 2024. doi: 10.1109/ICPEICES62430.2024.10719256.

[5] Grisham Garg, Dhruv Talan, Himanshu, Gaurav Yadav, and Mukhtiar Singh. Implementing ml and dl based controllers for improving efficiency in ev charging application. In *2024 IEEE Third International Conference on Power Electronics, Intelligent Control and Energy Systems (ICPEICES)*, pages 235–240, 2024. doi: 10.1109/ICPEICES62430.2024.10719347.

[6] Harsh Pandey, Kanishk Kumar Singh, Sujay Sakalkar, Gaurav Yadav, and Mukhtiar Singh. Enhancing wireless charging for electric vehicles: A comparative study of coil designs and their impact on power transfer efficiency. In *2024 IEEE Third International Conference on Power Electronics, Intelligent Control and Energy Systems (ICPEICES)*, pages 1207–1212, 2024. doi: 10.1109/ICPEICES62430.2024.10719184.

[7] Yalavarthi Lalith Sai Ram, Akshay Kumar Singh, Sanat Kumar, Gaurav Yadav, and Mukhtiar Singh. Adaptive fuzzy logic based controller for grid-interactive ev systems in charging application. In *2024 IEEE Third International Conference on Power Electronics, Intelligent Control and Energy Systems (ICPEICES)*, pages 1213–1218, 2024. doi: 10.1109/ICPEICES62430.2024.10719087.

[8] Anurag Singh, Gaurav Yadav, and Mukhtiar Singh. Performance analysis of 3-phase active front end pwm rectifier for air-core two-coil wpt system configuration. In *2023 9th IEEE India International Conference on Power Electronics (IICPE)*, pages 1–6, 2023. doi: 10.1109/IICPE60303.2023.10474683.

[9] Gaurav Yadav and Mukhtiar Singh. Unveiling the superiority: comparative analysis of anfis, fopid, and pi controllers in grid-connected ev systems for g2v/v2g applications. In *2023 International Conference on Electrical, Electronics, Communication and Computers (ELEXCOM)*, pages 1–6. IEEE, 2023.

[10] Gaurav Yadav and Mukhtiar Singh. Robust control design for grid-tied ev system with sogi-based architecture in wide voltage range scenarios. In *2023 international conference on electrical, electronics, communication and computers (ELEXCOM)*, pages 1–6. IEEE, 2023.

[11] Gaurav Yadav and Mukhtiar Singh. Cnisogi and llmf based controller design for grid-interactive ev chargers in wide voltage range scenarios. In *2024 IEEE 4th International Conference on Sustainable Energy and Future Electric Transportation (SEFET)*, pages 1–6. IEEE, 2024.